RESEARCH AND DEVELOPMENT TECHNICAL REPORT
CECOM-81-0136-4

UHF RADIOWAVE PROPAGATION THROUGH FORESTS

PREPARED BY:

R.H. Lang, A. Schneider, S. Seker, and F.J. Altman

CyberCom Corporation
4105 North Fairfax Drive
Arlington, Virginia 22203

CyberCom Technical Report: CTR-108-01
September 1982

Distribution Statement: Approved for Public Release; Distribution Unlimited

CECOM
Center For Communication Systems (Mr. P. Sass)
U S Army Communications-Electronics Command
Fort Monmouth, New Jersey 07703

NOTICES

Disclaimers

The citation of trade names and names of manufacturers in this report is not to be construed as official Government indorsement or approval of commercial products or services referenced herein.

Disposition

Destroy this report when it is no longer needed. Do not return it to the originator.

RESEARCH AND DEVELOPMENT TECHNICAL REPORT
CECOM-81-0136-4

UHF RADIOWAVE PROPAGATION THROUGH FORESTS

PREPARED BY:

R.H. Lang, A. Schneider, S. Seker, and F.J. Altman

CyberCom Corporation
4105 North Fairfax Drive
Arlington, Virginia 22203

CyberCom Technical Report: CTR-108-01
September 1982

CECOM
Center For Communication Systems (Mr. P. Sass)
U S ARMY COMMUNICATIONS-ELECTRONICS COMMAND
FORT MONMOUTH, NEW JERSEY 07703

SECURITY CLASSIFICATION OF THIS PAGE (When Data Entered)

REPORT DOCUMENTATION PAGE

RE... STRUCTIONS BEFOR... COMPLETING FORM

1. REPORT NUMBER: CECOM-81-0136-4	2. GOVT ACCESSION NO.
3. RECIPIENT'S CATALOG NUMBER	
4. TITLE (and Subtitle): UHF Radiowave Propagation Through Forests	5. TYPE OF REPORT & PERIOD COVERED: Technical report SEPT 81-SEPT 82
6. PERFORMING ORG. REPORT NUMBER: CTR-108-01	
7. AUTHOR(s): R.H. Lang, A. Schneider, S. Seker and F. Altman	8. CONTRACT OR GRANT NUMBER(s): DAAK80-81-C-0136
9. PERFORMING ORGANIZATION NAME AND ADDRESS: CyberCom Corporation, 4105 North Fairfax Drive, Arlington, Virginia 22203	10. PROGRAM ELEMENT, PROJECT, TASK AREA & WORK UNIT NUMBERS: 1L1.61102.AH48.PF.01
11. CONTROLLING OFFICE NAME AND ADDRESS: Center for Communication Systems, ATTN: DRSEL-COM-RF-2 (Sass), U.S. Army Communications-Electronics Command, Fort Monmouth, New Jersey 07703	12. REPORT DATE: SEPT 82
	13. NUMBER OF PAGES: 180
14. MONITORING AGENCY NAME & ADDRESS (if different from Controlling Office)	15. SECURITY CLASS. (of this report): unclassified
	15a. DECLASSIFICATION/DOWNGRADING SCHEDULE

16. DISTRIBUTION STATEMENT (of this Report)

Distribution unlimited

17. DISTRIBUTION STATEMENT (of the abstract entered in Block 20, if different from Report)

18. SUPPLEMENTARY NOTES

19. KEY WORDS (Continue on reverse side if necessary and identify by block number)

UHF Radiowave Propagation, Forests, Foliage, Vegetation, Trees, Attenuation, Transmission loss, Channel Characterization, Pulse Response, Lateral Waves

20. ABSTRACT (Continue on reverse side if necessary and identify by block number)

A model for UHF radiowave propagation through a forest of tree trunks, branches, and leaves is developed using the discrete scattering theory of Foldy and Lax. The forest is represented as a time-invariant ensemble of tree trunks, branches, and leaves all having prescribed location and orientation statistics. Tree trunks are modelled as infinitely-long, circular, lossy-dielectric cylinders; branches as finitely-long, circular, lossy-dielectric cylinders; and leaves as flat, circular, lossy-dielectric discs. Mathematical expressions are found for the effective dyadic susceptibilities of the equivalent

DD FORM 1 JAN 73 1473 EDITION OF 1 NOV 65 IS OBSOLETE

SECURITY CLASSIFICATION OF THIS PAGE (When Data Entered)

continuous medium and for the specific attenuation associated with the mean (coherent) fields. Using biophysical parameters typical of a deciduous, hardwood forest, these expressions are found to be in reasonable agreement with experimental results. An anisotropic half-space model of the forest is developed based upon the effective dyadic susceptibility and the direct-, reflected-, and lateral wave components of the mean field presented for a pulse of a few nanoseconds duration and a frequency of 600 Megahertz. A preliminary analysis shows the importance of the random (incoherent) field at a distance of one kilometer and at frequencies above 100 Megahertz.

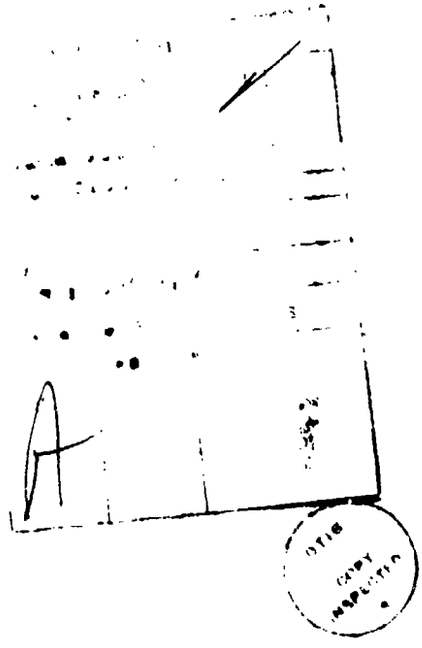

CONTENTS

FIGURES

EXECUTIVE SUMMARY

1.0 Introduction

In the early 1960's, the United States Army supported an extensive experimental and theoretical research program [47] on radiowave propagation in the environment of a tropical, thickly vegetated jungle. The experimental data acquired during this program were later used by Tamir [93,107,108] to validate a theoretical propagation model which shows that, for frequencies less than 200 MHz, the principal mechanism responsible for long-distance propagation is the so-called lateral wave. According to Tamir's theory, a lateral wave propagates upward from the transmitting antenna through the vegetative canopy to the tree tops, along the air-canopy interface, and downward from the tree tops through the canopy to the receiving antenna.

Recently, the Army has become interested in the development of several spread-spectrum radio systems (e.g. Packet Radio, PLRS, JTIDS) operating in the frequency band 200-2000 MHz. From the perspective of radio wave propagation, these newer systems differ from earlier ones in three important respects: (1) their higher operational frequencies, (2) their broader spectral occupancy, and/or (3) their pulsed (digital) mode of operation. The Tamir model, however, is valid primarily below 200 MHz and, further, considers only the propagation of an unmodulated, time-harmonic signal in a continuous isotropic medium.

This report describes a stochastic radiowave propagation model useful for assessing the effects of forests and other vegetation upon digital spread-spectrum radio communication systems operating in the 200 - 2000 MHz band. According to this model, the forest is represented as a time-invariant ensemble of lossy, randomly positioned and oriented discrete canonical scatterers. Tree trunks are modelled as infinitely-long, circular, dielectric cylinders; branches as finitely-long, circular dielectric cylinders; and leaves as flat, circular, dielectric discs. The orientation of these elements must be specified (statistically) because their scattering is directional. Thus the model is anisotropic, with different properties in different directions. The model is developed in sufficient detail to be useful in the prediction of attenuation and pulse distortion of mean scattered radiowaves. Areas for future study are identified below in Sections 3, 4, 5, 7, and 8.

2.0 Radiowave Scattering in Discrete Random Media

The forest is viewed as a random ensemble of tree trunks, branches, and leaves all having prescribed location and orientation statistics. Because of the inherent randomness associated with this medium of discrete scatterers, the behavior of propagating radiowaves within the forest cannot be described by traditional, deterministic electromagnetic models but rather only by modern stochastic models. Such models provide the basis for determining the two most important characteristics of the propagating electromagnetic wave: the mean field component, and the space-frequency correlation function which characterizes the random (or fluctuating) field component. See Section 2.2.4.

The stochastic electromagnetic model employed by CyberCom as the basis for this study of radiowave propagation through the forest is described in Section 2 of this report. The model was first developed by Foldy [53] and later extended by Lax [55a], Twersky [64], Lang [57], and others. The forest is considered to be a discrete medium representable as a time-invariant ensemble of randomly

positioned and oriented discrete canonical scatterers. Tree trunks are modeled as infinitely-long, circular, dielectric cylinders; branches as finitely-long, circular, dielectric cylinders; and leaves as flat, circular dielectric discs.

The electromagnetic waves scattered by the canonical scatterers (the cylinders and discs) are related to the fields induced within them by the incident fields. The fields induced within a single scatterer are related to the incident electromagnetic wave through the transition operator. This latter relation arises as a direct consequence of the linearity implicit in Maxwell's equations. Scatterers are also characterized by the amplitude of the scattered field when the scatterer is illuminated by a plane-wave. Both the transition operator and the scattering amplitude are employed in the development of the theory. CyberCom has utilized the Foldy-Lax model in considering radiowave scattering within an unbounded forest comprised of either two-dimensional scatterers (infinitely-long, circular, cylinders representing tree trunks) or three-dimensional scatterers, (finitely-long, circular, cylinders representing branches, and flat, circular, discs representing leaves). For these media, CyberCom used the Twersky model to derive mathematical expressions describing the behavior of the mean scattered field and the space-frequency correlation function. These expressions, which represent the principal results of Section 2, provide the basis for subsequent studies addressed in later sections of this report relating to the effective permittivity (susceptibility) of the forest, the specific attenuation of radiowaves propagating through the forest, the estimation of contributions by the lateral wave propagating above an anisotropic forest, the dispersion of broadband radiowave pulses, and the assessment of the relative strength of the mean and random components of the scattered radiowave.

3.0 Dyadic Scattering Amplitude

The stochastic electromagnetic model employed by CyberCom as the basis for this study of radiowave propagation through forests is predicated upon the assertion that the far-field scattering behavior of the individual canonical scatterers (the cylinders and discs) can be characterized by a (dyadic) transition operator and/or scattering amplitude. In Chapter 3 of this report, mathematical expressions are derived relating the scattering amplitudes of the three canonical scatterers to the dimensions, orientation, and permittivity of the scatterer and to the frequency and polarization of the propagating radiowave. Approximate expressions valid only in the low-frequency (Rayleigh) regime have been obtained for all three canonical scatterers. In addition, exact expressions valid for all frequency bands have been obtained for infinite-length, circular, dielectric cylinders (tree trunks) and approximate expressions suitable for the resonant regime have been obtained for discs (leaves). These expressions represent the principal results of Section 3. A resonant model for finite-length, circular, dielectric cylinders (branches) has yet to be developed.

4.0 Coherent Forest Scattering

A physically-appealing representation for the mean field component can be obtained by postulating that the mean (or coherent) field component satisfies Maxwell's equations "in the mean" and that the ensemble of discrete scatterers can be replaced by an equivalent continuous medium described by an effective

dyadic permittivity $\underline{\underline{\varepsilon}}$. In general, $\underline{\underline{\varepsilon}}$ has been found to depend upon the direction of radiowave propagation through the forest; such media are termed spatially dispersive. See Section 4.1. Because $\underline{\underline{\varepsilon}}$ is a dyadic, the forest is found, in general, to be anisotropic.

A constitutive parameter of the equivalent continuous medium closely allied to the effective dyadic permittivity $\underline{\underline{\varepsilon}}$ is the effective dyadic susceptibility $\underline{\underline{\chi}}$, so defined that $\underline{\underline{\varepsilon}} = \underline{\underline{I}} + \underline{\underline{\chi}}$ where $\underline{\underline{I}}$ is the unit dyadic. CyberCom has found that $\underline{\underline{\chi}}$ is directly proportional to the fractional volume of the forest occupied by the scatterers. As a consequence, it is a parameter which is conveniently scaled to scatterer density and, therefore, is preferred over $\underline{\underline{\varepsilon}}$ for the characterization of the equivalent medium. Mathematical expressions for the effective dyadic susceptibility of unbounded forests of tree trunks, branches, and leaves have been obtained in Section 4 under the hypothesis that the orientation distribution of the canonical scatterers is azimuthally uniform about the vertical. Numerical computations based upon typical forest parameters show reasonably good agreement with values inferred from measurements.

CyberCom has solved the wave equation for the mean scattered field propagating through an unbounded forest consisting solely of tree trunks, branches, or leaves. The solution reveals that, to a first approximation, the horizontally- and vertically polarized waves propagate independently and without any depolarization. Further, these waves propagate with velocities dependent upon the inclination of their wave-normal to the forest floor. These effects are a consequence of the anisotropy and spatially-dispersive character of the equivalent forest medium.

In general, the wave propagation constant has both real and imaginary components. The real part is expressed in radians per meter; the imaginary part, also called the specific attenuation, is expressed in nepers per meter or, alternatively, in decibels per meter. Mathematical expressions for the specific attenuation of radiowaves propagating through unbounded forests of tree trunks, branches, and leaves have been obtained in Section 4 using the dispersion relation and the effective dyadic susceptibility. Numerical computations based upon typical forest parameters show reasonably good agreement with measured values.

Experimental verification of the electromagnetic model and, ultimately, prediction of radio system performance requires the identification of measureable quantitative parameters to characterize the forest. Some of these parameters have already been identified by CyberCom during the course of this study. Some of these parameters (e.g., the size and relative permittivity of individual tree trunks, branches or leaves) are termed "microscopic"; others (e.g., number of trees per hectare or branches or leaves per cubic meter, foliage orientation distribution) are termed "macroscopic". In the low-frequency (Rayleigh) regime, CyberCom has been able to derive fairly simple engineering expressions relating specific attenuation to salient parameters of the forest. One composite parameter, especially important at low frequencies is the fractional volume occupied by the vegetation. Prior to this study, no such expressions were available for predicting the relationship between specific attenuation (dB/m) and salient forest parameters. More work is required to identify real-world forest types and to derive the associated susceptibilities and specific attenuations.

5.0 Anisotropic Forest-Slab Model

The forest model described in previous sections of this report (an unbounded ensemble of randomly-positioned tree trunks, branches and leaves having prescribed location and orientation statistics) can be refined by assuming the trees to be spread uniformly in height above a smooth forest floor and bounded above by air. Earlier efforts [93,104,107] have shown, however, that the presence of the ground complicates the model significantly. These complications can be avoided, however, by allowing the ground plane to recede from the air-forest interface so that the model adopted by CyberCom provides a very good approximation to the basic slab model if both the transmitting and receiving antennas are not located too close to the ground [107]. Further work should include the effects of the ground plane.

The lower half-space representing the forest is characterized (at least so far as the mean scattered fields are concerned) by effective dyadic permittivity $\underline{\underline{\varepsilon}}$ and so may be considered, in general, to be electrically anisotropic and spatially dispersive. The relation between the effective dyadic permittivity $\underline{\underline{\varepsilon}}$ and the biophysical parameters of the forest has been discussed previously. A transmitting antenna representable as a vertical (Hertzian) dipole having a time-harmonic current moment of angular frequency ω is assumed to be immersed a distance d below the air-forest interface.

The electromagnetic boundary value problem suggested by the anisotropic half-space model has been solved by CyberCom using the classical approach first described by Sommerfeld [111] and later extended by Brekhovskikh [87]. In effecting this solution, CyberCom considered the forest to be uniaxially anisotropic (a consequence of the prescribed azimuthal uniformity in the scatterer-orientation probability distributions). Earlier, Sachs and Wyatt [101], and Tamir and others [93,107] had considered similar, but isotropic, slab-type models based upon postulated effective permittivities which could not be related directly to the biophysical parameters of the forest. A principal conclusion derived from the earlier efforts was the experimentally-confirmed conjecture that radiowave propagation over long distances between antennas within forests is dominated by a so-called lateral wave. According to those models, the lateral wave propagates from the transmitting antenna up through the forest at the critical angle to the air-forest interface, through the air along the air-forest interface, and down through the forest at the critical angle from the air-forest interface to the receiver. Because a substantial fraction of the transmission path of the lateral wave can lie in the dissipationless air, the transmission loss associated with the lateral wave can be significantly lower than that associated with the direct wave through the forest. The former was characterized by Tamir as inversely proportional to the square of the distance.

The anisotropic half-space model considered by CyberCom also shows that the propagation of the mean field scattered from randomly-positioned tree trunks, branches, and leaves is dominated at low frequencies and large distances by the lateral wave. Preliminary studies reported in Section 7 suggest that in the frequency band 200 - 2000 MHz the non-coherent random field is larger that the coherent mean field, causing large spatial fluctuations.

6.0 Forest Pulse Response

The anisotropic forest-slab model developed by CyberCom in Section 5 of this report is a time-harmonic model in the sense that the signal radiated by the antenna is a sinusoidal waveform of angular frequency ω. However, because the

equivalent continuous medium characterized by the effective dyadic permittivity $\underline{\underline{\varepsilon}}$ is a linear medium, Fourier-transform techniques can be employed to generalize the model so that it can accommodate such arbitrarily-modulated waveforms as the pulse transmissions employed for spread-spectrum digital systems. Due to the complex frequency dependence exhibited by the effective dyadic permittivity of the forest, the model employs numerical techniques based upon the fast Fourier transform. Using this model, in Section 6 of this report, the forest pulse response, defined here as the vertically-polarized component of the mean scattered electric field, is found for a transmitted 5.8 nanosecond rectangular pulse having a carrier frequency of 600 Megahertz. The model can be used to assess medium-induced pulse distortion and inter-symbol interference and can be easily extended to accommodate other field components of the mean wave, arbitrary antenna types, and even Doppler effects induced by terminal antenna movement.

7.0 Non-Coherent Forest Scattering

As a radiowave propagates through the forest, power associated with the mean (or coherent) field is transformed to the random (or non-coherent) scattered field. In Section 7, this phenomenom is examined and the mechanism related to specific biophysical parameters of the forest. To ease the mathematical burden, the forest has been represented as an unbounded medium of infinitely-long, parallel tree trunks with transmitting antenna represented as a line-source parallel to the trees. Attention has been focused upon the Rayleigh-scattered field intensity of a radiowave propagating normal to the trunks. The results show that the intensity of the non-coherent scattered field increases relative to that of the coherent (mean) field with increasing distance from the source and with increasing frequency. Is is desirable to study the non-coherent field further and to attempt to include the effects of leaves.

8.0 Conclusions

In summary, the homogenous, isotropic, refracting slab of a forest has been replaced by CyberCom with an inhomogenous, anisotropic, scattering ensemble of trunks, branches, and leaves. In consequence:

1. The lateral-wave contribution has been found even above 200 Megahertz.
2. Preliminary validation of the model has shown rough agreement with experiments.
3. Results have been obtained for narrow pulse transmission at 600 MHz.
4. A preliminary study has emphasized the importance of the incoherent component of the transmitted field.

As the CyberCom approach is ambitious in both scope and depth, the following remain to be done:

a. The techniques already developed must be exercised to determine the relative importance of forest components and the effects of varying critical parameters. For example, if the contribution of branches is major, the difficult characterization of the scattering properties should be advanced in the resonant region.
b. The effects of antenna directivity, the ground, and terminal movement should be incorporated into the model.
c. The difficult transport theory for the important non-coherent scattered wave should be developed as far as practical.
d. Forest studies must be pursued to quantify important biophysical parameters in areas of interest.

1.0 Introduction

This report describes a stochastic radiowave propagation model useful for assessing the effects of forests and other vegetation upon radio communication systems operating in the 200 - 2000 Megahertz frequency band. In this introductory section, the background leading to the requirement for such a model is presented, with a summary of the approach employed for its development and an outline of this report.

1.1 Background

The United States Army has had a long and continuing interest in radiowave propagation through forest, jungle, or otherwise vegetated environments. In the early 1960's, the Army supported an extensive experimental and theoretical research program [47] on radiowave propagation in the environment of a tropical, thickly vegetated jungle. The experimental data acquired during this program were later used by Tamir [93, 107, 108] to validate a theoretical propagation model which shows that, for frequencies less than 200 MHz, the principal mechanism responsible for long-distance propagation is the so-called lateral wave. According to this theory, a lateral wave propagates upward from the transmitting antenna, through the vegetative canopy to the tree tops, along the air-canopy interface, and downward from the tree tops through the canopy to the receiving antenna. Prior to the Army's research program, it was generally believed, primarily on the basis of measurements made in England by Saxton and Lane [36], that the excess (specific) attenuation contributed by the foliage per meter of path length was independent of distance and unacceptably high for the tactical deployment of VHF radio sets on long paths in forests. Some of the experimental data used by Tamir and the Army in refuting this erroneous contention are shown in Figure 1-1 along with the experimental data of Saxton and Lane.

Recently, the Army has become interested in the development of several spread-spectrum radio systems (e.g., Packet Radio, PLRS, JTIDS) [163]. From the perspective of radiowave propagation, these

Experimental Data of Saxton and Lane [36]

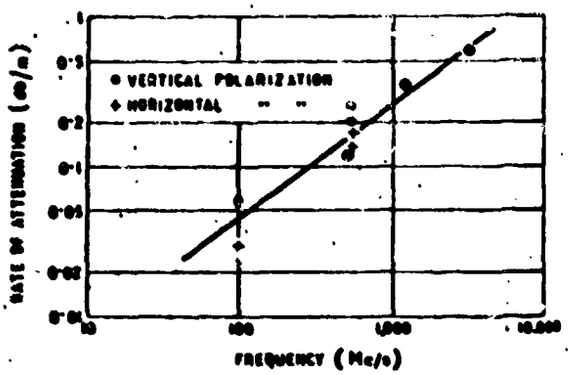

Fig. 1. Rate of attenuation in woods with trees in leaf as a function of frequency.

Experimental Data of Tamir [107]

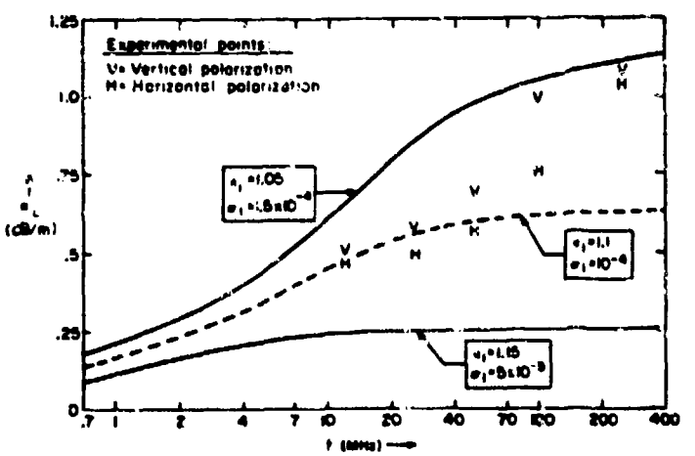

Fig. 8. Theoretical and experimental values of the lateral-wave attenuation α_L versus frequency f.

Figure 1-1: Experimental Data of Saxton and Lane [36] and Tamir [107]

newer systems differ from earlier ones in three important respects; (1) their higher operational frequencies, (2) their broader spectral occupancy, and (3) their pulsed (digital) mode of transmission. The intelligent deployment of these systems in vegetative environments requires a radiowave propagation model capable of describing (1) the attenuating characteristics of whatever propagation mechanism is likely to prove dominant at these higher frequencies, and (2) the time-variant, dispersive characteristics of the vegetation as it affects wideband, pulsed, transmission modes.

To support this requirement for enhanced propagation models, the Army has again embarked upon an ambitious research and development program, [164] but now directed toward the higher frequency bands (200 - 2000 MHz) and digital spread-spectrum modulation techniques typifying the modern electronic battlefield. Experimental aspects of this program have included wideband propagation measurements in the presence of forests [29], the derivation of empirical path-loss propagation models [45], and, most recently, the development of sophisticated, microprocessor-controlled, spread-spectrum, mobile radio measurement equipment. Complementary theoretical aspects of the program are described in this report.

Prior to the publication of this report, there had been no theoretically-based radiowave propagation model for vegetative environments suitable for frequencies in the band 200 - 2000 MHz and capable of describing not only transmission path attenuation but also pulse distortion. The Tamir model is valid primarily below 200 MHz and, further, considers only the propagation of an unmodulated, time-harmonic wave; no attempt is made to examine the effect of frequency-dispersive multipath on pulsed signals. Recently, Brown and Curry [25] have developed a UHF vegetative model for airborne, synthetic aperture radars operating near grazing incidence. Their model, however, neglects the effects of leaves and, further, does not consider the lateral wave found to be so important by Tamir.

1.2 Technical Approach

The forest is considered to be a discrete random medium representable as a time-invariant ensemble of randomly positioned and oriented discrete canonical scatterers. Tree trunks are modelled as infinitely-long, circular, dielectric cylinders; branches as finitely-long, circular dielectric cylinders; and leaves as flat, circular dielectric discs. The electromagnetic wave propagating within this medium is representable as the sum of two components: a mean field component and a residual random (or fluctuating) field component. The scatterers are assumed to be characterized by either their transition operator or their scattering amplitudes. Using a discrete scattering model originally proposed by Foldy [53] and later extended by Twersky, [64] Lax, [55a] Lang [57] and others, equations are derived which describe the behavior of the mean field and the space-frequency correlation function of the random field.

In this report, attention is concentrated on the behavior of the mean field.* It is shown that with regard to this component, the ensemble of discrete scatterers can be represented by an equivalent continuous medium characterized by an effective dyadic permittivity which can, in turn, be related directly to the size, shape, orientation, number density and permittivity of the scatterers themselves. This equivalent medium is then used to determine the wave propagating within an unbounded forest, and to define an anisotropic forest slab model analogous to the isotropic slab model introduced by Sachs and Wyatt [101] and studied by Tamir [107].

The electromagnetic fields scattered from the tree trunks, branches, and leaves are assumed to be linearly related to the mutually-induced currents excited within them by the propagating radio wave. As a consequence, the forest transmission channel between the transmitter and receiver can be considered linear, and Fourier spectral techniques employed to extend the time-harmonic forest slab model to encompass arbitrarily-modulated transmissions.

---

*Chapter 7 shows the importance of the random or noncoherent field.

1.3 Scope

This report uses a stochastic model for describing the behavior of radiowaves propagating through forests or other vegetated regions. The discrete scattering theory supporting the model is developed in Sections 2 and 3. In Section 4, the forest is represented (at least so far as the mean scattered field is concerned) by an equivalent continuous medium, and characterized by an effective dyadic permittivity which is directly related to the biophysical parameters of the forest. Also in Section 4, expressions for the specific attenuation are developed, and evaluated for typical biophysical parameters of a deciduous, hardwood forest. In Section 5, an anisotropic forest slab model is introduced and the relative contributions of the different propagation modes (direct wave, reflected wave, and lateral wave) assessed. The anisotropic forest slab model is applied in Section 6 to accommodate arbitrarily-modulated waveforms; numerical results are presented for the case of a broadband r-f pulse. Section 7 considers the relative importance of the random (fluctuating) field.

Although the model described herein can accommodate transmitting and receiving antennas of arbitrary directivity and polarization, this initial study emphasizes vertically-polarized, electrically-short, linear antennas. Further, although Doppler effects due either to wind-induced tree motion and/or terminal (antenna) motion can also be accommodated by the model, they are disregarded here. Finally, although the validity of the model is supported tentatively by comparison with measurements, this will be pursued further as the model is developed and additional experimental data become available.

2.0 Radiowave Propagation in Discrete Random Media

The basic methodology for describing radiowave propagation through the forest is formulated in this section. Because of the complexity of vegetation, stochastic or random methods are used rather than deterministic techniques. The forest is viewed as a random ensemble of trunks, branches and leaves. Equations are then developed for the mean and correlation of the electromagnetic fields. From these averages, physical quantities such as attenuation, propagation delay and pulse dispersion are obtained.

2.1 Representation of Scattered Electromagnetic Fields

The stochastic approach takes the viewpoint that the field quantities are composed of a mean component and a random (or fluctuating) component. If ψ represents an electromagnetic field quantity such as E or H, it is in general a function of the location and orientation of the vegetative components. Since these are randomly located and oriented, the field quantity ψ is a random variable. As such, it can be broken up into a mean component, $\langle\psi\rangle$, and a fluctuating component, $\tilde{\psi}$, i.e.

$$\psi = \langle\psi\rangle + \tilde{\psi} \qquad (2\text{-}1\text{-}1)$$

Here the brackets, < >, have been used to denote an ensemble average. Taking the average of Equation (2-1-1) shows that $\langle\tilde{\psi}\rangle = 0$, a reasonable result since the mean has already been extracted from ψ.

The correlation function of ψ (see Section 2.2.4) can be determined by multiplying ψ and its complex conjugate ψ^* and averaging over the ensemble. By using Equation (2-1-1) and the fact that the average fluctuations are zero, the correlation function of ψ can be written as

$$\langle\psi\psi^*\rangle = \langle\psi\rangle\langle\psi^*\rangle + \langle\tilde{\psi}\tilde{\psi}^*\rangle$$

Here the correlation is broken up into two components: a mean part, $\langle\psi\rangle\ \langle\psi^*\rangle$, and a fluctuating component $\langle\psi\psi^*\rangle$. When absorption is important than scattering, the fluctuating component is small. This is typically the case when the wavelength is large compared

to the size of the scatterers. In this regime, the correlation can be approximated by

$$\langle \psi \psi^* \rangle \approx \langle \psi \rangle \langle \psi^* \rangle \qquad (2\text{-}1\text{-}3)$$

It is this approximation that is inherent in early attempts at forest modeling [92, 93, 100, 101, 106, 107, 108]. The forest was replaced by a dielectric slab and, in effect, mean fields were computed.

The development of equations for the mean and correlation can be approached in two different ways. They are the continuous and discrete modeling procedures. The continuous approach uses the mean and correlation of the effective forest permittivity as input information to the model. The discrete approach, on the other hand, uses the scattering amplitudes of individual scatterers, as well as the position and orientation statistics of scatterers. Examples of modeling by the continuous approach are provided by Keller [56], Besieris and Kohler [49] and Tsang and Kong [62], while the discrete approach has been used by Twersky [63, 64], Ishimaru [54, 55] and Lang [57, 58]. The continuous modeling approach tends to be somewhat simpler than the discrete method. This is due to the need for scattering amplitudes of individual scatterers in the discrete method. The discrete technique, however, provides a closer connection with reality. Individual scatterer sizes and dielectric constants can be measured; the effective dielectric permittivity and its correlation, as required by the continuous approach, are difficult quantities to determine.

For the discrete case, an approximate equation for the mean field was obtained by Foldy [53] for dipole scatterers and later by Lax [55a] for resonant-size scatterers. The mean equation is valid when the fractional volume of vegetation is small. This criterion appears to be satisfied within most forests (see Section 4.3). Twersky [63] subsequently derived an approximate equation for the correlation which again is valid when the fractional volume is small. It is these basic equations that will be used to obtain the macroscopic effects of vegetation on radiowave propagation.

2.2 Two-Dimensional Scattering Media

Scattering by an aggregate of parallel dielectric cylinders is considered in this section. Because of the planar symmetry of the problem, scalar rather than vector equations can be used. This substantially simplifies the analysis and thus makes the derivation of the mean and correlation equations more transparent. In addition, the problem provides a good model for a forest consisting wholly of trunks or one in which trunks have the dominant effect on the channel properties.

2.2.1 Model Formulation

Consider a collection of N identical parallel dielectric cylinders each having complex relative permittivity ε_p and cross-sectional surface area S_p. These scatterers are shown in Figure 2-1. In this figure a cross-sectional view of the forested region is shown. The forest is totally contained within the area S.

Analysis of the problem begins by considering Maxwell's time-harmonic equations (with an $\exp\{j\omega t\}$ time dependence assumed)

$$\begin{aligned} \nabla \times \underline{E} &= -j\omega\mu_o \underline{H} \\ \nabla \times \underline{H} &= j\omega\varepsilon_o \varepsilon(\underline{x}_t)\underline{E} + \underline{J}_s \end{aligned} \tag{2-2-1}$$

where μ_o and ε_o are the permeability and permittivity, respectively, of free space, ω is the angular frequency, and

$$\varepsilon(\underline{x}_t) = 1 + \sum_{j=1}^{N} \chi_j(\underline{x}_t) \tag{2-2-2}$$

is the relative permittivity of the scatterers as a function of transverse vector position $\underline{x}_t$. The susceptibility function $\chi_j(\underline{x}_t)$ represents the susceptibility of the j^{th} scatterer as a function of position. It is given by

$$\chi_j(\underline{x}_t) = \begin{cases} \chi_\ell \ , & \underline{x}_t \ \text{inside } j^{th} \text{ scatterer} \\ 0 \ , & \underline{x}_t \ \text{outside } j^{th} \text{ scatterer} \end{cases} \tag{2-2-3}$$

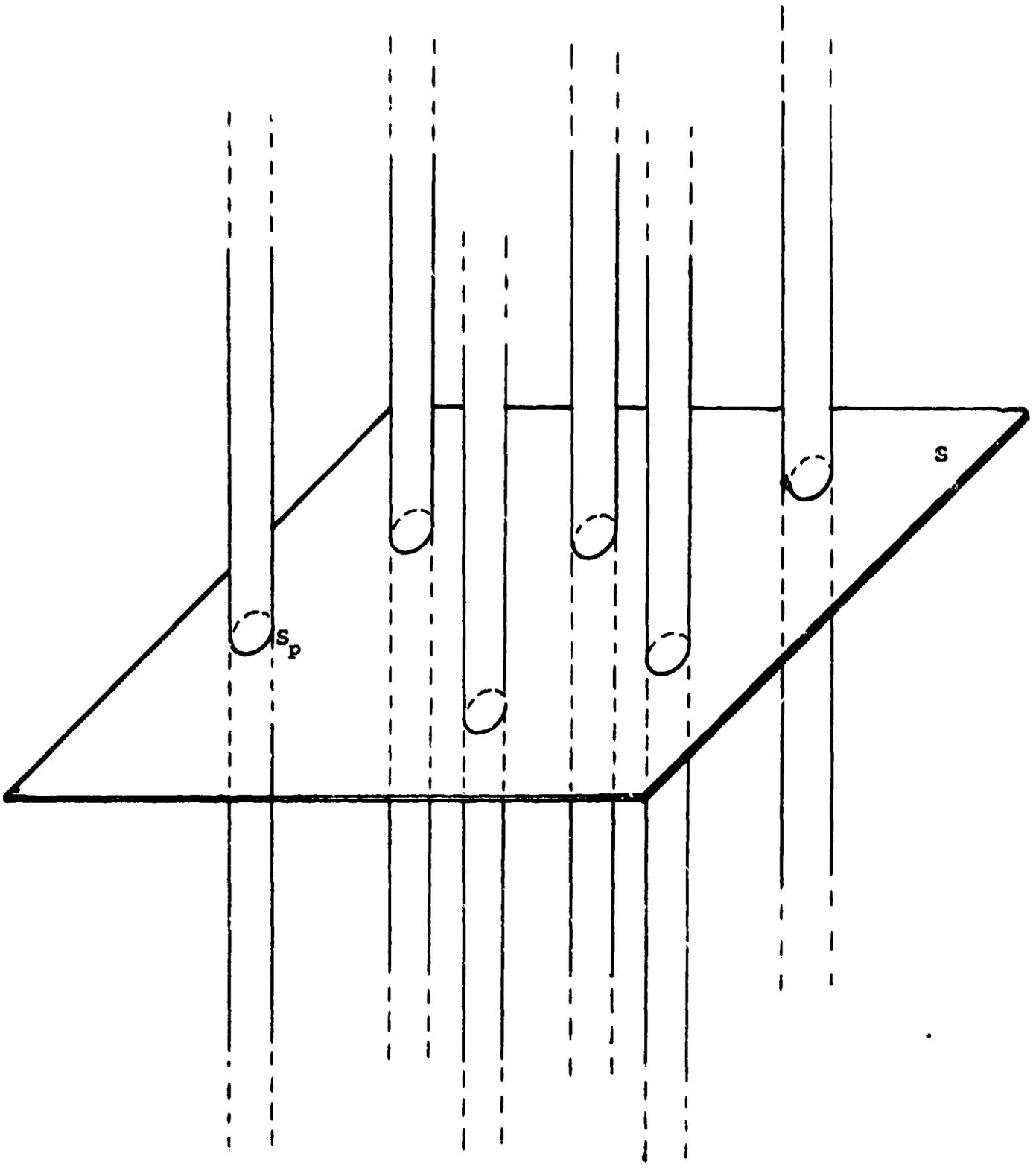

Figure 2-1: Two-Dimensional Ensemble of Scatterers

Here χ_ℓ is the susceptibility of a scatterer, which is related to ϵ_p by $\chi_\ell = \epsilon_p - 1$.

To reduce the vector field problem to a scalar field problem, the current $\underline{J}_s$ is assumed to have the following form

$$\underline{J}_s = J_z(\underline{x}_t)\underline{z}^\circ \quad * \tag{2-2-4}$$

It has been tacitly assumed in writing Equation (2-2-4) that the scatterers are parallel to the z-axis. The electromagnetic fields are decomposed into transverse and z-directed components so that

$$\begin{aligned} \underline{E} &= \underline{E}_t + E_z\underline{z}^\circ \\ \underline{H} &= \underline{H}_t + H_z\underline{z}^\circ \end{aligned} \tag{2-2-5}$$

Substitution of Equations (2-2-4) and (2-2-5) into Equation (2-2-1) reveals that E_z and $\underline{H}_t$ are the only field components excited, and that they satisfy

$$[\nabla_t^2 + k_o^2\epsilon(\underline{x}_t)]E_z(\underline{x}_t) = j\omega\mu_o J_z(\underline{x}_t) \tag{2-2-6}$$

Here ∇_t is the transverse del operator and $k_o^2 = \omega^2\mu_o\epsilon_o$. The problem has been scalarized. As a result, the complete field behavior can be obtained from the scalar field E_z.

It is convenient at this point to introduce an operator notation. This notation will highlight the important aspects of the development while suppressing unimportant details. It will also make the parallelism that exists between the scalar and vector models more apparent. The operator notation is introduced by defining the following quantities:

$$L = -(\nabla_t^2 + k_o^2) \qquad V_j = k_o^2\chi_j(\underline{x}_t) \tag{2-2-8}$$

$$\Psi = E_z \qquad g = -j\omega\mu_o J_z \tag{2-2-9}$$

By using this notation in Equation (2-2-6) the wave equation can be written as

$$\left(L - \sum_{j=1}^{N} V_j\right)\Psi = g \tag{2-2-10}$$

---

*$\underline{z}^\circ$ is a unit vector in the $\underline{z}$ direction.

For later use, the field Ψ can be decomposed into incident and scattered parts. This is written as

$$\Psi = \Psi_i + \Psi_s \tag{2-2-11}$$

where Ψ_i is the incident wave and Ψ_s is the scattered wave. The incident field Ψ_i is the field that would exist if the scatterers were not present, thus

$$L\Psi_i = g \tag{2-2-12}$$

2.2.2 Single-Scatterer Characterization

Before the N-particle problem can be addressed the single scatterer must be characterized electromagnetically. For this purpose, the transition operator and scattering amplitude are introduced in this section.

Consider a single scatterer located at the origin as shown in Figure 2-2. The electric field satisfies the wave equation given by Equation (2-2-10) with N=1. This equation is

$$(L - V)\psi = g \tag{2-2-13}$$

where

$$V = k_o^2 X(\underline{x}_t) \tag{2-2-14}$$

with

$$\psi = e_z \qquad g = -j\omega\mu_o J_z \tag{2-2-15}$$

and

$$X(\underline{x}_t) = \begin{cases} \chi_\ell \ , \ \underline{x}_t & \text{inside } S_p \\ 0 \ , \ \underline{x}_t & \text{outside } S_p \end{cases} \tag{2-2-16}$$

Lower-case notation has been employed for the field as a reminder that only one scatterer is being considered.

The transition operator will now be introduced. This operator relates the induced sources within the scatterer to the incident field upon the scatterer. To develop this relation, the field is separated into incident and scattered components so that

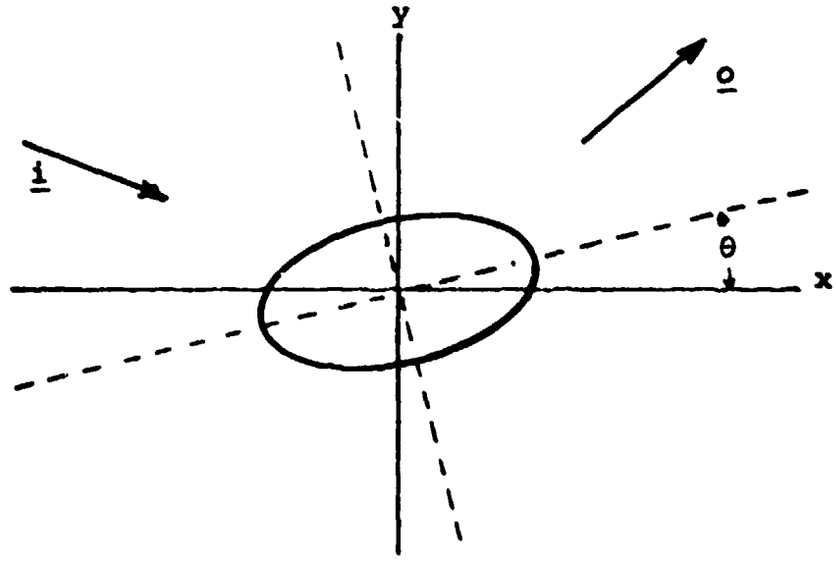

Figure 2-2: Single Scatterer Geometry (Cross-Section)

$$\psi = \psi_i + \psi_s \quad , \quad L\psi_i = g \tag{2-2-17}$$

Substitution of Equation (2-2-17) into Equation (2-2-13) gives the equation for the scattered field, viz.

$$L\psi_s = g_{eq} \quad , \quad g_{eq} = V\psi \tag{2-2-18}$$

The equivalent sources that generate the scattered field, g_{eq}, are given by $V\psi$. The transition operator T can now be defined as

$$g_{eq} = T\psi_i \tag{2-2-19}$$

From the above equation, it is seen that once the incident field is specified, the induced sources can be calculated if T is known. Since bounded ψ_i yields bounded induced source distributions, this implies that T is a bounded operator. As a result, T can be represented in integral form as

$$g_{eq}(\underline{x}_t) = \int d\underline{x}_t' \, t(\underline{x}_t, \underline{x}_t') \psi_i(\underline{x}_t') \tag{2-2-20}$$

The kernel $t(\underline{x}_t, \underline{x}_t')$ is analogous to the time-varying impulse response $h(t,\tau)$. One can show that $t(\underline{x}_t, \underline{x}_t') = 0$ for $\underline{x}_t$ or $\underline{x}_t'$ outside of S_p. This just means that the equivalent sources are located within the boundaries of the scatterer.

In the low-frequency case, where the wavelength is large compared to the characteristic size of the scatterer's cross-section, the equivalent source distribution looks like a line current. In this case, the transition operator's kernel can be written as

$$t(\underline{x}_t, \underline{x}_t') = k_o^2 \alpha \delta(\underline{x}_t) \delta(\underline{x}_t') \tag{2-2-21}$$

The introduction of the coefficient α is motivated by three-dimensional scatterers for which α is the polarizability [57].

The scatterer can be characterized in an alternative manner by specifying its far-field response to a unit-amplitude incident plane wave. If the incident plane wave is given by

$$\psi_i(\underline{x}_t) = \exp\{-jk_o \underline{i} \cdot \underline{x}_t\} \tag{2-2-22}$$

then the scattered field in the radiation zone has the form

$$\psi_s(\underline{x}_t) = f(\underline{o},\underline{i}) \cdot \frac{\exp\{-jk_o x_t\}}{\sqrt{x_t}} \quad , \quad x_t = |\underline{x}_t| \qquad (2\text{-}2\text{-}23)$$

where $\underline{i}$ and $\underline{o}$ ($= \underline{x}_t/x_t$) are unit vectors in the direction of the incident wave and the observation point respectively as is shown in Figure 2-2. Equation (2-2-23) serves as a defining equation for the scattering amplitude, $f(\underline{o},\underline{i})$.

The scattering amplitude and the transition operator are related to each other. The relationship is

$$f(\underline{o},\underline{i}) = \gamma \tilde{t}(k_o\underline{o},k_o\underline{i}) \quad , \quad \gamma = \frac{2\pi^3}{k_o} e^{-j\pi/4} \qquad (2\text{-}2\text{-}24)$$

where $\tilde{t}(\underline{k}_t,\underline{k}_t')$ is the Fourier transform of $t(\underline{x}_t,\underline{x}_t')$ with respect to $\underline{x}_t$ and $\underline{x}_t'$, i.e.,

$$\tilde{t}(\underline{k}_t,\underline{k}_t') = (2\pi)^{-2} \int d\underline{x}_t d\underline{x}_t' \, t(\underline{x}_t,\underline{x}_t') e^{j(\underline{k}_t\cdot\underline{x}_t - \underline{k}_t'\cdot\underline{x}_t')} \qquad (2\text{-}2\text{-}25)$$

The relationship between f and t is derived in Appendix B.

In developing the multiple-scattering equations the transition operator for a scatterer not located at the origin will be needed. Denote the transition operator kernel for the j^{th} scatterer by $t_j(\underline{x}_t,\underline{x}_t')$. It can be related to the transition operator of the scatterer located at the origin. If the j^{th} scatterer's center is located at $\underline{X}_{tj}$ where $\underline{X}_{tj}$ is measured from the origin, then by a simple shift of the incident field and the induced charge, one finds

$$t_j(\underline{x}_t,\underline{x}_t') = t(\underline{x}_t-\underline{X}_{tj},\underline{x}_t'-\underline{X}_{tj}) \qquad (2\text{-}2\text{-}26)$$

Here $t(\underline{x}_t,\underline{x}_t')$ is the transition kernel for a scatterer located at the origin. It should be noted here t is a function of θ_j - the orientation angle of the j^{th} scatterer.

2.2.3 Mean-Wave Equation

An approximate equation for the mean field can be derived using the Foldy-Lax method [57]. This method is valid in the case of small fractional volume.

Consider the total field Ψ at some point $\underline{x}_t$ to consist of the incident field, Ψ_i, and the various scattered fields from the individual particles, i.e.

$$\Psi = \Psi_i + \sum_{j=1}^{N} \Psi_s^{(j)} \quad , \quad L\Psi_i = g \tag{2-2-27}$$

where $\Psi_s^{(j)}$ is the scattered field from the j^{th} particle. The transition operator for the j^{th} particle can then be used to relate the j^{th} scattered field to the incident field on the j^{th} particle. This is expressed mathematically as

$$L\Psi_s^{(j)} = g_{eq}^{(j)} = T_j \Psi^{(j)} \tag{2-2-28}$$

where T_j is the transition operator for the j^{th} particle and $\Psi^{(j)}$ is the field at the location of j^{th} particle with the j^{th} particle removed. Substituting Equation (2-2-28) into Equation (2-2-27) and multiplying from the left by L, gives the following equation

$$L\Psi = g + \sum_{j=1}^{N} T_j \Psi^{(j)} \tag{2-2-29}$$

Averaging the above equation over the ensemble of scatterer configurations yields

$$L\langle\Psi\rangle = g + \sum_{j=1}^{N} \langle T_j \Psi^{(j)} \rangle \tag{2-2-30}$$

where the fact that L is deterministic has been used. To obtain an equation for the mean field $\langle\Psi\rangle$, the Foldy-Lax approximation

$$\Psi^{(j)} = \langle\Psi\rangle_j \tag{2-2-31}$$

is introduced. This says that the field incident upon the j^{th} scatterer is approximately equal to the mean field at the j^{th} scatterer. It can be shown by scaling techniques that this approximation is valid when the fractional volume occupied by the scatterers is small. Using this approximation

$$\langle T_j \Psi^{(j)} \rangle \approx \langle T_j \langle\Psi\rangle \rangle = \langle T_j \rangle \langle\Psi\rangle_j \tag{2-2-32}$$

Putting this approximation into Equation (2-2-30) yields the following equation for the mean field

$$L\langle\Psi\rangle - \sum\langle T_j\rangle\langle\Psi\rangle_j = g \qquad (2\text{-}2\text{-}33)$$

The equation for the mean field can be simplified by explicitly writing out $\langle T_j\rangle$ and assuming that all particles are identically distributed in location and orientation. Doing this, the expression for $\langle T_j\rangle$ becomes

$$\langle T_j\rangle = \int_S d\underline{s}_t \int_0^{2\pi} d\theta p(\underline{s}_t,\theta) T_j(\underline{s}_t,\theta) \qquad (2\text{-}2\text{-}34)$$

where $p(\underline{s}_t,\theta)d\underline{s}_t d\theta$ is the joint probability that the position vector $\underline{X}_t$ will take on a value close to $\underline{s}_t$ and simultaneously the orientation angle θ will take on a value close to θ. Note that the average is identical for all particles since the probability density is independent of j.

Before proceeding, Equation (2-2-34) can be written in a somewhat more convenient form by suppressing the orientation average and writing

$$\langle T_j\rangle = \int_S d\underline{s}_t p(\underline{s}_t)\bar{T}_j(\underline{s}_t) \qquad (2\text{-}2\text{-}35)$$

where $\bar{T}(\underline{s}_t)$, the orientation average over θ at a particular $\underline{s}_t$, is given by

$$\bar{T}(\underline{s}_t) = \int_0^{2\pi} d\theta p(\theta|\underline{s}_t) T(\underline{s}_t,\theta) \qquad (2\text{-}2\text{-}36)$$

A simplified equation for the mean can now be written. Using Equation (2-2-35) in Equation (2-2-33) and noting that the terms of the sum are identical gives

$$L\langle\Psi\rangle - \int_S d\underline{s}_t \rho(\underline{s}_t)\bar{T}(\underline{s}_t)\langle\Psi\rangle = g \qquad (2\text{-}2\text{-}37)$$

where the number density of the scatterers $\rho(\underline{s}_t)$ is just

$$\rho(\underline{s}_t) = Np(\underline{s}_t) \qquad (2\text{-}2\text{-}38)$$

The notation in this equation can be simplified by defining the mean wave operator $\mathcal{L}$

$$\mathcal{L} = L - \int_S d\underline{s}_t \rho(\underline{s}_t)\bar{T}(\underline{s}_t) \qquad (2\text{-}2\text{-}39)$$

Equation (2-2-37) then becomes

$$\mathcal{L}\langle\Psi\rangle = g \qquad (2\text{-}2\text{-}40)$$

The mean equation as given above is in its most compact form. For later use, it will prove expedient to write it in the more explicit form

$$(\nabla_t^2+k_o^2)\langle\Psi(\underline{x}_t)\rangle+\int_S d\underline{s}_t \rho(\underline{s}_t)\int d\underline{x}_t' t(\underline{x}_t-\underline{s}_t,\underline{x}_t'-\underline{s}_t)\langle\Psi(\underline{x}_t')\rangle=-g(\underline{x}_t) \qquad (2\text{-}2\text{-}41)$$

This equation is an integro-differential equation; however, it is deterministic and not random. Further, the equation substantially simplifies in the case of dipole scatterers as may be seen by substituting Equation (2-2-21) into Equation (2-2-41) to obtain

$$[\nabla_t^2+k_o^2(1+\rho(\underline{x}_t)\alpha]\langle\Psi(\underline{x}_t)\rangle = -g(\underline{x}_t) \qquad (2\text{-}2\text{-}42)$$

where it is understood that $\rho(\underline{x}_t) = 0$ for $\underline{x}_t$ outside of S. This simplification is possible, however, only at low frequencies (large wave lengths) where the incident field is essentially constant over the scatterer. Since this low-frequency approximation involves the assumption that the incident wavelength must be large compared to the size of the scatterers, scattering from resonant-size scatterers must be treated by the more general mean Equation (2-2-41).

2.2.4 Space-Frequency Correlation Function

A basic quantity of interest for characterizing such communications channels as the forest medium is the space-frequency correlation function of the scatterer field, $\langle\psi(\underline{x}_t,\omega)\psi^*(\hat{\underline{x}}_t,\hat{\omega})$. This is the ensemble average of a field component at $\underline{x}_t$ and angular frequency ω times the conjugate of the field component evaluated at $\hat{\underline{x}}_t$ and $\hat{\omega}$. At a fixed point ($\underline{x}_t=\hat{\underline{x}}_t$), the resulting frequency

correlation function indicates the effective bandwidth, and its Fourier transform gives the delay spread. At a fixed frequency ($\omega=\hat{\omega}$), the width of the space correlation function indicates the minimum separation required for efficient space diversity.

In Section 2.1, it was pointed out that if the medium was mostly absorptive in nature rather than scattering, the space-frequency correlation function can be obtained as in Equation (2-1-3) by way of the mean field as follows

$$\langle\Psi(\underline{x}_t,\omega)\Psi^*(\hat{\underline{x}}_t,\hat{\omega})\rangle \approx \langle\Psi(\underline{x}_t,\omega)\rangle\langle\Psi^*(\hat{\underline{x}}_t,\hat{\omega})\rangle \qquad (2\text{-}2\text{-}43)$$

In general, however, as the frequency increases, scattering becomes more important and Equation (2-2-43) no longer holds. The correlation of the field must then be obtained from first principles as in the case of the mean.

An equation for the correlation can be obtained by paralleling the development of the mean wave equation. The equation must again be derived under the assumption of small fractional volume. However, there is no restriction on the absorptive or scattering properties of the particles. Because of the amount of technical detail involved, the derivation of this equation has been relegated to Appendix C.

The correlation equation obtained in Appendix C is

$$ff^*\langle\Psi\Psi^*\rangle - \int_s d\underline{s}_t\rho(\underline{s}_t)\overline{T(\underline{s}_t)T^*(\underline{s}_t)}\langle\Psi\Psi^*\rangle = gg^* \qquad (2\text{-}2\text{-}44)$$

where

$$\overline{T(\underline{s}_t)T^*(\underline{s}_t)} = \int_0^{2\pi} d\theta p(\theta|\underline{s}_t)T_j(\underline{s}_t,\theta)T_j^*(\underline{s}_t,\theta) \qquad (2\text{-}2\text{-}45)$$

Note that, as in Equation (2-2-43), the unstarred and starred quantities are functions of unhatted and hatted quantities, respectively. The mean operator f is given in Equation (2-2-39). The correlation equation can be put in a slightly different form by multiplying from the left by $f^{-1}f^{*-1}$ where the inverse mean operator f^{-1} is given by

$$\mathcal{L}^{-1}\psi(\underline{x}_t) = \int d\underline{x}_t' G(\underline{x}_t, \underline{x}_t')\psi(\underline{x}_t') \tag{2-2-46}$$

and the kernel of the integral operator is the mean Green's function which satisfies

$$\mathcal{L}G(\underline{x}_t, \underline{x}_t') = \delta(\underline{x}_t - \underline{x}_t') \tag{2-2-47}$$

The result is

$$\langle\Psi\Psi^*\rangle = \langle\Psi\rangle\langle\Psi^*\rangle - \mathcal{L}^{-1}\mathcal{L}^{*-1}\int_S d\underline{s}_t \rho(\underline{s}_t)T(\underline{s}_t)T^*(\underline{s}_t)\langle\Psi\Psi^*\rangle \tag{2-2-48}$$

This is equivalent to the correlation equation given by Ishimaru [55], although his equation is given for the three-dimensional scalar case.

As in the case of the mean, Equation (2-2-46) will now be written out more explicitly

$$\begin{aligned}\langle\Psi(\underline{x}_t)\Psi^*(\hat{\underline{x}}_t)\rangle &= \langle\Psi(\underline{x}_t)\rangle\langle\Psi^*(\hat{\underline{x}}_t)\rangle \\ &- \int d\underline{x}_t' d\underline{x}_t'' d\hat{\underline{x}}_t' d\hat{\underline{x}}_t'' d\underline{s}_t \rho(\underline{s}_t) G(\underline{x}_t, \underline{x}_t') G^*(\hat{\underline{x}}_t, \hat{\underline{x}}_t') \\ &\cdot t(\underline{x}_t' - \underline{s}_t, \underline{x}_t'' - \underline{s}_t) t^*(\hat{\underline{x}}_t' - \underline{s}_t, \hat{\underline{x}}_t'' - \underline{s}_t) \cdot \langle\Psi(\underline{x}_t'')\Psi(\hat{\underline{x}}_t'')\rangle\end{aligned} \tag{2-2-49}$$

In the above equation it has been assumed that $\omega = \hat{\omega}$ and then this variable has been suppressed.

As in the case of the mean-wave equation, when the frequency is low, the correlation Equation (2-2-49) can be substantially simplified. By using Equation (2-2-21) in Equation (2-2-49), it is found that

$$\begin{aligned}\langle\Psi(\underline{x}_t)\Psi^*(\hat{\underline{x}}_t)\rangle &= \langle\Psi(\underline{x}_t)\rangle\langle\Psi^*(\underline{x}_t')\rangle \\ &- k_o^4|\alpha|^2 \int_S d\underline{s}_t \rho(\underline{s}_t) G(\underline{x}_t, \underline{s}_t) G^*(\hat{\underline{x}}_t, \underline{s}_t) \cdot \langle\Psi(\underline{s}_t)\Psi^*(\underline{s}_t)\rangle\end{aligned} \tag{2-2-50}$$

The solution to this equation will be found in Chapter 7 for an unbounded medium ($S = \infty$) with constant density ρ and $\underline{x}_t = \hat{\underline{x}}_t$

2.3 Three-Dimensional Scattering Media

2.3.1 Model Formulation

In the preceding section, equations were derived for the mean and correlation of the field in a medium of two-dimensional scatterers. Attention will now be focused on ensembles of three-dimensional scatterers. These scatterers will be used to model leaves and branches. Because of the three-dimensional character of the scatterers, the problem can no longer be scalarized, thus the vector wave equation must be used.

The configuration of scatterers to be discussed is shown in Figure 2-3. There are N identical, nonaligned scatterers contained within volume V. Each scatterer has volume V_p and relative dielectric constant ε_p. A deterministic background medium is also assumed to be present. The relative permittivity of the composite medium is given by

$$\varepsilon(\underline{x}) = \varepsilon_b(\underline{x}) + \sum_{j=1}^{N} \chi_j(\underline{x}) \qquad (2\text{-}3\text{-}1)$$

where $\varepsilon_b(\underline{x})$ is the relative permittivity of the background medium which is assumed to be unity inside V and arbitrary outside V, i.e.

$$\varepsilon_b(\underline{x}) = \begin{cases} 1 & , \ \underline{x} \text{ inside V} \\ \varepsilon_b(\underline{x}) & , \ \underline{x} \text{ outside V} \end{cases} \qquad (2\text{-}3\text{-}2)$$

By appropriately choosing V and $\varepsilon_b(\underline{x})$, a half-space or slab configuration of scatterers can be constructed. In addition, the ground can be accounted for through the background medium. The $\chi_j(\underline{x})$ used in Equation (2-3-1) is the susceptibility of the j^{th} scatterer. It can be written as

$$\chi_j(\underline{x}) = \begin{cases} \chi_\ell & , \ \underline{x} \text{ inside } j^{th} \text{ scatterer} \\ 0 & , \ \underline{x} \text{ outside } j^{th} \text{ scatterer} \end{cases} \qquad (2\text{-}3\text{-}3)$$

Here, as in the case of the two-dimensional scatterers, χ_ℓ is the bulk susceptibility of the scatterer material.

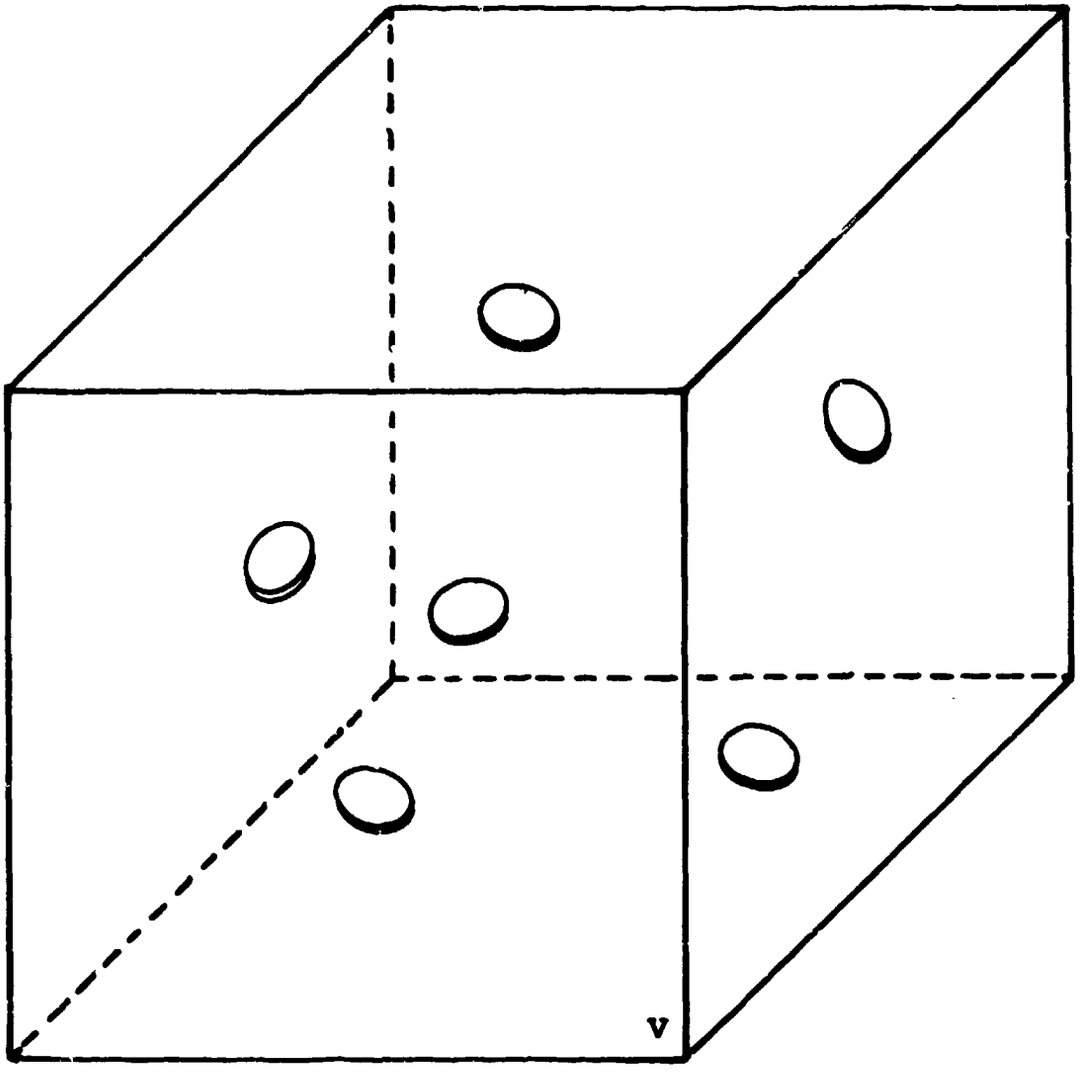

Figure 2-3: Three-Dimensional Ensemble of Scatterers

A vector wave equation for the electric field can be obtained by using Equation (2-3-1) in Maxwell's equations as given by Equation (2-2-1). The resulting equation is

$$\nabla x \nabla x \underline{E} - k_o^2 \varepsilon_b(\underline{x}) \underline{E} - \sum_{j=1}^{N} k_o^2 \chi_j(\underline{x}) \underline{E} = -j\omega\mu_o \underline{J} \qquad (2\text{-}3\text{-}4)$$

An operator notation is again introduced. By using the following notation

$$\underline{\underline{L}} = \nabla x (\nabla x \underline{\underline{I}}) - k_o^2 \varepsilon_b(\underline{x}) \underline{\underline{I}} \qquad (2\text{-}3\text{-}5)$$

$$\underline{\underline{V}}_j = k_o^2 \chi_j(\underline{x}) \underline{\underline{I}} \qquad (2\text{-}3\text{-}6)$$

$$\underline{\Psi} = \underline{E} \qquad \underline{g} = -j\omega\mu_o \underline{J} \qquad (2\text{-}3\text{-}7)$$

Equation (2-3-4) can be written as

$$(\underline{\underline{L}} - \sum_j \underline{\underline{V}}_j) \cdot \underline{\Psi} = \underline{g} \qquad (2\text{-}3\text{-}8)$$

The double underlined notation is used to signify a dyadic; thus $\underline{\underline{L}}$ and $\underline{\underline{V}}_j$ are dyadic operators. The unit dyadic $\underline{\underline{I}}$ has been introduced in the definition of $\underline{\underline{L}}$ and $\underline{\underline{V}}_j$. As its name indicates, it has the property that $\underline{\underline{I}} \cdot \underline{\Psi} = \underline{\Psi} \cdot \underline{\underline{I}} = \underline{\Psi}$ [see Appendix D]. This property is used to reduce the abstract form of the vector equation as given in Equation (2-3-8) to the standard form as given in Equation (2-3-4).

One of the principal advantages of the abstract operator notation is now evident. A comparison of the vector wave equation as given by Equation (2-3-8) with the two-dimensional scalar wave equation as given by Equation (2-2-10) shows that the two equations have basically the same form. Thus derivations carried out in the vector case will parallel those already performed in the scalar case.

2.3.2 Single-Scattering Problem

Before a mean equation can be derived for the field, the scatterers must be electromagnetically characterized. The dyadic transition operator and the dyadic scattering amplitude can be

used for this purpose. The development in this subsection parallels the development for the scalar two-dimensional problem as given in 2.2.2.

Consider a three-dimensional scatterer located at the origin. The electric field $\underline{\psi}$ satisfies the equation

$$(\underline{L} - \underline{V}) \cdot \underline{\psi} = \underline{g} \tag{2-3-9}$$

where

$$\underline{V} = k_o^2 X(\underline{x}) \underline{I} \tag{2-3-10}$$

and $\underline{L}$, $\underline{g}$ are defined in Equations (2-3-5) and (2-3-7) respectively. Here, as before, $X(\underline{x})$ is X_ℓ inside the scatterer and zero outside the scatterer. The orientation of the scatterer as specified by the polar angle θ and the azimuth angle ϕ is contained implicitly in the definition of $X(\underline{x})$, i.e., $X(\underline{x}) = X(\underline{x},\theta,\phi)$.

To define the transition operator, the field is broken up into a free-space component $\underline{\psi}_i$ and a scattered component $\underline{\psi}_s$ so that

$$\underline{\psi} = \underline{\psi}_i + \underline{\psi}_s \tag{2-3-11}$$

where $\underline{L} \cdot \underline{\psi}_i = g$ and $\underline{L} \cdot \underline{\psi}_s = \underline{V}\,\underline{\psi}$. Here as in the scalar case, $\underline{V} \cdot \underline{\psi}$ can be viewed as equivalent sources $\underline{g}_{eq}$ that create the scattered field. The dyadic transition operator can now be introduced. This operator acts on the incident field to produce the equivalent sources; thus

$$\underline{g}_{eq} = \underline{T} \cdot \underline{\psi}_i \tag{2-3-12}$$

Since the relationship is linear and bounded, Equation (2-3-12) can be written explicitly as

$$\underline{g}_{eq}(\underline{x}) = \int d\underline{x}' \underline{t}(\underline{x},\underline{x}') \cdot \underline{\psi}_i(x') \tag{2-3-13}$$

where $\underline{t}(\underline{x},\underline{x}')$ is called the transition operator kernel. The knowledge of $\underline{t}$ completely specifies the scattered field once the incident field is given.

The relationship between $\underline{\psi}_i$ and $\underline{g}_{eq}$ is substantially simplified in the low-frequency limit. In this limit the induced source distribution can be approximated by an electric dipole. Thus

$$\underline{q}_{eq} = -j\omega\mu_o \underline{J}_{eq} = -j\omega\mu_o [j\omega \underline{p}\delta(\underline{x})] \qquad (2\text{-}3\text{-}14)$$

where $\underline{p}$ is the electric dipole moment of the induced source distribution and $\delta(\underline{x})$ is the three-dimensional Dirac delta function. The dipole moment $\underline{p}$ can be directly related to the incident electric field $\underline{\psi}_i$ by the dyadic polarizability $\underline{\alpha}$. This relationship is

$$\underline{p} = \varepsilon_o \underline{\alpha} \cdot \underline{\psi}_o \qquad (2\text{-}3\text{-}15)$$

Comparing this equation with Equations (2-3-12) and (2-3-13) the transition operator and its kernel can be written as

$$\underline{T} = k_o^2 \underline{\alpha} \delta(\underline{x}) \qquad (2\text{-}3\text{-}16)$$

and

$$\underline{t}(\underline{x},\underline{x}') = k_o^2 \underline{\alpha} \delta(\underline{x}) \delta(\underline{x}') \qquad (2\text{-}3\text{-}17)$$

The far-field behavior of the scatterer's response to a plane wave can also be used to characterize the scatterer. Consider a plane wave

$$\underline{\psi}_i(\underline{x}) = \underline{q}_i^o e^{-jk_o \underline{i} \cdot \underline{x}} \qquad (2\text{-}3\text{-}18)$$

incident upon the scatterer. Here $\underline{q}_i^o$ is a unit polarization vector and $\underline{i}$ is a unit vector in the direction of propagation. The scattered field in the far-field zone of the scatterer is written as

$$\underline{\psi}_s(\underline{x}) \sim \underline{f}(\underline{o},\underline{i}) \cdot \underline{q}_i^o \frac{e^{-jk_o x}}{x}, \quad \underline{o} = \frac{\underline{x}}{|\underline{x}|} \qquad (2\text{-}3\text{-}19)$$

where $\underline{f}(\underline{o},\underline{i})$ is the dyadic scattering amplitude. Here $\underline{o}$ is a unit vector in the direction of observation and $x = |\underline{x}|$.

The scattering amplitude $\underline{f}$ can be understood more easily in terms of its components. To do this, incident and scattered polarization vectors need to be defined. An arbitrary incident polarization vector $\underline{q}_i^o$ can be decomposed into two orthogonal components; call them $\underline{h}_i^o$ and $\underline{v}^o{}_i$ indicating horizontal and vertical polarization, respectively. Similarly, the scattered field can be decomposed into two mutual orthogonal components $\underline{h}_s^o$ and $\underline{v}_s^o$. The notation has been employed that a superscript zero indicates a unit vector.

By using the unit polarization vectors introduced above the dyadic scattering amplitude can be written as

$$\underline{f} = f_{hh}\underline{h}_s^\circ\underline{h}_i^\circ + f_{hv}\underline{h}_s^\circ\underline{v}_i^\circ + f_{vh}\underline{v}_s^\circ\underline{h}_i^\circ + f_{vv}\underline{v}_s^\circ\underline{v}_i^\circ \qquad (2\text{-}3\text{-}20)$$

where the components f_{pq} are given by

$$f_{pq} = \underline{p}_s^\circ \cdot \underline{f} \cdot \underline{q}_i^\circ \quad , \quad p,q\varepsilon\{h,v\} \qquad (2\text{-}3\text{-}21)$$

Thus if the incident polarization is horizontal, $\underline{q}_i^\circ = \underline{h}_i^\circ$, the scattered far field will be

$$\underline{\psi}_s \sim (f_{hh}\underline{h}_s^\circ + f_{vh}\underline{v}_s^\circ)\frac{e^{-jk_\circ x}}{x} \qquad (2\text{-}3\text{-}22)$$

The dyadic scattering amplitude $\underline{f}$ can be directly related to the Fourier transform of the transition operator. This relationship is derived in Appendix A of Lang [57]. It is

$$\underline{f}(\underline{o},\underline{i}) = 2\pi^2(\underline{I}-\underline{o}\,\underline{o})\cdot\tilde{\underline{t}}(k_\circ\underline{o},k_\circ\underline{i})\cdot(\underline{I}-\underline{i}\,\underline{i}) \qquad (2\text{-}3\text{-}23)$$

where

$$\tilde{\underline{t}}(\underline{k},\underline{k}') = \frac{1}{(2\pi)^3}\int d\underline{x}d\underline{x}'\underline{t}(\underline{x},\underline{x}')e^{j(\underline{k}\cdot\underline{x}-\underline{k}'\cdot\underline{x}')} \qquad (2\text{-}3\text{-}24)$$

The relationship between $\underline{f}$ and $\underline{t}$ as given in Equation (2-3-23) is in dyadic form. By using the polarization unit vectors already defined, the unit dyadic can be decomposed as follows

$$\underline{I} = \underline{h}_s^\circ\underline{h}_s^\circ + \underline{v}_s^\circ\underline{v}_s^\circ + \underline{o}\,\underline{o}$$

or (2-3-25)

$$\underline{I} = \underline{h}_i^\circ\underline{h}_i^\circ + \underline{v}_i^\circ\underline{v}_i^\circ + \underline{i}\,\underline{i}$$

This is a result of the fact that I can be decomposed in the above form by any system of mutually orthogonal unit vectors. The scalar form of the relationship can be found by dotting Equation (2-3-22) from the right by $\underline{h}_i^\circ$ or $\underline{v}_i^\circ$ and by dotting from the left by $\underline{h}_s^\circ$ or $\underline{v}_s^\circ$ and then using Equation (2-3-25). The result is

$$f_{pq}(\underline{o},\underline{i}) = 2\pi^2\tilde{t}_{pq}(k_\circ\underline{o},k_\circ\underline{i}) \quad , \quad p,q\varepsilon\{h,v\} \qquad (2\text{-}3\text{-}26)$$

where $\tilde{t}_{pq} = \underline{p}_s^\circ\cdot\tilde{\underline{t}}\cdot\underline{q}_i^\circ$.

Both the transition operator and scattering amplitude forms of characterizing the scatterer are used. Usually the transition

operator is employed in the derivation of approximate equations, while the scattering amplitude appears when these equations are solved.

2.3.3 Mean-Wave Equation

An approximate equation for the mean field will now be given. The method for obtaining this mean field equation exactly parallels the two-dimensional procedure as given in Section 2.2.3. As a result, the derivation will not be given here.

Starting with the vector wave equation as given by Equation (2-3-8), introducing the dyadic transition operator, averaging and using the Foldy-Lax approximation, the three-dimensional vector mean-field equation is found to be

$$\underline{\underline{L}}\langle\underline{\Psi}\rangle - \int_V d\underline{s}\rho(\underline{s})\underline{\underline{T}}(\underline{s})\cdot\langle\underline{\Psi}\rangle = \underline{g} \qquad (2\text{-}3\text{-}27)$$

where $\underline{\underline{T}}(\underline{s})$ is the orientational average for a particle located at $\underline{s}$, i.e.

$$\underline{\underline{T}}(\underline{s}) = \int_0^{\pi} d\theta \int_0^{2\pi} d\phi p(\theta,\phi|\underline{s})\underline{\underline{T}}(\underline{s},\theta,\phi) \qquad (2\text{-}3\text{-}28)$$

where $p(\theta,\phi)$ is the angular probability density function given the particle is located at $\underline{s}$.

As before, it will be of use to write the mean-field equation explicitly. Equation (2-3-27) becomes

$$\nabla x\nabla x\langle\underline{E}(\underline{x})\rangle - k_o^2\varepsilon_b(\underline{x})\langle\underline{E}(\underline{x})\rangle$$

$$- \int_V d\underline{s}(\underline{s})\rho d\underline{x}'\underline{\underline{t}}(\underline{x}-\underline{s},\underline{x}'-\underline{s}')\cdot\langle\underline{E}(\underline{x}')\rangle = -j\omega\mu_o\underline{J}(\underline{x}) \qquad (2\text{-}3\text{-}29)$$

Equation (2-3-29) differs from the vector Helmholtz equation only because of the added integral term arising as a result of the scatterers. A similar scatterer-related integral term is also observed in the case of two-dimensional scatterers [Equation (2-2-41)].

The mean-field equation can be substantially simplified in the low-frequency (Rayleigh) regime. This is easily shown by substituting Equation (2-3-17) into Equation (2-3-29) and obtaining

$$\nabla x \nabla x \langle \underline{E} \rangle - k_o^2 [\varepsilon_b(\underline{x})\underline{I} + \rho \underline{\bar{\alpha}}] \langle \underline{E} \rangle = -j\omega\mu_o \underline{J}(\underline{x}) \qquad (2\text{-}3\text{-}30)$$

In this low-frequency (Rayleigh) regime where the wavelength is large relative to the size of the scatterers, it is apparent from Equation (2-3-30) that solutions to the mean-field equation can be obtained using classical techniques.

2.4 Three-Dimensional Scattering in Two-Dimensional Media

In this section, mean-wave propagation in a medium of two-dimensional scatterers with three-dimensional sources $\underline{g}(x)$ is considered. The equation for the mean field is derived from the three-dimensional mean-field equation given in Equation (2-3-29). The scattering being considered differs from the two-dimensional waves considered in Section 2.2 because it doesn't reduce simply to a scalar treatment; in general the complete vector problem must be considered. This results from the fact that three-dimensional sources produce waves that travel at oblique angles with respect to the scatterers.

The scatterers are characterized by the dyadic transition operator $\underline{t}(\underline{x},\underline{x}')$ as defined in Equation (2-3-13). Since the scatterers do not vary with z, translations of the incident field and of the equivalent or induced sources by the same amount in any direction will have no effect on the transition operator; thus $\underline{t}(\underline{x}_t,\underline{x}_t',z,z')$ is just a function of z-z' or

$$\underline{t}(\underline{x},\underline{x}') = \underline{t}(\underline{x}_t,\underline{x}_t',z-z') \qquad (2\text{-}4\text{-}1)$$

This is analogous to the impulse response of a time-invariant filter; one obtains the same response independently of when the impulse was applied.

Now using this two-dimensional form of $\underline{t}$ in Equation (2-3-39),

$$\nabla x\nabla x\langle \underline{E}(\underline{x}_t,z)\rangle - k_o^2\langle \underline{\Xi}(\underline{x}_t,z)\rangle$$

$$- \int_S d\underline{s}_t \int ds_z \rho(\underline{s}) \int d\underline{x}_t' dz' \underline{\underline{t}}(\underline{x}_t-\underline{s}_t, \underline{x}_t'-\underline{s}_t, z-z')$$

$$\cdot \langle \underline{E}(\underline{x}_t',z)\rangle = \underline{g}(\underline{x}_t,z) \qquad (2\text{-}4\text{-}2)$$

Here it is assumed $\varepsilon_b(\underline{x}) = 1$, and for all $\underline{x}$ that the total volume V under consideration is an infinite z-directed cylinder having cross-section S. An examination of this mean equation shows that it is Fourier-transformable in the z direction. Introducing the Fourier representation.

$$\langle \underline{E}(\underline{x}_t,z)\rangle = \frac{1}{2\pi}\int dk_z \langle \hat{\underline{E}}(\underline{x}_t,k_z)\rangle e^{-jk_z z} \qquad (2\text{-}4\text{-}3)$$

into Equation (2-4-2) yields

$$\hat{\nabla}x\hat{\nabla}x\langle \hat{\underline{E}}(\underline{x}_t,k_z)\rangle - k_o^2\langle \hat{\underline{E}}(\underline{x}_t,k_z)\rangle$$

$$- \int_S d\underline{s}_t \rho(\underline{s}_t) \int d\underline{x}_t' \hat{\underline{\underline{t}}}(\underline{x}_t-\underline{s}_t, \underline{x}_t'-\underline{s}_t, k_z)$$

$$\cdot \langle \hat{\underline{E}}(\underline{x}_t',k_z)\rangle = \hat{\underline{g}}(\underline{x}_t,k_z) \qquad (2\text{-}4\text{-}4)$$

where $\hat{\nabla} = \nabla_t - jk_z\underline{z}^\circ \qquad \nabla_t = \underline{x}^\circ\partial/\partial x + \underline{y}^\circ\partial/\partial y$

$$\hat{\underline{\underline{t}}}(\underline{x}_t,\underline{x}_t',k_z) = \int dz \underline{\underline{t}}(\underline{x}_t,\underline{x}_t',z) e^{jk_z z} \qquad (2\text{-}4\text{-}5)$$

The hat notation has been used to indicate a Fourier transform with respect to z. The transverse density $\rho(\underline{s}_t)$ is related to $\rho(\underline{s})$ as follows

$$\int ds_z \rho(\underline{s}) = N\int ds_z p(\underline{s}) = Np(\underline{s}_t) = \rho(\underline{s}_t) \qquad (2\text{-}4\text{-}6)$$

Thus $\rho(\underline{s}_t)$ is measured in units of particles per area rather than particles per volume.

As in the case of scalar two-dimensional fields and vector three-dimensional fields, the fields scattered by an isolated

two-dimensional scatterer can be characterized by a scatt ring amplitude. The difference between this vector two-dimens onal scattering amplitude and the scalar case is that the direction vector $\underline{i}$ of the incident plane wave of unit amplitude and polarization $\underline{q}^\circ$ is not necessarily perpendicular to the generating element of the cylindrical scatterer (z-axis). The dyadic scattering amplitude is defined in terms of the transformed scattered field as follows

$$\underline{e}_s(\underline{x}_t, z) \sim \underline{f}(\underline{o}, \underline{i}) \cdot \underline{q}^\circ \frac{e^{-jk_t x_t - jk_z z}}{\sqrt{x_t}} \tag{2-4-7}$$

where

$$\underline{i} = \underline{i}_t + i_z \underline{z}^\circ \quad , \quad i_z = \underline{i} \cdot \underline{z}^\circ \tag{2-4-8}$$

and

$$\underline{o} = \underline{o}_t + i_z \underline{z}^\circ \tag{2-4-9}$$

The wavenumber in the z direction is $k_z = k_o i_z$. This is determined wholly by the incident wave. Because of the two-dimensional property of the scatterer, the wave number k_z is preserved by the scattering process; thus the scattered wave in direction $\underline{o}$ must also have a z component i_z. This means that scattering is restricted to lie on a cone of angle θ_i as shown in Figure 2-4.

Since both $\underline{f}$ and $\underline{t}$ describe the single-scattering process, they should be related in a similar manner to the $\underline{f}$ and $\underline{t}$ of the three-dimensional scatterers. In Appendix B, it is shown that this is indeed the case. The result is

$$\underline{f}(\underline{o}, \underline{i}; k_z) = \gamma (\underline{I} - \underline{o}\,\underline{o}) \cdot \tilde{\underline{t}}(k_t \underline{o}_t, k_t \underline{i}_t; k_z) \cdot (\underline{I} - \underline{i}\,\underline{i}) \tag{2-4-10}$$

where γ is given by Equation (2-2-24) and

$$\tilde{\underline{t}}(\underline{k}_t, \underline{k}_t'; k_z) = \frac{1}{(2\pi)^2} \int d\underline{x}_t d\underline{x}_t' \hat{\underline{t}}(\underline{x}_t, \underline{x}_t'; k_z) e^{j(\underline{k}_t \cdot \underline{x}_t - \underline{k}_t' \cdot \underline{x}_t')} \tag{2-4-11}$$

These relationships will be used in Section 4 where expressions are derived for the propagation constants of the mean wave in an unbounded medium of two-dimensional scatterers.

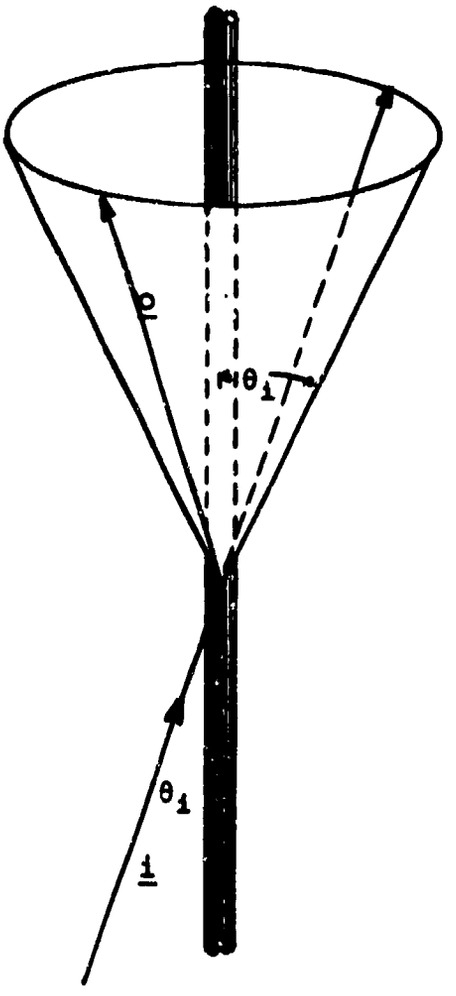

Figure 2-4: Scattering Cone for Two-Dimensional Scatterers

3.0 Dyadic Scattering Amplitudes

The theory of electromagnetic scattering presented in Section 2 assumed the knowledge or availability of the dyadic transition operators ($\underline{\underline{t}}$) or dyadic scattering amplitudes ($\underline{\underline{f}}$). It is the purpose of this section to provide the dyadic scattering amplitudes for trunks, branches and leaves.

For both two- and three-dimensional objects, the scattering amplitude is determined by illuminating the object with a unit-amplitude plane wave

$$\underline{E}_i(\underline{x}) = \underline{q}^\circ e^{-jk_\circ(\underline{i}\cdot\underline{x})} \tag{3-0-1}$$

where $\underline{i}$ is a unit vector in the direction of propagation and $\underline{q}^\circ$ is the unit polarization vector. The $-\underline{i}$ is often specified by the spherical angles θ_i and ϕ_i measured with respect to a polar axis z. One can then write:

$$-\underline{i} = \underline{x}^\circ \sin\theta_i \cos\phi_i + \underline{y}^\circ \sin\theta_i \sin\phi_i + \underline{z}^\circ \cos\theta_i \tag{3-0-2}$$

Incident waves with both horizontal, $\underline{q}^\circ = \underline{h}_i^\circ$, and vertical $\underline{q}^\circ = \underline{v}_i^\circ$, polarizations are considered. Here the horizontal polarization vector $\underline{h}_i^\circ$ is taken parallel to the x-y plane of the forest floor. More specifically,

$$\underline{h}_i^\circ = \frac{\underline{i} \times \underline{z}^\circ}{|\underline{i} \times \underline{z}^\circ|} \tag{3-0-3}$$

The vertical polarization vector is taken perpendicular to both $\underline{i}$ and $\underline{h}_i^\circ$; thus

$$\underline{v}_i^\circ = \underline{h}_i^\circ \times \underline{i} \tag{3-0-4}$$

For three-dimensional scatterers the dyadic scattering amplitude is defined by

$$\underline{E}_s(\underline{x}) \sim \underline{\underline{f}}(\underline{o},\underline{i})\cdot\underline{q}^\circ \frac{e^{-jk_\circ(\underline{o}\cdot\underline{x})}}{x} \tag{3-0-5}$$

where $\underline{o}$ is a unit vector in the direction of the observation point $\underline{x}$. The $\underline{o}$ vector can be described by angles θ_s and ϕ_s

measured with respect to the z and x axes, respectively. In terms of these angles, $\underline{o}$ is written as

$$\underline{o} = \underline{x}^{\circ}\sin\theta_s \cos\phi_s + \underline{y}^{\circ}\sin\theta_s \sin\phi_s + \underline{z}^{\circ}\cos\theta_s \qquad (3\text{-}0\text{-}6)$$

The scattered wave in general can have components in the horizontal $\underline{h}^{\circ}_s$ and the vertical $\underline{v}^{\circ}_s$ directions. These scattered polarization vectors are defined by

$$\underline{h}^{\circ}_s = \frac{\underline{o} \times \underline{z}^{\circ}}{|\underline{o} \times \underline{z}^{\circ}|}$$

$$\underline{v}^{\circ}_s = \underline{h}^{\circ}_s \times \underline{o} \qquad (3\text{-}0\text{-}7)$$

As pointed out in Section 2, $\underline{f}(\underline{o},\underline{i})$ has only four components since $\underline{o}\cdot\underline{f}(\underline{o},\underline{i}) = 0$ and $\underline{f}(\underline{o},\underline{i})\cdot\underline{i} = 0$. Thus,

$$\underline{f}(\underline{o},\underline{i}) = f_{hh}\underline{h}^{\circ}_s\underline{h}^{\circ}_i + f_{vh}\underline{h}^{\circ}_s\underline{v}^{\circ}_i + f_{vh}\underline{v}^{\circ}_s\underline{h}^{\circ}_i + f_{vv}\underline{v}^{\circ}_s\underline{v}^{\circ}_i \qquad (3\text{-}0\text{-}8)$$

The dyadic scattering amplitude for two-dimensional scatterers is identified as the coefficient of a cylindrically-expanding wave:

$$\underline{E}_s(\underline{x}) \sim \underline{f}(\underline{o},\underline{i})\cdot\underline{q}^{\circ} \frac{e^{-jk_o(\underline{o}\cdot\underline{x})}}{\sqrt{x}} \qquad (3\text{-}0\text{-}9)$$

where $\theta_s = \pi - \theta_i$. This restriction on the angle θ_s results from the requirement that scattered fields have the same variation in a as the incident wave. This means that $\underline{o}$ must lie on the surface of a cone of angle θ_i.

3.1 Infinitely-Long, Circular Cylinder (Tree Trunk)

In this section, the dyadic scattering amplitude for an infinite circular cylinder of radius a and dielectric constant ε_ℓ is given. Assume that the axis of the cylinder is the polar z axis [Refer to Figure 3-1]. There is no need to find the scattering amplitude from first principles since the required results are given by Wait [82] and summarized by Ruck et al. [78]. These results are:

$$f_{pp}(\underline{o},\underline{i}) = \sqrt{\frac{2}{\pi}} \frac{e^{j\,\pi/4}}{\sqrt{k_o \sin\theta_i}} \sum_{n=-\infty}^{\infty} (-1)^n C_n^{pp} e^{jn(\phi_i-\phi_s)} \quad , \quad p\varepsilon\{h,v\} \qquad (3\text{-}1\text{-}1)$$

$$f_{vh}(\underline{o},i) = -f_{hv}(\underline{o},\underline{i}) = \sqrt{\frac{2}{\pi}} \frac{e^{j\,\pi/4}}{\sqrt{k_o \sin\theta_i}} \sum_{n=-\infty}^{\infty} (-1)^n \bar{C}_n e^{jn(\phi_i-\phi_s)} \qquad (3\text{-}1\text{-}2)$$

where

$$C_n^{vv} = - \frac{V_n P_n - q_n^2 J_n(x_0) H_n^{(2)}(x_0) J_n^2(x_1)}{P_n N_n - [q_n H_n^{(2)}(x_0) J_n(x_1)]^2} \qquad (3\text{-}1\text{-}3)$$

$$C_n^{hh} = - \frac{M_n N_n - q_n^2 J_n(x_0) H_n^{(2)}(x_0) J_n^2(x_1)}{P_n N_n - [q_n H_n^{(2)}(x_0) J_n(x_1)]^2} \qquad (3\text{-}1\text{-}4)$$

$$\bar{C}_n = \frac{-j2}{\pi x_0} \left[\frac{s_0 q_n J_n^2(x_1)}{P_n N_n - [q_n H_n^{(2)}(x_0) J_n(x_1)]^2} \right] \qquad (3\text{-}1\text{-}5)$$

$$x_0 = k_o a \qquad (3\text{-}1\text{-}6)$$

$$x_1 = k_o a \sqrt{\varepsilon_\ell - \cos^2\theta_i} \qquad (3\text{-}1\text{-}7)$$

$$q_n = \frac{n \cos\theta_i}{k_o a} \left[\frac{1}{\varepsilon_\ell - \cos^2\theta_i} - \frac{1}{\sin^2\theta_i} \right] \qquad (3\text{-}1\text{-}8)$$

$$V_n = s_1 J_n(x_1) J_n'(x_1) - s_0 J_n'(x_0) J_n(x_1) \qquad (3\text{-}1\text{-}9)$$

$$P_n = r_1 H_n^{(2)}(x_0) J_n'(x_1) - s_0 H_n^{(2)\prime}(x_0) J_n(x_1) \qquad (3\text{-}1\text{-}10)$$

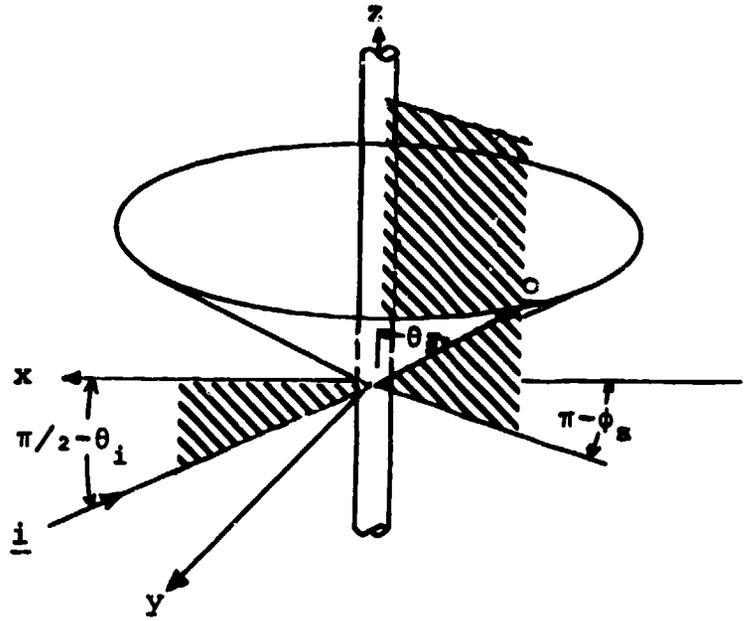

Figure 3-1: Infinitely-Long Circular Cylinder Scattering Geometry

$$N_n = s_1 H_n^{(2)}(x_0) J_n'(x_1) - s_0 H_n^{(2)'}(x_0) J_n(x_1) \qquad (3\text{-}1\text{-}11)$$

$$M_n = r_1 J_n(x_0) J_n'(x_1) - s_0 J_n'(x_0) J_n(x_1) \qquad (3\text{-}1\text{-}12)$$

$$s_0 = \frac{1}{\sin\theta_i} \qquad s_1 = \frac{\varepsilon_\ell}{\sqrt{\varepsilon_\ell - \cos^2\theta_i}} \qquad (3\text{-}1\text{-}13)$$

$$r_1 = \frac{1}{\sqrt{\varepsilon_\ell - \cos^2\theta_i}} \qquad (3\text{-}1\text{-}14)$$

with $J_n(\cdot)$ being the Bessel function of order n and $H_n^{(2)}(\cdot)$ being the Hankel function of the second kind of order n. The primes over the cylinder functions mean derivatives with respect to their arguments.

An examination of the results shows that, in general, scattering from the cylinder gives rise to depolarization since $f_{hv} \neq 0$. It should be noted that this depolarization does not exist when the incident wave is normal to the cylinder ($\theta_i = \pi/2$) because then $q_n = 0$. The cross-polarized terms are also zero in the forward-scattered direction. In this case, $\theta_s = \theta_i + \pi$ which leads to $C_n^{(vh)} = -C_{-n}^{(vh)}$ $(n = 1,2,\ldots)$ and $C_0 = 0$. Thus,

$$f_{hv}(\underline{i},\underline{i}) = -f_{vh}(\underline{i},\underline{i}) = 0 \qquad (3\text{-}1\text{-}15)$$

3.2 Finitely-Long, Circular Cylinder (Branch)

Consider a planar electromagnetic wave to be incident upon a finitely-long, circular cylinder of complex relative permittivity ε_ℓ. Without loss of generality, the longitudinal axis of the cylinder can be taken as inclined to the z-axis by an angle ϑ, and the plane defined by the cylinder axis and the z-axis as rotated an angle ϕ from the x-z plane [refer to Figure 3-2]. An incident electric field of unit amplitude can be represented as

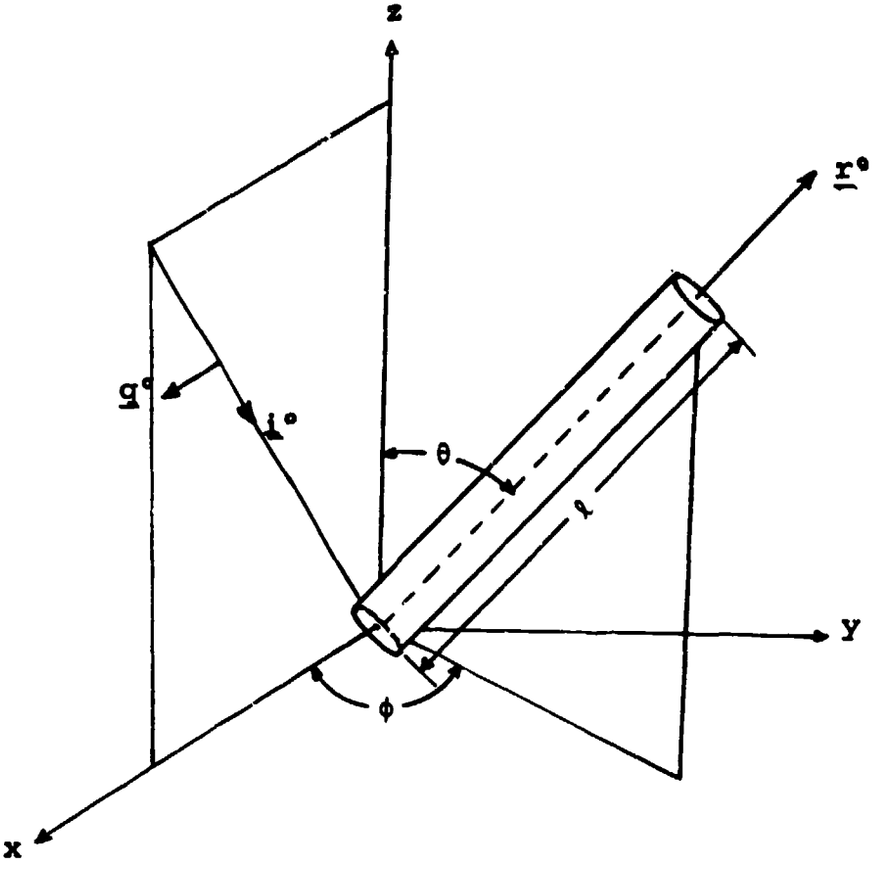

Figure 3-2: Finitely-Long Circular Cylinder Scattering Geometry

$$\underline{E}_i(\underline{x}) = \underline{q}^\circ e^{-jk_\circ(\underline{i}\cdot\underline{x})} \tag{3-2-1}$$

where

$$k_\circ = \omega\sqrt{\mu_\circ\varepsilon_\circ} \tag{3-2-2}$$

$$-\underline{i} = \underline{x}^\circ\cos\phi_i \sin\theta_i + \underline{y}^\circ\sin\phi_i \sin\theta_i + \underline{z}^\circ\cos\theta_i \tag{3-2-3}$$

$$\underline{x} = \underline{x}^\circ x + \underline{y}^\circ y + \underline{z}^\circ z \tag{3-2-4}$$

and θ_i is the angle between the direction of the incident wave, and the z-axis, and ψ_i is the angle between the plane defined by $\underline{i}$ and the z-axis and the x-z plane.

If the cylinder is sufficiently long, and thin in comparison to the wavelength within, the induced electric field $\underline{E}_i$ within the cylinder may be ascertained using quasi-static techniques. Under this approximation, the electromagnetic boundary condition requiring the continuity of the tangential field components ($\underline{E}$ and $\underline{H}$) can be employed to show that the induced electric field component directed along the axis of the cylinder is given by

$$\underline{r}^\circ \cdot \underline{E}_\ell = \underline{r}^\circ \cdot \underline{E}_i \tag{3-2-5}$$

whereas the induced electric field component normal to the axis of the cylinder is given by

$$\underline{r}^\circ \times \underline{E}_\ell = \underline{r}^\circ \times \underline{E}_i \left(\frac{2}{\varepsilon_\ell + 1}\right) \tag{3-2-6}$$

where $\underline{r}^\circ$, a unit vector directed along the axis of the cylinder, is given by

$$\underline{r}^\circ = \underline{x}^\circ\cos\phi \sin\theta + \underline{y}^\circ\sin\phi \sin\theta + \underline{z}^\circ\cos\theta \tag{3-2-7}$$

As a consequence of Equations (3-2-1), (3-2-5), and (3-2-6), the induced electric field within the cylinder may be shown to be

$$\underline{E}_\ell(\underline{x}) = \left\{(\underline{q}^\circ\cdot\underline{r}^\circ)\underline{r}^\circ + \left(\frac{2}{\varepsilon_\ell + 1}\right)[\underline{q}^\circ\cdot\underline{r}^\circ)\underline{r}^\circ]\right\} e^{-jk_\circ(\underline{i}\cdot\underline{x})} \tag{3-2-8}$$

As a consequence of the radiation condition, the electric field $\underline{E}$ in free-space attributable to the current distribution $\underline{J}$ within the closed volume V_p is given by

$$\underline{E}(\underline{x}) = -j\omega\mu_o \int_{V_p} d\underline{x}' \underline{G}(\underline{x},\underline{x}') \cdot \underline{J}(\underline{x}') \qquad (3\text{-}2\text{-}9)$$

where $\underline{G}(\underline{x},\underline{x}')$ is the free-space dyadic Green's function [126]. Although the total current induced within the finite cylinder is

$$\underline{J} = j\omega\varepsilon_o\varepsilon_\ell \underline{E}_i \qquad (3\text{-}2\text{-}10)$$

that part of the total current responsible for the scattered field $\underline{E}_s$ is only

$$\underline{J}_s = j\omega\varepsilon_o(\varepsilon_\ell - 1)\underline{E}_\ell = j\omega\varepsilon_o\chi_\ell\underline{E}_\ell \qquad (3\text{-}2\text{-}11)$$

where χ_ℓ is the susceptibility of the cylinder. Substitution of Equation (3-2-11) into Equation (3-2-9) provides the following relation between the field $\underline{E}_s$, scattered by the cylinder and the field $\underline{E}_\ell$ induced within the cylinder

$$\underline{E}_s(\underline{x}) = k_o^2\chi_\ell \int_{V_p} d\underline{x}' \underline{G}(\underline{x},\underline{x}') \cdot \underline{E}_\ell(\underline{x}') \qquad (3\text{-}2\text{-}12)$$

The far-field free-space dyadic Green's function is given by

$$\underline{G}(\underline{x},\underline{x}') = (\underline{I} - \underline{o}\,\underline{o}) \frac{e^{-jk_o[\underline{o}\cdot(\underline{x}-\underline{x}')]}}{4\pi x} \qquad (3\text{-}2\text{-}13)$$

with

$$\underline{o} = \underline{x}^\circ\cos\phi_s \sin\theta_s + \underline{y}^\circ\sin\phi_s \sin\theta_s + \underline{z}^\circ\cos\theta_s \qquad (3\text{-}2\text{-}14)$$

Substitution of Equations (3-2-8) and (3-2-13) into Equation (3-2-12) yields

$$\underline{E}_s(\underline{x}) = \underline{f} \cdot \underline{q}^\circ \frac{e^{-jk_o x}}{x} \qquad (3\text{-}2\text{-}15)$$

where $\underline{f}$, the dyadic scattering amplitude, is given by

$$\underline{f}(\underline{o},\underline{i}) = \beta(\underline{I} - \underline{o}\,\underline{o}) \cdot \left[\underline{r}^\circ\underline{r}^\circ + \left(\frac{2}{\varepsilon_\ell + 1}\right)(\underline{I} - \underline{r}^\circ\underline{r}^\circ)\right] \frac{e^{jk_\Delta \ell} - 1}{jk_\Delta} \qquad (3\text{-}2\text{-}16)$$

and

$$k_\Delta = k_o(\underline{o} - \underline{i}) \cdot \underline{r}^o \tag{3-2-17}$$

$$\beta = (\pi\chi_\ell)(\pi a^2)(k_o/2\pi)^2 \tag{3-2-18}$$

3.3 Circular Disc (Leaf)

Consider a planar electromagnetic wave to be incident upon a circular disc of radius a, thickness t, and complex relative permittivity ε_ℓ. Without loss of generality, the orientation of the disc can be defined in terms of the two eulerian angles θ and ϕ shown in Figure 3-3. An incident electric field of unit amplitude can be represented as

$$\underline{E}_i(\underline{x}) = \underline{q}^o e^{-jk_o(\underline{i}\cdot\underline{x})} \tag{3-3-1}$$

where

$$k_o = \omega\sqrt{\mu_o\varepsilon_o} \tag{3-3-2}$$

$$-\underline{i} = \underline{x}^o\cos\phi_i \sin\theta_i + \underline{y}^o\sin\phi_i \sin\theta_i + \underline{z}^o\cos\theta_i \tag{3-3-3}$$

$$\underline{x} = \underline{x}^o x + \underline{y}^o y + \underline{z}^o z \tag{3-3-4}$$

and θ_i is the angle between the direction of the incident wave and the z-axis, and ϕ_i is the angle between the x-z plane and the plane defined by $\underline{i}$ and the z-axis.

If the disc is relatively thin (a>>t) and the radius large in comparison with the wavelength (a>>λ), the induced electric field $\underline{E}_\ell$ within the disc may be approximated by the electric field in an unbounded slab having the same orientation as the disc. Under this approximation, the electromagnetic boundary condition requiring the continuity of the tangential field components ($\underline{E}$ and $\underline{H}$) across an arbitrary interface can be employed to show that the induced electric field within the disc is given, approximately, by

$$\underline{E}_\ell(\underline{x}) = \underline{E}(n)e^{-jk_o(\underline{i}_t\cdot\underline{x})} \tag{3-3-5}$$

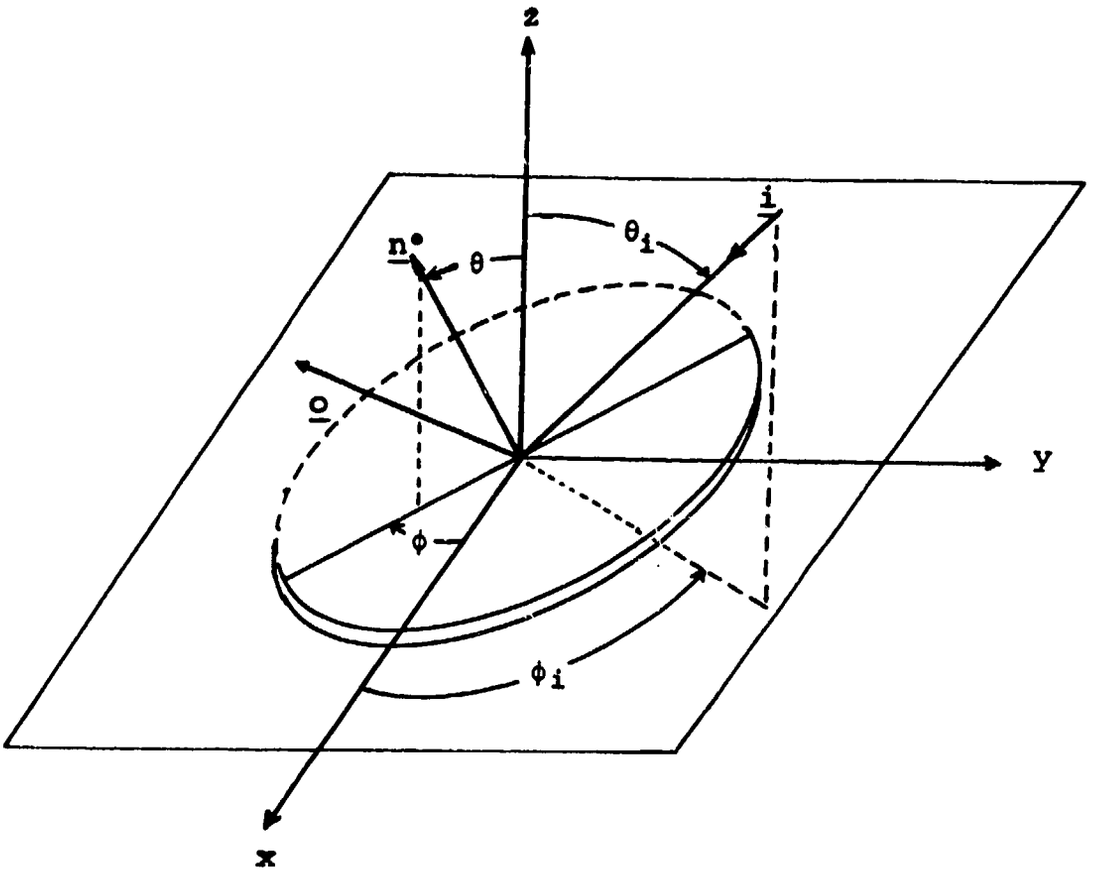

Figure 3-3: Circular Disc Scattering Geometry

where,

$$\underline{E}(n) = \underline{q}^{\circ}_{+} e^{+}_{q} e^{j\kappa n} + \underline{q}^{\circ}_{-} e^{-}_{q} e^{-j\kappa n} \qquad (3\text{-}3\text{-}6)$$

and

$$\underline{n}^{\circ} = \underline{x}^{\circ}\sin\phi\,\sin\theta - \underline{y}^{\circ}\cos\phi\,\sin\theta + \underline{z}^{\circ}\cos\theta \qquad (3\text{-}3\text{-}7)$$

$$n = \underline{n}^{\circ} \cdot \underline{x} \qquad (3\text{-}3\text{-}8)$$

$$\underline{i}_t = \underline{i} - (\underline{n}^{\circ} \cdot \underline{i}^{\circ})\underline{n}^{\circ} \qquad (3\text{-}3\text{-}9)$$

$$\kappa = k_o(\varepsilon_\ell - i_t^2)^{\frac{1}{2}} \quad , \quad i_t = |\underline{i}_t| \qquad (3\text{-}3\text{-}10)$$

The unit polarization vectors appearing in Equation (3-3-6) depend upon the relative orientation of the disc. As a consequence

$$\underline{q}^{\circ}_{\pm} = \left\{ \begin{array}{c} \underline{h}^{\circ}_{\pm} \\ \\ \underline{v}^{\circ}_{\pm} \end{array} \right\} = \left\{ \begin{array}{c} \dfrac{(\underline{i}_{\pm} \times \underline{n}^{\circ})}{|\underline{i}_{\pm} \times \underline{n}^{\circ}|} \\ \\ \underline{h}^{\circ}_{\pm} \times \underline{i}^{\circ} \end{array} \right\} \qquad (3\text{-}3\text{-}11)\ (3\text{-}3\text{-}12)$$

and $$\underline{i}_{\pm} = [\underline{i}_t \pm \underline{n}^{\circ}(\varepsilon_\ell - i_t^2)^{\frac{1}{2}}]/\sqrt{\varepsilon_\ell} \qquad (3\text{-}3\text{-}13)$$

The amplitudes of the induced field components, $e^{\pm}_{q}$, are given by

$$e^{+}_{q} = \frac{t_q e^{-jk(\kappa - k_o)t/2}}{1 - r_q^2 e^{-j2\kappa t}} \qquad (3\text{-}3\text{-}14)$$

$$e^{-}_{q} = r_q e^{+}_{q} e^{-j\kappa t} \qquad (3\text{-}3\text{-}15)$$

where

$$r_q = \left\{ \begin{array}{c} r_h \\ \\ r_v \end{array} \right\} = \left\{ \begin{array}{c} \dfrac{(\varepsilon_\ell - i_t^2)^{\frac{1}{2}} - (1 - i_t^2)^{\frac{1}{2}}}{(\varepsilon_\ell - i_t^2)^{\frac{1}{2}} + (1 - i_t^2)^{\frac{1}{2}}} \\ \\ \dfrac{(\varepsilon_\ell - i_t^2)^{\frac{1}{2}} - \varepsilon_\ell(1 - i_t^2)^{\frac{1}{2}}}{(\varepsilon_\ell - i_t^2)^{\frac{1}{2}} + \varepsilon_\ell(1 - i_t^2)^{\frac{1}{2}}} \end{array} \right\} \qquad (3\text{-}3\text{-}16)\ (3\text{-}3\text{-}17)$$

$$t_q = \begin{Bmatrix} t_h \\ \\ t_v \end{Bmatrix} = \begin{Bmatrix} \dfrac{2(1-i_t^2)^{\frac{1}{2}}}{(\varepsilon_\ell - i_t^2)^{\frac{1}{2}} + (1-i_t^2)^{\frac{1}{2}}} \\ \\ \dfrac{2\sqrt{\varepsilon_\ell}\,(1-i_t^2)^{\frac{1}{2}}}{(\varepsilon_\ell - i_t^2)^{\frac{1}{2}} + \varepsilon_\ell(1-i_t^2)^{\frac{1}{2}}} \end{Bmatrix} \qquad \begin{matrix} (3\text{-}3\text{-}18) \\ \\ (2\text{-}3\text{-}19) \end{matrix}$$

As a consequence of the radiation condition, the electric field scattered by the disc $\underline{E}_s$ and the electric field induced within the disc $\underline{E}_\ell$ are related by the Kirchhoff integral

$$\underline{E}_s(\underline{x}) = k_o^2 \chi_\ell \int_{V_p} d\underline{x}' \underline{G}(\underline{x},x') \cdot \underline{E}_\ell(\underline{x}') \qquad (3\text{-}3\text{-}20)$$

where $\underline{G}(\underline{x},x')$ is the free-space dyadic Green's function and χ_ℓ is the susceptibility of the disc ($\chi_\ell = \varepsilon_\ell - 1$). The far-field free-space dyadic Green's function, needed to find the dyadic scattering amplitude $\underline{f}$ which has been defined so that

$$\underline{E}_s(\underline{x}) = \underline{f} \cdot \underline{q}^o \frac{e^{-jk_o x}}{x} \qquad (3\text{-}3\text{-}21)$$

is given by

$$\underline{G}(\underline{x},\underline{x}') = (\underline{I} - \underline{o}\,\underline{o}) \frac{e^{-jk_o[\underline{o}\cdot(\underline{x}-\underline{x}')]}}{4\pi x} \qquad (3\text{-}3\text{-}22)$$

If Equation (3-3-20) is generalized to accommodate a dyadic field representation so that

$$\underline{E}_s(\underline{x}) = k_o^2 \chi_\ell \int_{V_p} d\underline{x}' \underline{G}(\underline{x},\underline{x}') \cdot \underline{E}_\ell(\underline{x}') \qquad (3\text{-}3\text{-}23)$$

then it is apparent from Equations (3-3-21), (3-3-22), and (3-3-23) that

$$\underline{f}(\underline{o},\underline{i}) = (\pi\chi_\ell)(k_o/2\pi)^2 \int_{V_p} d\underline{x}' (\underline{I} - \underline{o}\,\underline{o}) \cdot \underline{E}_\ell(\underline{x}') e^{jk_o(\underline{o}\cdot\underline{x}')} \qquad (3\text{-}3\text{-}24)$$

and where, as a consequence of Equation (3-3-5)

$$\underline{E}_\ell(\underline{x}) = [\underline{e}^+ e^{j\kappa n} + \underline{e}^- e^{-j\kappa n}] e^{-jk_o(\underline{i}_t\cdot\underline{x})} \qquad (3\text{-}3\text{-}25)$$

with

$$\underline{e}^{\pm} = e^{\pm}_{h}\underline{h}^{\circ}\underline{h}^{\circ} + e^{\pm}_{v}\underline{v}^{\circ}\underline{v}^{\circ} \tag{3-3-26}$$

Substituting Equation (3-3-25) into Equation (3-3-24) and introducing the identity

$$\underline{o} = \underline{o}_t + (\underline{o}\cdot\underline{n}^{\circ})\underline{n}^{\circ} \tag{3-3-27}$$

yields

$$\underline{f}(\underline{o},\underline{i}) = (\pi X_{\ell})(k_{\circ}/2\pi)^2 \int_{V_p} d\underline{x}' (\underline{I} - \underline{o}\,\underline{o})\cdot[\underline{e}^{+}e^{jk\underline{n}} + \underline{e}^{-}e^{-jk\underline{n}}]$$

$$\cdot\, e^{jk_{\circ}(\underline{o}\cdot\underline{n}^{\circ})} \cdot e^{jk\underline{\nu}_t\cdot\underline{x}'} \tag{3-3-28}$$

where

$$\underline{\nu}_t = \underline{o}_t - \underline{i}_t \tag{3-3-29}$$

For a circular disc of radius a and thickness t, Equation (3-3-28) can be evaluated directly to obtain

$$\underline{f}(\underline{o},\underline{i}) = (\pi X_{\ell})(k_{\circ}/2\pi)^2[(a/\nu_t)J_1(2\pi a\nu_t)]$$

$$\cdot\, (\underline{I} - \underline{o}\,\underline{o})\cdot[e^{+}\mathrm{sinc}\theta^{+} + e^{-}\mathrm{sinc}\theta^{-}] \tag{3-3-30}$$

where $J_1(\cdot)$ is the Bessel function of order unity and

$$\theta^{\pm} = (k_{\circ}t/2)[(\underline{o}\cdot\underline{n}^{\circ}) \mp (\varepsilon_{\ell} - i_t^2)^{\frac{1}{2}}] \tag{3-3-31}$$

$$|\underline{\nu}_t| = \nu_t = (k_{\circ}/2\pi)(\xi^2 + \eta^2)^{\frac{1}{2}}$$

$$\xi = \cos\theta[\sin\theta_i \sin(\phi-\phi_i) + \sin\theta_s \sin(\phi-\phi_s)]$$

$$- \sin\theta[\cos\theta_i + \cos\theta_s] \tag{3-3-33}$$

$$\eta = \sin\theta_i \cos(\phi-\phi_i) + \sin\theta_s \cos(\phi-\phi_s) \tag{3-3-34}$$

The dyadic scattering amplitude of the circular disc as given by Equation (3-3-30) simplifies substantially in the case of an electrically thin disc where

$$k_o\sqrt{\varepsilon_\ell}\, t << 1 \qquad (3\text{-}3\text{-}35)$$

In this case, the phase angles κt and θ are small and Equation (3-3-30) can be approximated by

$$\underline{f}(\underline{o},\underline{i})\cdot\underline{q}^\circ = (\pi\chi_\ell)(k_o/2\pi)^2 t[(a/\nu_t)J_1(2\pi a\nu_t)]$$

$$\cdot\ (\underline{I}-\underline{o}\,\underline{o})\cdot\left[\underline{q}^\circ - \frac{\chi_\ell}{1+\chi_\ell}(\underline{n}^\circ\cdot\underline{q}^\circ)\underline{n}^\circ\right] \qquad (3\text{-}3\text{-}36)$$

For this thin disc case in the low-frequency (Rayleigh) regime where, in addition to inequality (3-3-35),

$$a << \lambda \qquad (3\text{-}3\text{-}37)$$

then $a\nu_t \simeq 0$ and

$$\underline{f}(\underline{o},\underline{i})\cdot\underline{q}^\circ = \chi_\ell t(k_o a/2)^2(\underline{I}-\underline{o}\,\underline{o})\cdot\left[\underline{q}^\circ - \frac{\chi_\ell}{1+\chi_\ell}(\underline{n}^\circ\cdot\underline{q}^\circ)\underline{n}^\circ\right] \qquad (3\text{-}3\text{-}38)$$

Note that in the direction of forward scatter where $\underline{o} = \underline{i}$,

$$\theta_s = \pi - \theta_i \quad , \quad \phi_s = \phi_i + \pi \qquad (3\text{-}3\text{-}39)$$

$\nu_t = 0$, and Equation (3-3-36) for the electrically thin disc reduces to the Rayleigh result of Equation (3-3-38).

4.0 Coherent Forest Scattering

A physically appealing representation for the mean field can be obtained by postulating that the mean (or coherent) field satisfies Maxwell's equation "in the mean" and that the ensemble of discrete scatterers can be replaced by an equivalent continuous medium described by an effective dyadic permittivity $\underline{\underline{\varepsilon}}$, or alternatively, by an effective dyadic susceptibility $\underline{\underline{\chi}}$. Because $\underline{\underline{\chi}}$ is found to be directly proportional to the fractional volume occupied by the scatterers, it is easily scaled with respect to the forest density and therefore preferable to $\underline{\underline{\varepsilon}}$ for characterization of the equivalent continuous medium. In Section 4.1, general expressions are derived which relate $\underline{\underline{\chi}}$ directly to the dyadic scattering amplitudes $\underline{\underline{f}}$. In subsequent sub-sections, these expressions are employed to determine for tree trunks, for branches and leaves, specific expressions for their respective effective dyadic susceptibilities. These specific expressions are exemplified by calculations which are then compared with experiment. It may be noted that, as all forest constituents are assumed uniformly distributed about the vertical, the equivalent continuous medium is uniaxially anisotropic.

Plane-wave propagation within an unbounded, equivalent continuous medium is considered in Section 4.2. Here, a general dispersion relation is derived relating the plane-wave propagation constants $\underline{\kappa}$ of the mean (or coherent) field and the dyadic scattering amplitudes $\underline{\underline{f}}$. In subsequent sub-sections, this dispersion relation is employed to determine, for plane-wave propagation through an unbounded forest of tree trunks, branches, or leaves, specific expressions for the wave-propagation constant. The imaginary part of the wave-propagation constant, the specific attenuation, is numerically evaluated and compared with experiment.

Experimental verification of the electromagnetic model and, ultimately, prediction of radio system performance requires the identification of measurable quantitative parameters to characterize the forest. In Section 4.3, some of these parameters are identified and related directly to the specific attenuation.

4.1 Effective Dyadic Permittivity of the Forest

The mean electric field propagating within an unbounded ensemble of three-dimensional scatterers can be determined, as shown in Section 2.3, from the mean wave-equation

$$\underline{\underline{L}}\cdot\langle\underline{E}(\underline{x})\rangle - \int d\underline{s}\rho(\underline{s})\int d\underline{x}'\underline{\underline{t}}(\underline{x}-\underline{s},\underline{x}'-\underline{s})\cdot\langle\underline{E}(\underline{x}')\rangle = -j\omega\mu_o\underline{J}(\underline{x}) \quad (4\text{-}1\text{-}1)$$

where

$$\underline{\underline{L}} = \nabla x\nabla x\underline{\underline{I}} - k_o^2\underline{\underline{I}} \quad (4\text{-}1\text{-}2)$$

From the physical viewpoint, a more appealing representation of the mean field can be obtained by postulating that the mean field satisfies Maxwell's equations in-the-mean and that the ensemble of discrete scatterers can be replaced by an equivalent continuous medium described by an effective dyadic permittivity $\underline{\underline{\varepsilon}}$. If Faraday's law

$$\nabla x\langle\underline{E}(\underline{x})\rangle = -j\omega\mu_o\langle\underline{H}(\underline{x})\rangle \quad (4\text{-}1\text{-}3)$$

is substituted into the first term of Equation (4-1-1), then

$$\nabla x\langle\underline{H}(\underline{x})\rangle = j\omega\varepsilon_o[\underline{\underline{I}}\cdot\langle\underline{E}(\underline{x})\rangle + \frac{1}{k_o^2}\int d\underline{s}\rho(\underline{s})\int d\underline{x}'\underline{\underline{t}}(\underline{x}-\underline{s},\underline{x}'-\underline{s})$$

$$\cdot\langle\underline{E}(\underline{x}')\rangle + \underline{J}(\underline{x})] \quad (4\text{-}1\text{-}4)$$

and, by Ampere's law

$$\nabla x\langle\underline{H}(\underline{x})\rangle = j\omega\langle\underline{D}(\underline{x})\rangle + \underline{J}(\underline{x}) \quad (4\text{-}1\text{-}5)$$

it follows that

$$\langle\underline{D}(\underline{x})\rangle = \varepsilon_o[\underline{\underline{I}}\cdot\langle\underline{E}(\underline{x})\rangle + \frac{1}{k_o^2}\int d\underline{s}\rho(\underline{s})\int d\underline{x}'\underline{\underline{t}}(\underline{x}-\underline{s},\underline{x}'-\underline{s})$$

$$\cdot\langle\underline{E}(\underline{x}')\rangle] \quad (4\text{-}1\text{-}6)$$

Taking the Fourier transform with respect to $\underline{x}$ transforms Equation (4-1-6) into

$$\langle\tilde{\underline{D}}(\underline{k})\rangle = \varepsilon_o[\underline{\underline{I}}\cdot\langle\tilde{\underline{E}}(\underline{k})\rangle + \frac{1}{k_o^2}\int d\underline{s}\rho(\underline{s})\int d\underline{x}'\tilde{\underline{\underline{t}}}(\underline{k},\underline{x}'-\underline{s})\cdot\langle\underline{E}(\underline{x}')\rangle e^{j\underline{k}\cdot\underline{s}} \quad (4\text{-}1\text{-}7)$$

The second integral appearing in Equation (4-1-7) may be recognized as a convolution with respect to the parameter $\underline{s}$; as a consequence

$$\langle\tilde{\underline{D}}(\underline{k})\rangle = \varepsilon_o[\underline{I}\cdot\langle\underline{E}(\underline{k})\rangle + \frac{(2\pi)^3}{k_o^2}\int d\underline{s}\rho(\underline{s})\int d\underline{k}'\tilde{\underline{t}}(\underline{k},\underline{k}') \cdot \langle\tilde{\underline{E}}(\underline{k}')\rangle e^{j(\underline{k}-\underline{k}')\cdot\underline{s}}] \quad (4\text{-}1\text{-}8)$$

If the number density $\rho(\underline{s})$ is independent of location so that

$$\rho(\underline{s}) = \rho \quad (4\text{-}1\text{-}9)$$

then the order of integration in Equation (4-1-8) may be inverted with the result

$$\langle\tilde{\underline{D}}(\underline{k})\rangle = \varepsilon_o[\underline{I} + \frac{(2\pi)^3\rho}{k_o^2}\tilde{\underline{t}}(\underline{k},\underline{k})]\cdot\langle\tilde{\underline{E}}(\underline{k})\rangle \quad (4\text{-}1\text{-}10)$$

The constitutive relation

$$\underline{D} = \varepsilon_o\underline{\varepsilon}\cdot\underline{E} \quad (4\text{-}1\text{-}11)$$

indicates that Equation (4-1-10) may be re-written in the form

$$\langle\tilde{\underline{D}}(\underline{k})\rangle = \varepsilon_o\underline{\varepsilon}\cdot\langle\underline{E}(\underline{k})\rangle \quad (4\text{-}1\text{-}12)$$

and that

$$\underline{\varepsilon} = \underline{I} + \frac{(2\pi)^3\rho}{k_o^2}\tilde{\underline{t}}(\underline{k},\underline{k}) \quad (4\text{-}1\text{-}13)$$

is the effective dyadic permittivity of the equivalent continuous medium. Note that $\underline{\varepsilon}$ depends upon the direction of propagation through the wave vector $\underline{k}$; such a medium is termed spatially dispersive*. Because $\underline{\varepsilon}$ is a dyadic, the medium is termed anisotropic. It is also interesting to note that, far from the source where the mean field $\langle\underline{E}(\underline{x})\rangle$ is essentially planar, only those components of $\underline{\varepsilon}$ which are orthogonal to the direction of propagation will be of significance. This is consistent with the relation established in Section 2.3 between $\tilde{\underline{t}}$ and the dyadic scattering amplitude of $\underline{f}$ [refer to Equation (2-3-23)].

In the low-frequency (Rayleigh scattering) limit, where each scatterer can be represented as an electric dipole with dyadic polarization $\underline{\alpha}$, the Fourier transform of Equation (2-3-17)

*Landau and Lifschitz.

$$\underline{\underline{t}}(\underline{k},\underline{k}') = k_o^2 \underline{\underline{\alpha}}/(2\pi)^3 \qquad (4\text{-}1\text{-}14)$$

can be substituted into Equation (4-1-13) to yield

$$\underline{\underline{\varepsilon}} = \underline{\underline{I}} + \rho\underline{\underline{\alpha}} \qquad (4\text{-}1\text{-}15)$$

in the Rayleigh regime. Note that in the Rayleigh regime, $\underline{\underline{\varepsilon}}$ is no longer dependent upon the direction of the wave vector $\underline{k}$; however, the medium can be anisotropic.

The effective dyadic susceptibility can be defined as

$$\underline{\underline{\chi}} = \underline{\underline{\varepsilon}} - \underline{\underline{I}} \qquad (4\text{-}1\text{-}16)$$

so that, in general, as a consequence of Equation (4-1-13)

$$\underline{\underline{\chi}} = \frac{(2\pi)^3 \rho}{k_o^2} \underline{\underline{t}}(\underline{k},\underline{k}) \qquad (4\text{-}1\text{-}17)$$

However, in the Rayleigh regime, as a consequence of Equation (4-1-15)

$$\underline{\underline{\chi}} = \rho\underline{\underline{\alpha}} \qquad (4\text{-}1\text{-}18)$$

It is apparent from Equations (4-1-17) and (4-1-18) that the effective dyadic susceptibility is directly proportional to the number density of the discrete scatterers. For this reason, $\underline{\underline{\chi}}$ is often preferred over $\underline{\underline{\varepsilon}}$ for the characterization of the equivalent medium. Because of the assumed $\exp\{j\omega t\}$ time-dependence of all field quantities, it proves convenient to define the real and imaginary parts of $\underline{\underline{\chi}}$ so that $\underline{\underline{\chi}} = \underline{\underline{\chi}}' - j\underline{\underline{\chi}}''$

In general, the effective dyadic sysceptibility $\underline{\underline{\chi}}$ can be written explicitly in terms of the unit vectors $\underline{h}^\circ$, $\underline{v}^\circ$, and $\underline{i}^\circ$. Here, $\underline{i}^\circ$ is a unit vector in the direction of propagation and $\underline{h}^\circ$ and $\underline{v}^\circ$ are the polarization vectors. In component form, $\underline{\underline{\chi}}$ is

$$\underline{\underline{\chi}} = \sum_{\underline{\alpha}^\circ \underline{\beta}^\circ} \chi_{\alpha\beta} \alpha^\circ \beta^\circ \quad , \quad \alpha^\circ, \beta^\circ \in \{\underline{h}^\circ, \underline{v}^\circ, \underline{i}^\circ\} \qquad (4\text{-}1\text{-}19)$$

There are nine components. However, only χ_{hh}, χ_{hv}, χ_{vh}, and χ_{vv} are important. The other components are either zero or do not contribute at this level of approximation. These four principal components of the effective dyadic susceptibility can be determined directly from the components of the dyadic scattering amplitude $\underline{\underline{f}}$. Equations (2-3-26), (4-1-17), and (4-1-19) yield

$$\chi_{pq} = \frac{4\pi\rho}{k_o^2} \overline{f_{pq}(\underline{i},\underline{i})} \qquad p,q \in \{h,v\} \qquad (4\text{-}1\text{-}20)$$

The development presented above leading to the concept of an effective dyadic permittivity was predicated upon the mean-wave equation for three-dimensional scattering from three-dimensional scatterers [Equation (4-1-1)]. An analogous result, the mean-wave equation for three-dimensional scattering from two-dimensional scatterers, was developed in Section 2.4 [Equation (2-3-29)]. As a consequence, an effective dyadic susceptibility for a continuous medium equivalent to an unbounded ensemble of two-dimensional scatterers can be analogously defined with the effective dyadic susceptiblility given by

$$\underline{\chi} = \frac{(2\pi)^2 \rho}{k_o^2} \overline{\underline{\tilde{f}}(k_t, k_t; k_z)} \qquad (4\text{-}1\text{-}21)$$

Here again only the χ_{hh}, χ_{hv}, χ_{vh} and χ_{vv} components are important. They can be directly related to the four components of the two-dimensional dyadic scattering amplitude by employing Equation (2-4-10) in component form. The result is

$$\chi_{pq} = \frac{(2\pi)^2 \rho}{\gamma k_o^2} \overline{f_{pq}(\underline{i}, \underline{i})} \quad , \quad p,q \varepsilon \{h,v\} \qquad (4\text{-}1\text{-}22)$$

where γ is given in Equation (2-2-24).

4.1.1 Effective Dyadic Susceptibility of Trunks

The radiowave propagation model developed in this report views the forest as a random ensemble of tree trunks, branches and leaves having prescribed location and orientation statistics. Tree trunks are modelled as vertical lossy dielectric circular cylinders of infinite length. The salient scattering properties of individual cylinders can be characterized in terms of the dyadic scattering amplitude $\underline{f}$ which was determined earlier in Section 3.1. The effective dyadic susceptibility for an unbounded forest of tree trunks can be found using Equation (4-1-22).

$$\chi_{pp} = \frac{j\rho 4}{(k_o)^2 \sin\theta_i} \left(C_o^{(pp)} + 2 \sum_{n=1}^{\infty} C_n^{(pp)} \right) \quad , \quad p \varepsilon \{h,v\} \qquad (4\text{-}1\text{-}1\text{-}1)$$

The $C_n^{(pp)}$ are given by Equations (3-1-3) and (3-1-4). As was pointed out in Section 3, there is no depolarization of the electromagnetic wave in the forward scattering direction by vertical circular cylinders, i.e. $f_{hv}(\underline{i},\underline{i}) = f_{hv}(\underline{i},\underline{i}) = 0$, thus

$$\chi_{hv} = \chi_{vh} = 0 \qquad (4\text{-}1\text{-}1\text{-}2)$$

and the equivalent continuous medium for vertical trunks is uniaxially anisotropic.

The effective dyadic susceptibility of tree trunks as expressed by Equation (4-1-1-1) is exemplified in Figures 4-1 and 4-2 for the case of a radiowave propagating parallel to the forest floor (θ_i=90°). These calculations are based upon a tree trunk radius of 10 centimeters and a trunk number density of 1 trunk per square meter. Three models are employed to describe the permittivity of the wood [refer to Appendix A], but only CyberCom model III can be considered realistic. The horizontal components of the effective dyadic susceptibility (denoted by χ_{hh}, in general, but here for θ_i=90° by χ_t) are shown in Figure 4-1; the vertical component of the effective dyadic susceptibility (denoted by χ_{vv}, in general, but here for θ_i=90° by χ_z) shown in Figure 4-2.

It is seen from these figures that the effective dyadic susceptibility $\underline{\chi}$ is relatively insensitive to the CyberCom model employed for wood permittivity. Further, although the resonant response apparent in these figures is not shown in detail (calculations having been made at 100 MHz intervals), it is clear that for tree trunks of this (10 centimeter) radius, resonance plays a major role in the frequency band 200 - 2000 MHz. In this frequency band the real parts of the dyadic susceptibility (χ_t',χ_z') decrease roughly as the square of the frequency; the imaginary part of the horizontal component (χ_t'') decreases roughly as the two-thirds power of the frequency; and the imaginary part of the vertical component (χ_z'') decreases roughly as the five-thirds power of the frequency.

Tamir [107], concerned only with frequencies below 200 MHz, has suggested that the forest could be represented by an effective

scalar permittivity (ε') of about 1.1 and an effective conductivity (σ) of about 10^{-4}mhos/meters [refer to Figure 1-1]. The relations

$$\chi' = \varepsilon' - 1 \qquad (4\text{-}1\text{-}1\text{-}3)$$

$$\chi'' = \sigma/\omega\varepsilon_o \qquad (4\text{-}1\text{-}1\text{-}4)$$

can be used to deduce the effective scalar susceptibilities suggested by Tamir; these susceptibilities are also plotted in Figure 4-1 and 4-2. It is apparent from these figures that the frequency-independent value of χ' suggested by Tamir differs significantly from the inverse frequency-squared dependent of χ_t', χ_z' found by CyberCom; the inverse frequency-dependent value of χ'' suggested by Tamir is about one order of magnitude smaller than the corresponding values of χ_t'', χ_z'' found by CyberCom. Near agreement between χ'' and χ_t'', χ_z'' could be achieved by decreasing the assumed tree trunk number density from 1 tree trunk per square meter to 0.2 tree trunk per square meter. Although not shown in this figure, the low-frequency (Rayleigh) behavior of the vertical component (χ_t', χ_t'') agrees with Tamir's model for CyberCom wood permittivity models II and III. This Rayleigh behavior is also anticipated in the frequency band 200 - 2000 MHz for tree trunks (and branches) of extremely small radius (less than 1 centimeter).

4.1.2 Effective Dyadic Susceptibility of Branches

Branches are modeled as lossy-dielectric circular cylinders of radius a and length ℓ. The salient scattering properties of individual finite-length cylinders can be characterized in terms of their dyadic scattering amplitude $\underline{f}$ which is given in Section 3.2. The component susceptibilities for an unbounded forest of branches can be found by employing Equation (4-1-20).

The four components of the dyadic scattering amplitude in the forward direction $\underline{o} = \underline{i}$ can be obtained from Equation (3-2-16) by dotting it from the left and right with the horizontal and vertical polarization vectors. Thus,

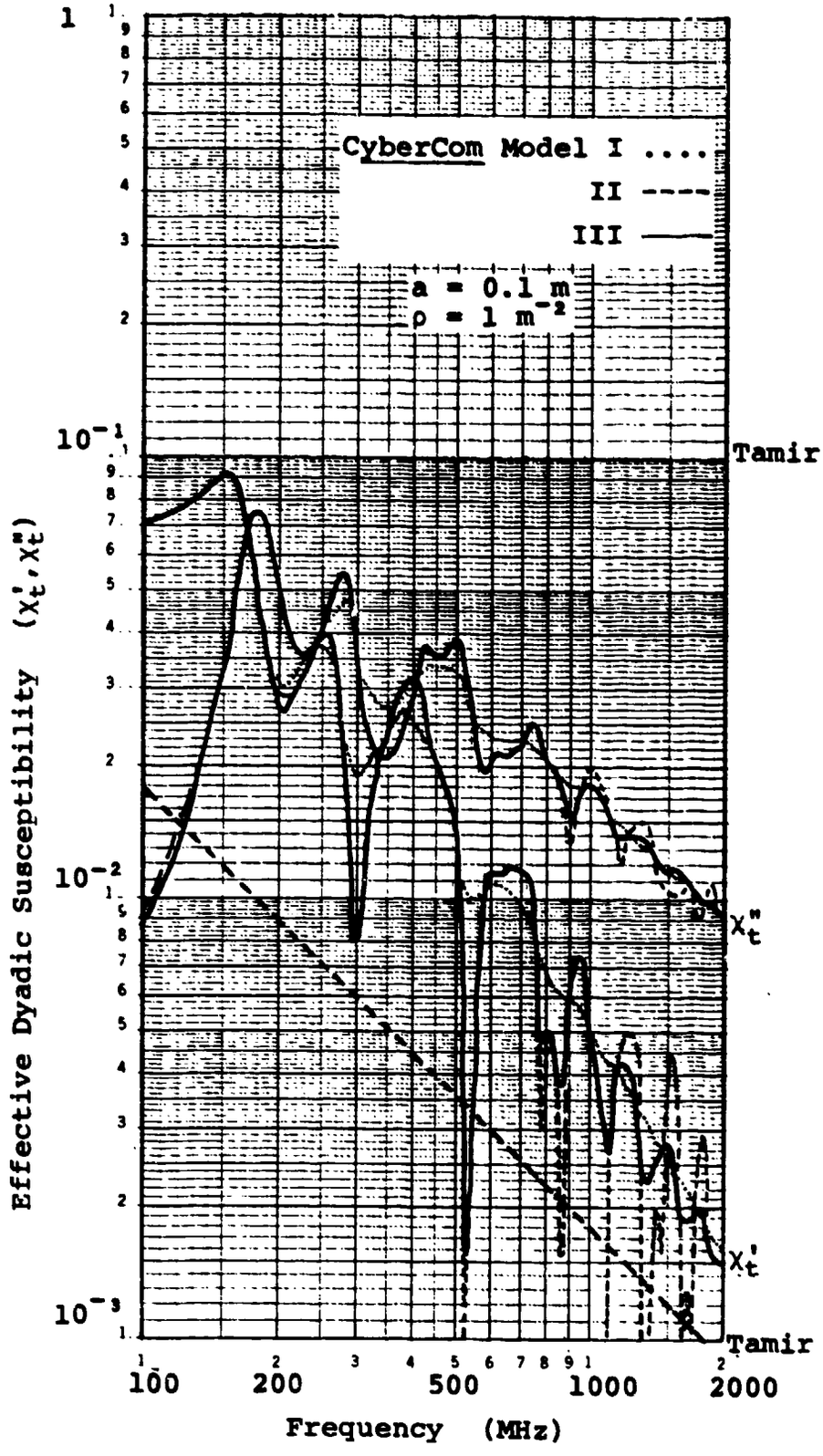

Figure 4-1: Effective Dyadic Susceptibility - Trunks

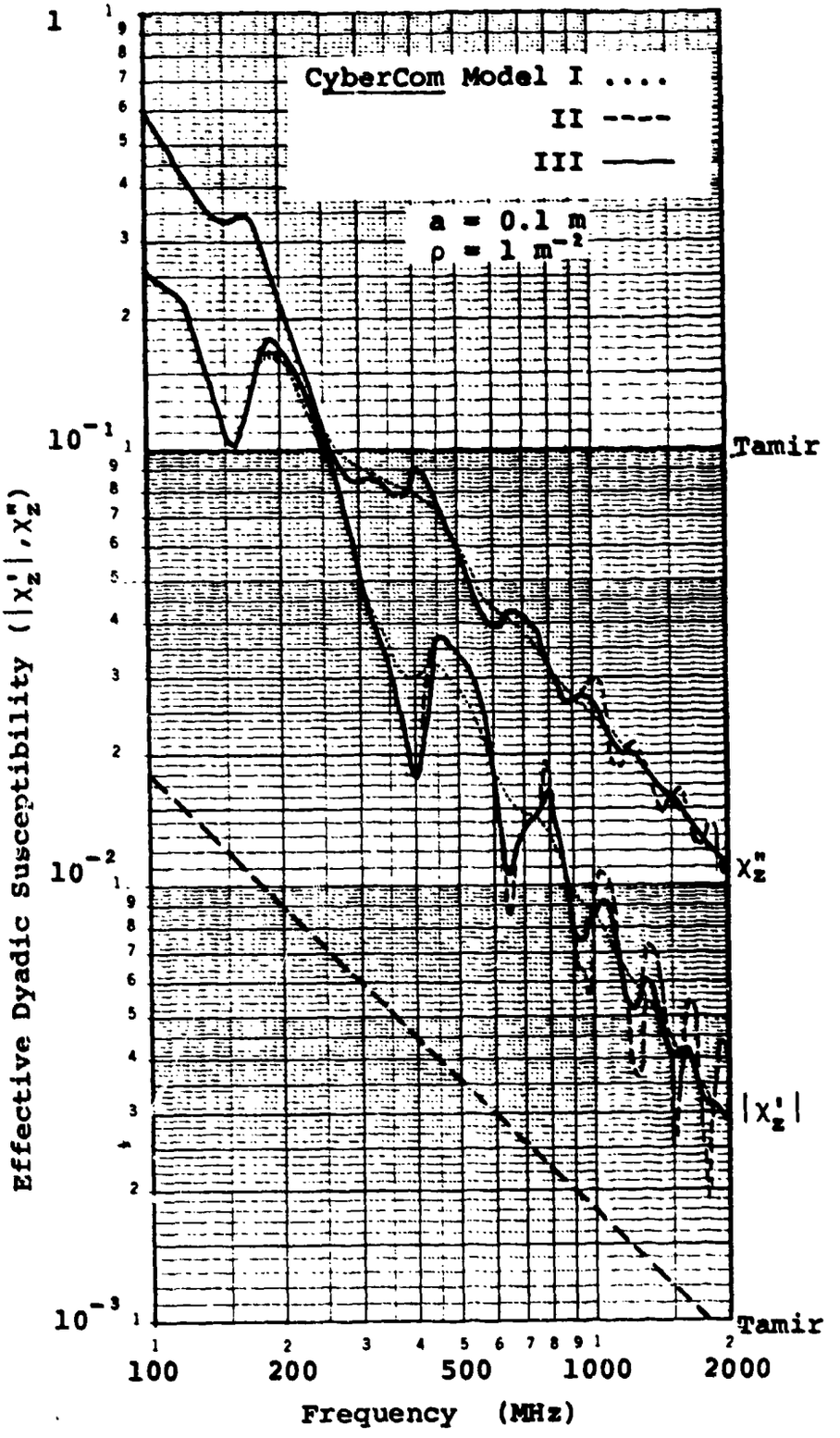

Figure 4-2: Effective Dyadic Susceptibility - Trunks

$$f_{p,q}(\underline{i},\underline{i}) = \left(\frac{k_o a}{2}\right)^2 \chi_\ell \ell \left\{ \frac{\chi_\ell}{\chi_\ell} (\underline{p}^\circ \cdot \underline{r}^\circ)(\underline{r}^\circ \cdot \underline{q}^\circ) + \frac{2\underline{p}^\circ \cdot \underline{q}^\circ}{2+\chi_\ell} \right\} \qquad (4\text{-}1\text{-}2\text{-}1)$$

The mean scattering amplitudes are given by

$$\overline{f_{pq}(\underline{i},\underline{i})} = \int_0^\pi d\theta \int_0^{2\pi} d\phi p(\theta,\phi) f_{pq}(\underline{i},\underline{i}) \qquad (4\text{-}1\text{-}2\text{-}2)$$

where $p(\theta,\phi)$ is the probability density function of branch inclinations. If it is assumed that the branches are distributed uniformly in the azimuthal angle ϕ and that all have the same polar angle θ_b then

$$p(\theta,\phi) = \frac{\delta(\theta-\theta_b)}{2\pi} \qquad (4\text{-}1\text{-}2\text{-}3)$$

Now, using $\underline{i}$ [as given in Equation (3-0-2)] in Equations (3-0-3) and (3-0-4), the following expressions can be obtained for $\underline{h}_i^\circ$ and $\underline{v}_i^\circ$

$$\underline{h}_i^\circ = -\underline{x}^\circ \sin\phi_i + \underline{y}^\circ \cos\phi_i \qquad (4\text{-}1\text{-}2\text{-}4)$$

$$\underline{v}_i^\circ = -\underline{x}^\circ \cos\phi_i \cos\theta_i - \underline{y}^\circ \sin\phi_i \cos\theta_i + \underline{z}^\circ \sin\theta_i \qquad (4\text{-}1\text{-}2\text{-}5)$$

In addition $\underline{r}^\circ$, which is a unit-vector directed along the branch, can be written as

$$\underline{r}^\circ = \underline{x}^\circ \sin\phi \sin\theta + \underline{y}^\circ \sin\phi \sin\theta + \underline{z}^\circ \cos\theta \qquad (4\text{-}1\text{-}2\text{-}6)$$

When these expressions for the unit vectors $\underline{h}_i^\circ$, $\underline{v}_i^\circ$ and $\underline{r}^\circ$ are used in Equation (4-1-2-1) and the result averaged over the probability density function given in Equation (4-1-2-3)

$$\overline{f_{hh}(\underline{i},\underline{i})} = \left(\frac{k_o a}{2}\right)^2 \chi_\ell \ell \left[\frac{\chi_\ell}{2(2+\chi_\ell)} \sin^2\theta_b + \frac{2}{2+\chi_\ell} \right] \qquad (4\text{-}1\text{-}2\text{-}7)$$

$$\overline{f_{vv}(\underline{i},\underline{i})} = \left(\frac{k_o a}{2}\right)^2 \chi_\ell \ell \left[\frac{\chi_\ell}{2(2+\chi_\ell)} (\cos^2\theta_i \sin^2\theta_b + 2\sin^2\theta_i \cos^2\theta_b) + \frac{2}{2+\chi_\ell}\right] \quad (4\text{-}1\text{-}2\text{-}8)$$

are obtained. The depolarized forward-scattering amplitudes both average to zero so that

$$\overline{f_{hv}(\underline{i},\underline{i})} = \overline{f_{vh}(\underline{i},\underline{i})} = 0 \quad (4\text{-}1\text{-}2\text{-}9)$$

The four principal components of the effective dyadic susceptibility are then found by substituting the above results into Equation (4-1-20) and obtaining

$$\chi_{hh} = \pi \chi_\ell \rho a^2 \ell \left[\frac{\chi_\ell}{2(2+\chi_\ell)} \sin^2\theta_b + \frac{2}{2+\chi_\ell}\right] \quad (4\text{-}1\text{-}2\text{-}10)$$

$$\chi_{vv} = \pi \chi_\ell \rho a^2 \ell \left[\frac{\chi_\ell}{2(2+\chi_\ell)} (\cos^2\theta_i \sin^2\theta_b + 2\sin^2\theta_i \cos^2\theta_b) + \frac{2}{2+\chi_\ell}\right] \quad (4\text{-}1\text{-}2\text{-}11)$$

$$\chi_{hv} = \chi_{vh} = 0 \quad (4\text{-}1\text{-}2\text{-}12)$$

Thus the equivalent continuous medium for an azimuthally symmetric distribution of branches is uniaxially anisotropic.

The effective dyadic susceptibility of the branches as expressed by Equations (4-1-2-10) and (4-1-2-11) is exemplified in Figure 4-3 for the case of a radiowave propagating parallel to the forest floor ($\theta_i = 90°$). These calculations are based upon a branch radius of 1 centimeter, a branch length of 1 meter, and a branch number density of 1 branch per cubic meter. All branches are assumed to be inclined 45 degrees with respect to the vertical, but uniformly oriented in azimuth. Three models are employed to describe the permittivity of the wood [refer to Appendix A], but only model III can be considered realistic. The horizontal

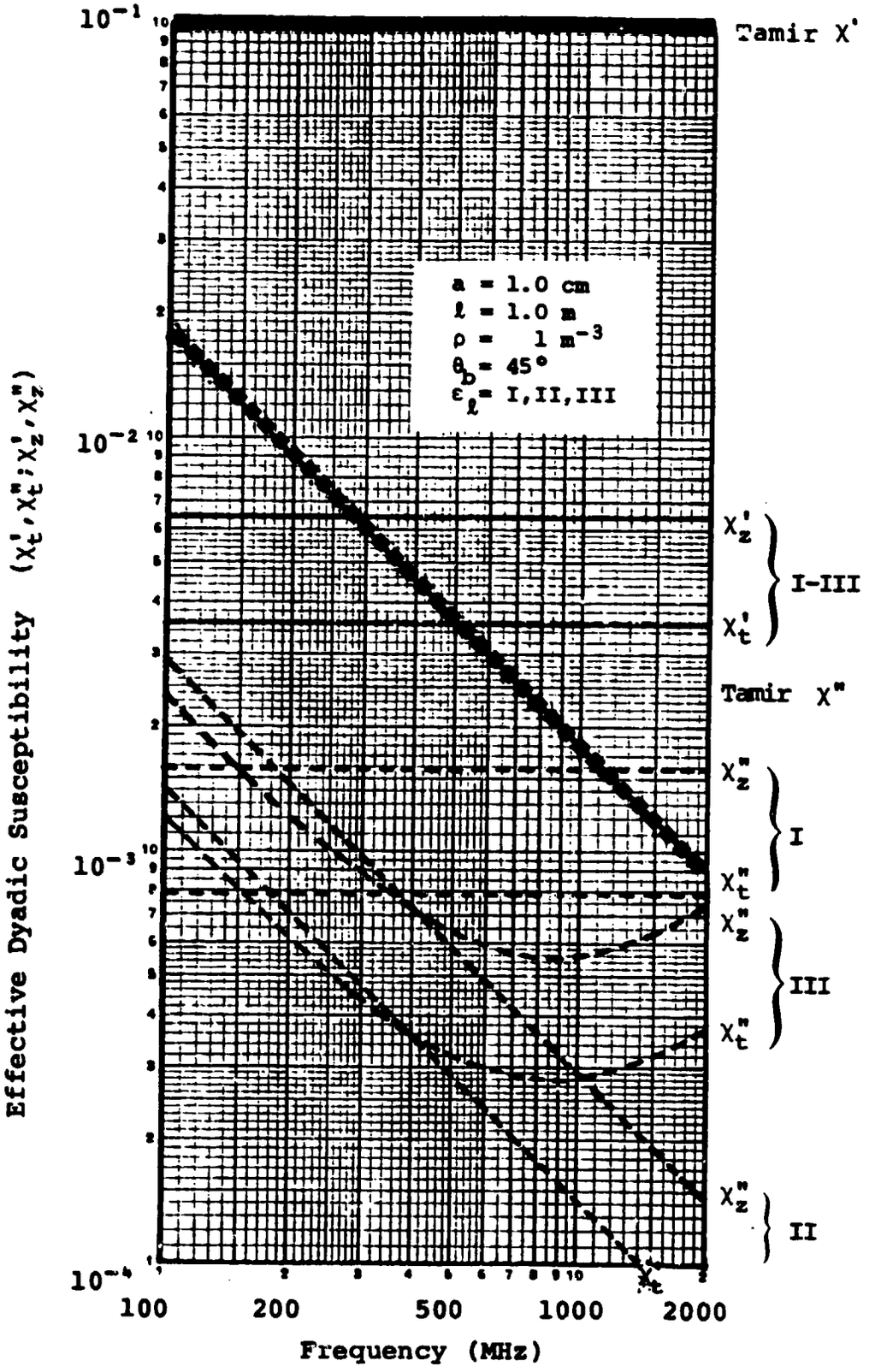

Figure 4-3: Effective Dyadic Susceptibility - Branches

and vertical components of the effective dyadic susceptibility (denoted by χ_{hh} and χ_{vv}, in general, but here for $\theta_o = 90°$ by χ_t and χ_z, respectively) are shown in Figure 4-3. Assumptions implicit in the development of the thin-branch scattering model preclude the consideration of branches of significantly greater radius over the frequency band 200 - 2000 MHz.

In the thin-branch frequency regime, the frequency behavior of the effective dyadic susceptibility is determined by the frequency behavior of the susceptibility of a single scatterer. For branches, this is clearly evident from Equations (4-1-2-10) and (4-1-2-11), where the only frequency-dependent parameter is the susceptibility of the wood χ_ℓ. Further, since all three models for wood permittivity satisfy the inequality [refer to Appendix A]

$$\chi''_\ell << \chi'_\ell = 39 \qquad (4\text{-}1\text{-}2\text{-}13)$$

it is apparent from Equations (4-1-2-10) and (4-1-2-11) that for branches

$$\chi''_{hh} \approx \pi \chi''_\ell \rho a^2 \ell \left[\frac{1}{2} \sin^2\theta_b + \frac{1}{20}\right] \qquad (4\text{-}1\text{-}2\text{-}14)$$

$$\chi''_{vv} \approx \pi \chi''_\ell \rho a^2 \ell \left[\frac{1}{2} (\cos^2\theta_i \sin^2\theta_b + 2\sin^2\theta_i \cos^2\theta_b) + \frac{1}{20}\right] \qquad (4\text{-}1\text{-}2\text{-}15)$$

These equations explain why the frequency behavior of χ''_t and χ''_z shown in Figure 4-3 so closely reflects the frequency behavior of χ''_ℓ shown in Figure A-2 of Appendix A. Note that, in contradistinction to resonant scattering, scatterer dimensions do not affect the frequency behavior of $\underline{\chi}$.

The effective scalar susceptibilities suggested by Tamir [refer to Section 4.1.1] are also shown in Figure 4-3. These values appear to be about one order of magnitude greater than the computed values of $\underline{\chi}$. This disparity may be attributed to the fairly low branch number density assumed for the calculations (1 branch per cubic meter) and also to the fact that Tamir's value includes, not only the effects of branches, but all other vegetative components as well.

4.1.3 Effective Dyadic Susceptibility of Leaves

Leaves are modelled as lossy-dielectric circular discs. The salient scattering properties of individual discs can be characterized in terms of their dyadic scattering amplitude $\underline{f}$ which is given in Section 3.3. The component susceptibilities for an unbounded forest of leaves can be found by employing Equation (4-1-20).

According to Equation (3-3-30), the four components of the dyadic scattering amplitude in the direction of forward scatter are

$$f_{pq}(\underline{i},\underline{i}) = \pi X_\ell (k_o/2\pi)^2 (e_{pq}^+ \operatorname{sinc}\theta^+ + e_{pq}^- \operatorname{sinc}\theta^-) \qquad (4\text{-}1\text{-}3\text{-}1)$$

where,

$$e_{pq}^\pm = \underline{p}^o \cdot \underline{e}^\pm \cdot \underline{q}^o \quad , \quad p,q\varepsilon\{h,v\} \qquad (4\text{-}1\text{-}3\text{-}2)$$

and all other parameters are defined in Section 3.3. The mean scattering amplitude, averaged over leaf orientation and required in Equation (4-1-20), is given by

$$\overline{f_{pq}(\underline{i},\underline{i})} = \int_0^\pi d\theta \int_0^{2\pi} d\phi p(\theta,\phi) f_{pq}(\underline{i},\underline{i}) \qquad (4\text{-}1\text{-}3\text{-}3)$$

where $p(\theta,\phi)$ is the probability density function of the leaf inclinations. Unfortunately, even under the assumption that the leaves are distributed uniformly in azimuth so that

$$p(\theta,\phi) = \frac{1}{2\pi} p(\theta) \qquad (4\text{-}1\text{-}3\text{-}4)$$

the expression

$$\overline{f_{pq}(\underline{i},\underline{i})} = \frac{1}{2\pi} \int_0^\pi d\theta p(\theta) \int_0^{2\pi} d\phi f_{pq}(\underline{i},\underline{i}) \qquad (4\text{-}1\text{-}3\text{-}5)$$

is difficult to evaluate analytically because of the complex dependence of $f_{pq}(i,i)$ on the azimuthal angle ϕ. Although it can be shown on the basis of symmetry that the cross-polarized components must average to zero so that

$$\overline{f_{hv}(\underline{i},\underline{i})} = \overline{f_{vh}(\underline{i},\underline{i})} = 0 \qquad (4\text{-}1\text{-}3\text{-}6)$$

the co-polarized components have been obtained only by using numerical integration.

Explicit expressions for the averaged co-polarized components can be found, however, when the discs are electrically thin and satisfy the inequality

$$k_o\sqrt{\varepsilon_\ell}\, t << 1 \qquad (4\text{-}1\text{-}3\text{-}7)$$

Then, according to Equation (3-3-38)

$$f_{pp}(\underline{i},\underline{i}) = \left(\frac{k_\ell a}{2}\right)^2 \chi_\ell t\left[1 - \frac{\chi_\ell}{1+\chi_\ell}(\underline{p}^o\cdot\underline{n}^o)^2\right] \qquad (4\text{-}1\text{-}3\text{-}8)$$

Using Equations (3-0-2), (3-0-3) and (3-0-4) to recast Equation (4-1-3-8) in terms of the angular variables , and substituting the result into Equation (4-1-3-5) yields the following explicit expressions for the co-polarized components

$$\overline{f_{hh}(\underline{i},\underline{i})} = \left(\frac{k_\ell a}{2}\right)^2 \chi_\ell t\left[1 - \frac{\chi_\ell}{2(1+\chi_\ell)} I_1\right] \qquad (4\text{-}1\text{-}3\text{-}9)$$

$$\overline{f_{vv}(\underline{i},\underline{i})} = \left(\frac{k_\ell a}{2}\right)^2 \chi_\ell t\left[1 - \frac{\chi_\ell}{2(1+\chi_\ell)} (I_1\cos^2\theta_i + 2I_2\sin^2\theta_i)\right] \qquad (4\text{-}1\text{-}3\text{-}10)$$

where,

$$I_1 = \int_0^\pi d\theta p(\theta)\sin^2\theta \qquad (4\text{-}1\text{-}3\text{-}11)$$

$$I_2 = \int_0^\pi d\theta p(\theta)\cos^2\theta \qquad (4\text{-}1\text{-}3\text{-}12)$$

The effective dyadic susceptibility for an unbounded forest of electrically thin leaves can be obtained by substituting Equations (4-1-3-6), (4-1-3-9) and (4-1-3-10) into Equation (4-1-20) and finding

$$\chi_{hh} = \pi\chi_\ell \rho a^2 t\left[1 - \frac{\chi_\ell}{2(1+\chi_\ell)} I_1\right] \qquad (4\text{-}1\text{-}3\text{-}13)$$

Again it is seen that the equivalent continuous medium for an azimuthally-symmetric distribution of leaves is uniaxially anisotropic.

$$\chi_{vv} = \pi\chi_{\ell}\rho a^2 t\left[1 - \frac{\chi_{\ell}}{2(1+\chi_{\ell})}\left(I_1\cos^2\theta_i + 2I_2\sin^2\theta_i\right)\right] \qquad (4\text{-}1\text{-}3\text{-}14)$$

$$\chi_{hv} = \chi_{vh} = 0 \qquad (4\text{-}1\text{-}3\text{-}15)$$

subject to the condition $k_o\sqrt{\varepsilon_{\ell}}\, t << 1$. Typically, leaves are no more than about 1 millimeter thick; according to Appendix A, $\varepsilon_{\ell} \approx 40$. As a consequence, Equations (4-1-3-13), (4-1-3-14) and (4-1-3-15) should prove valid over the entire frequency band 200 - 2000 HMz.

The effective dyadic susceptibility of leaves in the thin-disc approximation [Equations (4-1-3-13) and (4-1-3-14)] is exemplified in Figure 4-4 for the case of a radiowave propagating parallel to the forest floor ($\theta_i = 90°$). These calculations are based upon a leaf radius of 5 centimeters, a leaf thickness of 1 millimeter, and a leaf number density of 200 leaves per cubic meter, fairly typical values. The random orientation of the leaves is described by a probability density function assumed to be uniform in azimuth, and uniform in elevation angle over the range 0-30 degrees (the leaves tend to be horizontal). Three models are employed to describe the permittivity of the leaves [refer to Appendix A], but only model III can be considered realistic. The horizontal and vertical components of the effective dyadic susceptibility (denoted by χ_{hh} and χ_{vv}, in general, but here for $\theta_i = 90°$ by χ_t and χ_z, respectively) are shown in Figure 4-4.

The effective scalar susceptibilities suggested by Tamir [refer to Section 4.1.1] are also shown in Figure 4-4. The agreement between Tamir's values and those for χ_t'' based upon leaf permittivity models II and III for frequencies below 500 MHz is remarkable. At higher frequencies, relaxation losses attributable to polarization of the water molecule [refer to Appendix I] are likely to be appreciable, thereby invalidating both the Tamir values and those computed on the basis of leaf permittivity model II.

A comparison of Figures 4-3 and 4-4 reveals that for the leaves $\chi_t > \chi_z$ whereas for the branches $\chi_t < \chi_z$. This difference

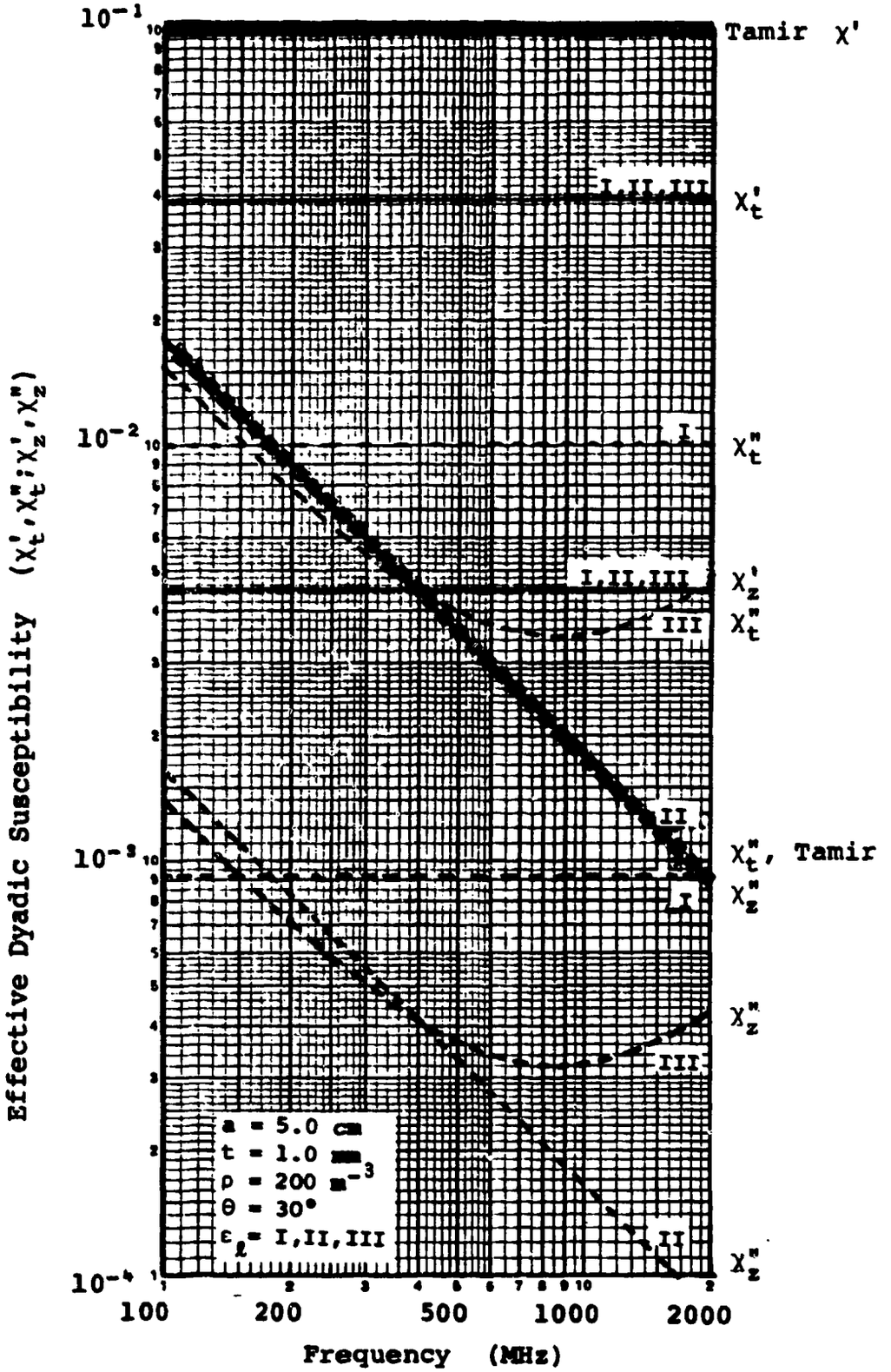

Figure 4-4: Effective Dyadic Susceptibility - Leaves

is explained by noting that, for the leaf and branch orientation distributions assumed in the calculations, the leaves present primarily a horizontal profile to a propagating radiowave (discs with axes at 0° to 30° from vertical), whereas the branches present primarily a vertical profile (rods at 45° that appear vertical when in plane with viewer). Under these conditions, a horizontally-polarized radiowave tends to be more susceptible to the effects of the leaves, whereas a vertically-polarized radiowave tends to be more susceptible to the effects of the branches.

4.2 Plane-Wave Propagation

4.2.1 Dispersion Relation

The mean electric field propagating within an unbounded ensemble of three-dimensional scatterers can be determined, as shown in Section 2.3, from the mean wave equation

$$\underline{\underline{L}}\cdot\langle\underline{E}(\underline{x})\rangle - \int d\underline{s}\,\rho(\underline{s})\int d\underline{x}'\,\underline{\underline{t}}(\underline{x}-\underline{s},\underline{x}'-\underline{s})\cdot\langle\underline{E}(\underline{x}')\rangle = -j\omega\mu_o\underline{J}(\underline{x}) \qquad (4\text{-}2\text{-}1)$$

where

$$\underline{\underline{L}} = \nabla x\nabla x\underline{\underline{I}} - k_o^2\underline{\underline{I}} \qquad (4\text{-}2\text{-}2)$$

Consider the plane-wave

$$\langle\underline{E}(\underline{x})\rangle = \underline{E}\, e^{-j\underline{\kappa}\cdot\underline{x}} \qquad (4\text{-}2\text{-}3)$$

to be propagating in a source-free region where

$$\underline{J}(\underline{x}) = 0 \qquad (4\text{-}2\text{-}4)$$

Substitution of Equation (4-2-3) and (4-2-4) into Equation (4-2-1) yields, upon taking the Fourier transformation with respect to the variable $\underline{x}$

$$\underline{\kappa}\times(\underline{\kappa}\times\underline{E}) + k_o^2\left[\underline{\underline{I}} + \frac{1}{k_o^2}\int d\underline{s}\,\rho(\underline{s})\int d\underline{x}'\,\overline{\underline{\underline{t}}(\underline{\kappa},\underline{x}'-\underline{s})}\, e^{j\underline{\kappa}\cdot\underline{s}}\right]\cdot\underline{E} = 0 \qquad (4\text{-}2\text{-}5)$$

Recognizing the second integral appearing in Equation (4-2-5) as a convolution with respect to the parameter $\underline{s}$ and assuming

the number density of the scatterers $\rho(\underline{s})$ to be independent of location so that

$$\rho(\underline{s}) = \rho \tag{4-2-6}$$

Equation (4-2-5) can be written as

$$\underline{\kappa} \times (\underline{\kappa} \times \underline{E}) + k_o^2 \left[\underline{I} + (2\pi)^3 \frac{\rho}{k_o^2} \overline{\underline{\tilde{t}}(\underline{\kappa},\underline{\kappa})} \right] \cdot \underline{E} = 0 \tag{4-2-7}$$

Because the fractional volume occupied by the scatterers is assumed small [see Section 4.3], the second term in the square brackets of Equation (4-2-7) is also small and perturbation techniques can be used to find an approximate solution for $\underline{E}$. For ordering purposes, it is then convenient to replace ρ in Equation (4-2-7) by $\delta\rho$ and expand both $\underline{E}$ and $\underline{\kappa}$ as power series in δ so that

$$\underline{E} = \underline{E}_0 + \underline{E}_1 + ... \tag{4-2-8}$$

$$\underline{\kappa} = (\kappa_0 + \delta\kappa_1 + ...)\underline{i} \tag{4-2-9}$$

Substituting Equations (4-2-8) and (4-2-9) into Equation (4-2-7) and setting to zero the coefficient of each power of δ yields

$$\kappa_0^2[\underline{i} \times (\underline{i} \times \underline{E}_0)] + k_o^2 \underline{E}_0 = 0 \tag{4-2-10}$$

and

$$2\kappa_0\kappa_1[\underline{i} \times (\underline{i} \times \underline{E}_0)] + \kappa_0^2[\underline{i} \times (\underline{i} \times \underline{E}_1)]$$

$$+ k_o^2 \underline{E}_1 + (2\pi)^3 \rho \overline{\underline{\tilde{t}}(\kappa_0\underline{i},\kappa_0\underline{i})} \cdot \underline{E}_1 = 0 \tag{4-2-11}$$

Equation (4-2-10) can be recognized as the free-space wave equation; as a consequence

$$\underline{E}_0 \cdot \underline{i} = 0 \tag{4-2-12}$$

$$\kappa_0 = k_o \tag{4-2-13}$$

Equation (4-2-11) can be simplified by expanding the vector triple-cross products and using Equations (4-2-12) and (4-2-13) to obtain

$$-2k_o\kappa_1\underline{E}_0 + k_o^2(\underline{E}_1 \cdot \underline{i})\underline{i} + (2\pi)^3 \rho \overline{\underline{\tilde{t}}(k_o\underline{i},k_o\underline{i})} \cdot \underline{E}_1 = 0 \tag{4-2-14}$$

This vector equation is equivalent to three linear algebraic equations and, in order for a non-trivial solution to exist, the determinant of the coefficients must be zero. The vector wave numbers (propagation constants) $\underline{\kappa}_1$ satisfying this condition can be determined by expressing $\underline{E}_0$ as

$$\underline{E}_0 = (\underline{E}_0 \cdot \underline{h}^\circ)\underline{h}^\circ + (\underline{E}_0 \cdot \underline{v}^\circ)\underline{v}^\circ \qquad (4\text{-}2\text{-}15)$$

and substituting Equation (4-2-15) into Equation (4-2-14) to obtain the following dispersion relation for κ_1

$$\begin{vmatrix} -2k_o\kappa_1 + (2\pi)^3 \rho \bar{\tilde{t}}_{hh} & (2\pi)^3 \rho \bar{\tilde{t}}_{hv} \\ (2\pi)^3 \rho \bar{\tilde{t}}_{vh} & -2k_o\kappa_1 + (2\pi)^3 \rho \bar{\tilde{t}}_{vv} \end{vmatrix} = 0 \qquad (4\text{-}2\text{-}16)$$

under the assumption that $(\underline{E}_1 \cdot \underline{i}) = 0$. The dispersion relation can also be written in the form

$$k_o^2\kappa_1^2 - Bk_o\kappa_1 + C = 0 \qquad (4\text{-}2\text{-}17)$$

where

$$B = 2\pi\rho[\overline{f_{hh}} + \overline{f_{vv}}] \qquad (4\text{-}2\text{-}18)$$

$$C = (2\pi\rho)^2[\overline{f_{hh}}\,\overline{f_{vv}} - \overline{f_{hv}}\,\overline{f_{vh}}] \qquad (4\text{-}2\text{-}19)$$

and Equation (2-3-23) has been employed to express $\underline{t}$ in terms of the dyadic scattering amplitude $\underline{f}$. As a consequence of Equation (4-2-17), the allowable propagation constants are

$$\kappa_1^{\pm} = \frac{B \pm \sqrt{B^2 - 4C}}{2k_o} \qquad (4\text{-}2\text{-}20)$$

$$\kappa_1^{\pm} = \frac{\pi\rho}{k_o}\left[(\overline{f_{hh}} + \overline{f_{vv}}) \pm \sqrt{(\overline{f_{hh}} - \overline{f_{vv}})^2 + 4\overline{f_{hv}}\,\overline{f_{vh}}}\right] \qquad (4\text{-}2\text{-}21)$$

For classes of scatterers for which

$$\overline{f_{vh}} = \overline{f_{hv}} = 0 \qquad (4\text{-}2\text{-}22)$$

(such as branches and leaves having azimuthally uniform orientation distributions),

$$\kappa_1^+ \equiv \kappa_{1h} = \frac{2\pi\rho}{k_o} \overline{f_{hh}(\underline{i},\underline{i})} \tag{4-2-23}$$

$$\kappa_1^- \equiv \kappa_{1h} = \frac{2\pi\rho}{k_o} \overline{f_{vv}(\underline{i},\underline{i})} \tag{4-2-24}$$

Thus, if $\delta\rho$ is now replaced by ρ (or, equivalently, δ is set equal to unity), Equations (4-2-9), (4-2-13), (4-2-23) and (4-2-24) can be used to show that to first order in the perturbation parameter δ,

$$\kappa_p = k_o + \frac{2\pi\rho}{k_o} \overline{f_{pp}} \quad , \quad p\varepsilon\{h,v\} \tag{4-2-25}$$

whenever Equation (4-2-22) is satisfied.

For three-dimensional wave propagation in two-dimensional media [refer to Section 2.4], a similar development can be pursued to show that, in general,

$$\underline{\kappa} = \underline{\kappa}_t + k_z\underline{z}^o \quad , \quad k_z = k_o\cos\theta_i \quad , \quad \underline{\kappa}_t = \kappa_t\underline{i}_t \tag{4-2-26}$$

where

$$\kappa_t = k_t + \frac{\pi^2\rho}{\gamma k_t}\left[(\overline{f_{hh}} + \overline{f_{vv}}) \pm \sqrt{(\overline{f_{hh}} - \overline{f_{vv}})^2 + 4f_{hv}f_{vh}}\right] \tag{4-2-27}$$

$$k_t = k_o\sin\theta_i$$

and

$$\gamma = \sqrt{\frac{2\pi^3}{k_o}}\, e^{-j\,\pi/4} \tag{4-2-28}$$

If

$$\overline{f_{vh}} = \overline{f_{hv}} = 0 \tag{4-2-29}$$

(as in the case of tree trunks) then Equation (4-2-27) can be simplified to

$$\kappa_{tp} = k_t + \frac{2\pi^2\rho}{\gamma k_o} \overline{f_{pp}(\underline{i},\underline{i})} \quad , \quad p\varepsilon\{h,v\} \tag{4-2-30}$$

4.2.2 Specific Attenuation

In general, the wave propagation constant $\underline{\kappa}$ has both real and imaginary components so that

$$\kappa_p = \kappa_p' - j\kappa_p'' \quad , \quad p\varepsilon\{h,v\} \tag{4-2-31}$$

and, as a consequence,

$$\langle \underline{E}(\underline{x}) \rangle = \underline{E}\, e^{-j\kappa_p'(\underline{i}\cdot\underline{x})} \cdot e^{-\kappa_p''(\underline{i}\cdot\underline{x})} \tag{4-2-32}$$

The real part of the propagation constant (κ_p') is expressed in radians per meter; the imaginary part (κ_p''), also called the specific attenuation, is expressed in nepers per meter or, alternatively, in decibels per meter through the relation

$$\alpha = (20\log_1 e)\kappa_p'' \simeq 8.686\, \kappa_p'' \tag{4-2-33}$$

Because the fractional volume occupied by the vegetation is small, the real part of the propagation constant (κ_p') is dominated by the free-space component (k_o); this is shown in Figure 4-5. The effect of the imaginary part (the specific attenuation κ_p''), however, can be appreciable and is considered further in the following sub-sections.

Some investigators [34, 35, 44, 45] have reported that the measured specific attenuation decreases with increasing path length. The theory developed in this report predicts no such behavior for the mean field of a radiowave propagating directly through an unbounded forest. Such behavior might conceivably arise, however, as a consequence of lateral-wave propagation modes along the air-forest interface [refer to Section 5], non-homogeneous transmission paths through non-uniformly forested regions, and/or random (non-coherent) scattered field behavior [refer to Section 7].

4.2.2.1 Specific Attenuation of Tree Trunks

The radiowave propagation model developed in this report views the forest as a random ensemble of tree trunks, branches and leaves having prescribed location and orientation statistics.

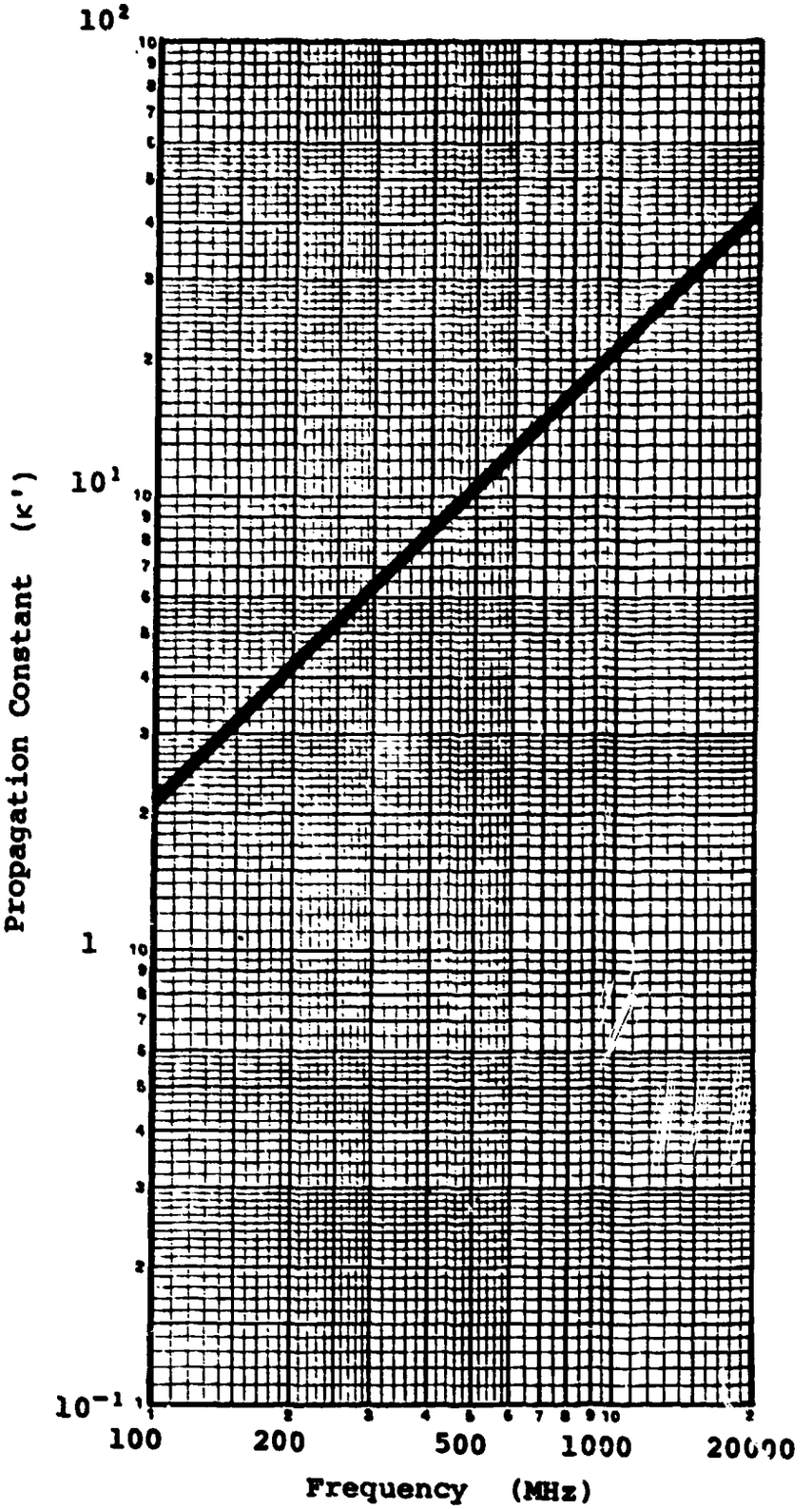

Figure 4-5: Propagation Constant (Real Part)
[Free-Space; Tree Trunks, Branches, Leaves]

Tree trunks are modelled as vertical lossy dielectric circular cylinders of infinite length. The salient scattering properties of individual cylinders can be characterized in terms of the dyadic scattering amplitude $\underline{f}$ which was determined earlier in Section 3.1. The specific attenuation for the mean field propagating through an unbounded forest of tree trunks can be found from the imaginary part of Equation (4-2-30).

The propagation constants for the horizontally- and vertically-polarized components of the mean field propagating through an unbounded forest of parallel tree trunks can be obtained by substituting Equation (3-1-1) into Equation (4-2-30). Recognizing that for a forward-scattered radiowave propagating parallel to the forest floor,

$$\underline{o} = \underline{i} \quad , \quad \theta_i = \pi/2 \quad , \quad \phi_i - \phi_s = -\pi \qquad (4\text{-}2\text{-}1\text{-}1)$$

then

$$C_n^{(pp)} = C_{-n}^{(pp)} \qquad (4\text{-}2\text{-}1\text{-}2)$$

and the equation for the propagation constants simplifies to

$$\kappa_p = k_o\left[1 - j\,\frac{2\rho}{k_o^2}\left(C_o^{(pp)} + 2\sum_{1}^{\infty} C_n^{(pp)}\right)\right] \qquad (4\text{-}2\text{-}1\text{-}3)$$

where,

$$C_n^{(pp)} = \begin{cases} -M_n/P_n \quad , & (p=h) \qquad (4\text{-}2\text{-}1\text{-}4) \\ -V_n/N_n \quad , & (p=v) \qquad (4\text{-}2\text{-}1\text{-}5) \end{cases}$$

and all other parameters are defined in Section 3.1.

The specific attenuation attributable to tree trunks as expressed by the imaginary part of Equation (4-2-1-3) is exemplified in Figure 4-6 for the case of a radiowave propagating parallel to the forest floor ($\theta_i = 90°$). These calculations are based upon a tree trunk radius of 10 centimeters and a trunk number density of 1 trunk per square meter. Three models are employed to describe

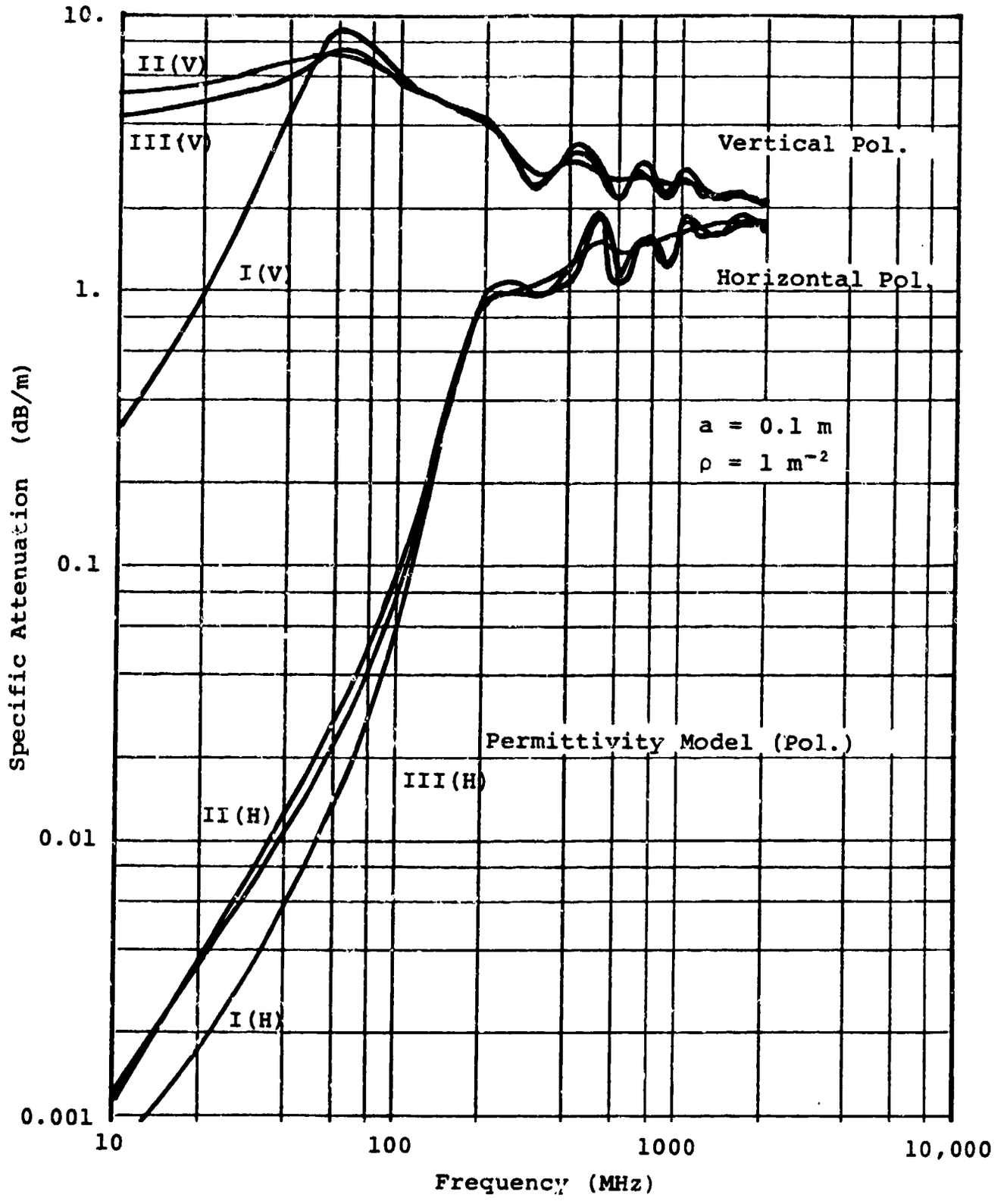

Figure 4-6: Specific Attenuation - Trunks

the permittivity of the wood [refer to Appendix A], but only model III can be considered realistic.

It is apparent from Figure 4-6 that, in agreement with experiment [33, 36, 39, 40], vertically polarized radiowaves are attenuated more severely than are horizontally polarized radiowaves. It is further apparent from Figure 4-6 that for horizontal polarization the specific attenuation is relatively insensitive to the particular choice of the wood permittivity model. This is also true for vertical polarization above 70 Megahertz. This behavior, as well as the oscillatory behavior evident at still higher frequencies and shown in greater detail in Figure 4-7 for several values of θ_o, can be attributed to resonance effects. It is also apparent that above 200 Megahertz resonance plays a major role in tree trunk scatter models and essentially precludes the utilization of simple dipole models at UHF for all but the smallest trees.

In the VHF band, when the radius of the tree trunk is small relative to the radio wavelength within the trunk, Equation (4-2-1-3) reduces to the dipole approximation

$$\kappa_h = k_o[1 + \rho\pi a^2 X_\ell/(2+X_\ell)] \qquad (4\text{-}2\text{-}1\text{-}6)$$

for horizontal polarization, and to

$$\kappa_v = k_o[1 + \rho\pi a^2 X_\ell/2] \qquad (4\text{-}2\text{-}1\text{-}7)$$

for vertical polarization. These equations have been compared with those derived by Brown and Curry [25]. Unfortunately, a direct comparison was not possible because Brown and Curry averaged their results over a uniform distribution of tree-trunk inclination angles and did not provide intermediate results. However, when their technique was used to find the propagation constant appropriate to an array of parallel cylinders, the derived expressions agreed exactly with Equations (4-2-1-6) and (4-2-1-7). This comparison provided an independent check of the CyberCom results.

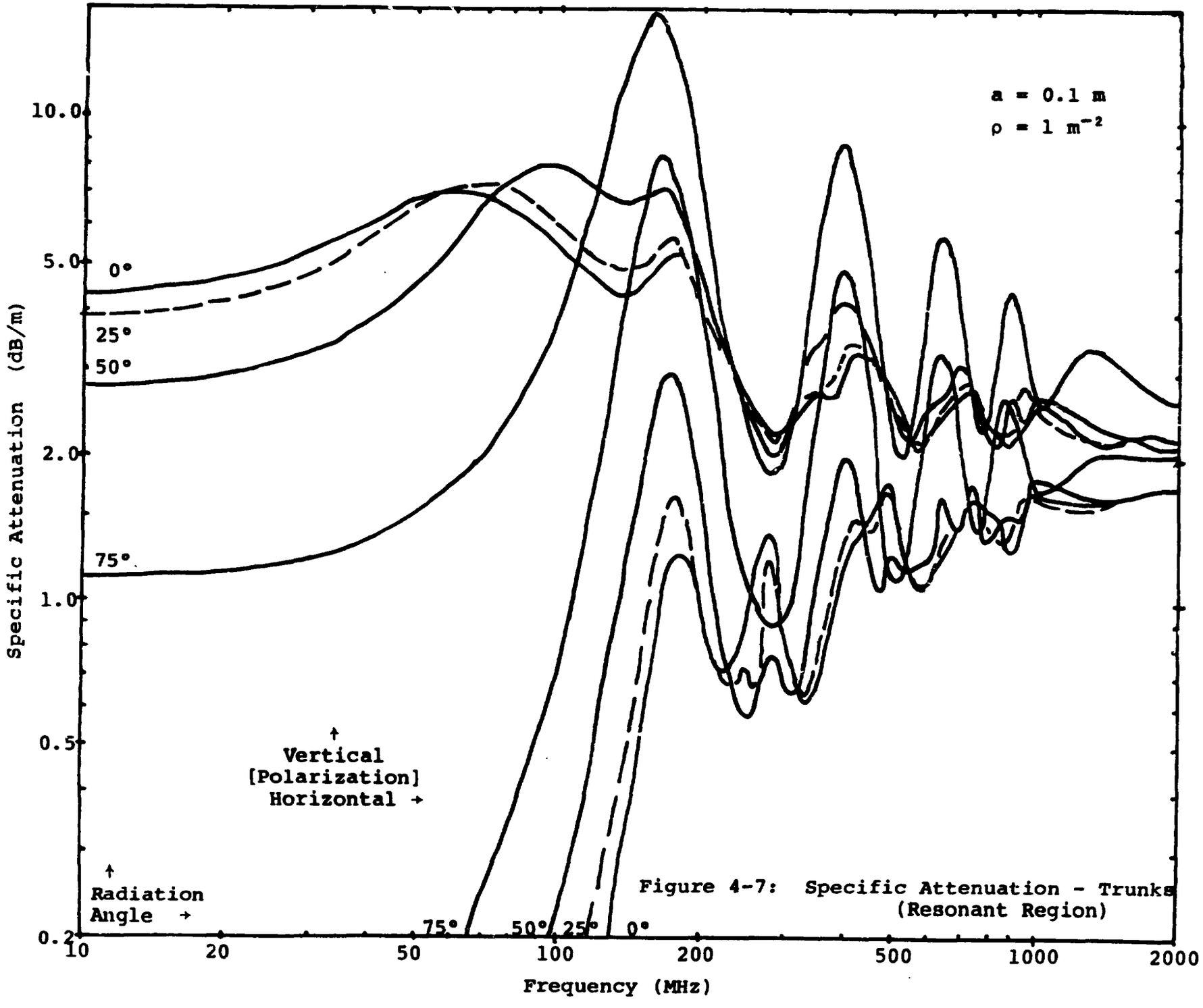

Figure 4-7: Specific Attenuation - Trunks (Resonant Region)

4.2.2.2 Specific Attenuation of Branches

Branches are modelled as lossy dielectric circular cylinders of finite length. The salient scattering properties of individual cylinders can be characterized in terms of the dyadic scattering amplitude $\underline{f}$ which was determined earlier in Section 3.2. The specific attenuation of the mean field propagating through an unbounded forest of branches can be found from the imaginary part of Equation (4-2-25).

The propagation constants of the mean scattered field propagating through an unbounded forest of branches can be obtained by substituting Equations (4-1-2-7) and (4-1-2-8) into Equation (4-2-25) and finding, for the horizontally-polarized component,

$$\kappa_h = k_o\left\{1 + (\rho/2)(\pi a^2 \ell)\chi_\ell\left[\frac{\chi_\ell}{2(2+\chi_\ell)}\sin^2\theta_b + \frac{2}{2+\chi_\ell}\right]\right\} \qquad (4\text{-}2\text{-}2\text{-}1)$$

and, for the vertically-polarized component,

$$\kappa_v = k_o\left\{1 + (\rho/2)(\pi a^2 \ell)\chi_\ell\left[\frac{\chi_\ell}{2(2+\chi_\ell)}(\cos^2\theta_i \sin^2\theta_b + 2\sin^2\theta_i \cos^2\theta_b) + \frac{2}{2+\chi_\ell}\right]\right\} \qquad (4\text{-}2\text{-}2\text{-}2)$$

The specific attenuation attributable to branches as expressed by the imaginary part of Equations (4-2-2-1) and (4-2-2-2) is exemplified in Figure 4-8 for the case of a radiowave propagating parallel to the forest floor ($\theta_i = 90°$). These calculations are based upon a branch radius of 1 centimeter, a branch length of 1 meter, and a branch number density of 1 branch per cubic meter. All branches are assumed to be inclined 45 degrees with respect to the vertical, but uniformly distributed in azimuth. Three models are employed to describe the permittivity of wood [refer to Appendix A], but only model III can be considered realistic. Assumptions implicit in the development of the thin branch scattering model preclude the consideration of branches of significantly greater radius over the frequency band 200 - 2000 MHz.

In the thin-branch frequency regime, the frequency behavior of the specific attenuation is determined by the frequency behavior of the susceptibility of a single scatterer. For branches, this is clearly evident from Equation (4-2-2-1) and (4-2-2-2), where the only frequency-dependent parameter is the susceptibility of the wood χ_ℓ. Further, since all three models for wood permittivity satisfy the inequality [refer to Appendix A].

$$\chi''_\ell << \chi'_\ell = 39 \qquad (4\text{-}2\text{-}2\text{-}3)$$

it is apparent from Equations (4-2-33), (4-2-2-1) and (4-2-2-2) that for radiowaves propagating parallel to the forest floor ($\theta_i = 90°$)

$$\alpha_h \approx (8.686)k_o(\rho/4)(\pi a^2 \ell)\chi''_\ell \sin^2\theta_b \qquad \text{(dB/m)} \qquad (4\text{-}2\text{-}2\text{-}4)$$

and

$$\alpha_v \approx (8.686)k_o(\rho/4)(\pi a^2 \ell)\chi'_\ell \cos^2\theta_b \qquad \text{(dB/m)} \qquad (4\text{-}2\text{-}2\text{-}5)$$

so long as θ_b is not too near 90 degrees.

The empirically-derived behavior predicted by Saxton and Lane [refer to Figure 1-1] is also shown in Figure 4-8. Although the model predictions agree reasonably well with experiment so far as order of magnitude is concerned, only computations based upon wood permittivity model I reflect a similar frequency dependence. However, because wood permittivity model I does not properly account for ohmic losses within the wood, it must be considered nonrealistic and the near agreement between the branch model employing it and experiment only coincidental. This is not to say, however, that the thin-branch model is invalid. It must be recognized that the empirically-derived behavior predicted by Saxton and Lane refers to attenuation through a forest (tree trunks, branches and leaves) and not solely to attenuation through branches. Thus, for example, if tree trunks were the dominant scatterers, the subresonant behavior contributed by the trunks [refer to Figure 4-6] could easily mask the essentially frequency-independent behavior predicted here for the branches using wood permittivity models II and III. Further study is required.

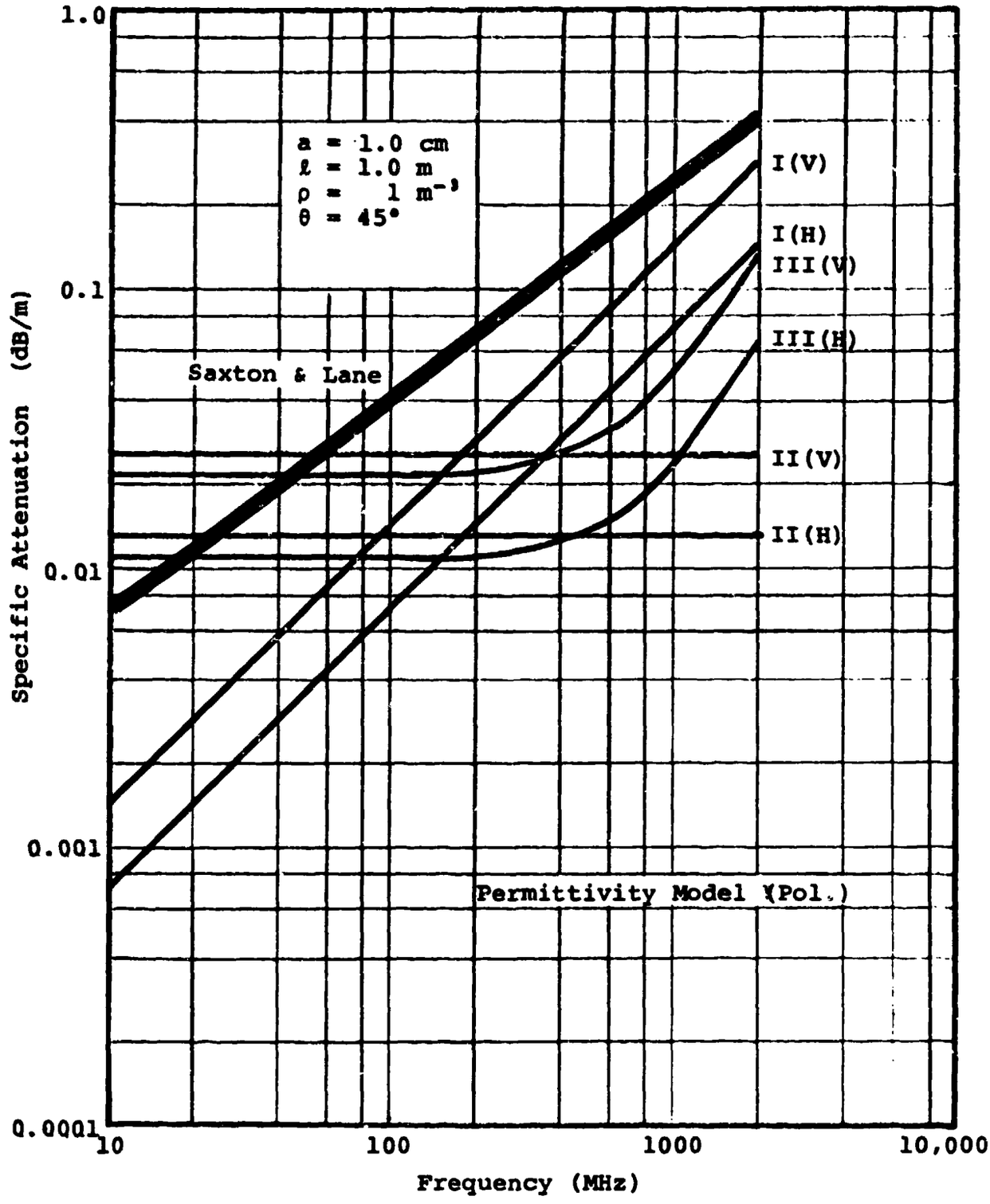

Figure 4-8: Specific Attenuation - Branches

4.2.2.3 Specific Attenuation of Leaves

Leaves are modelled as lossy-dielectric circular discs. The salient scattering properties of individual discs can be characterized in terms of the dyadic scattering amplitude $\underline{f}$ which was determined earlier in Section 3.3. The specific attenuation for the mean field propagating through an unbounded forest of leaves can be found from the imaginary part of Equation (4-2-25).

The propagation constants of the mean scattered field propagating through an unbounded forest of electrically thin leaves can be obtained by substituting Equations (4-1-3-9) and (4-1-3-10) into Equation (4-2-25) and finding, for the horizontally-polarized component

$$\kappa_h = k_o\left\{1 + (\rho/2)(\pi a^2 t)\chi_\ell\left[1 - \frac{\chi_\ell}{2(1+\chi_\ell)} I_1\right]\right\} \qquad (4\text{-}2\text{-}3\text{-}1)$$

and, for the vertically-polarized component

$$\kappa_v = k_o\ 1 + (\rho/2)(\pi a^2 t)\chi_\ell\left[1 - \frac{\chi_\ell}{2(1+\chi_\ell)} (I_1\cos^2\theta_i + 2I_2\sin^2\theta_i)\right] \qquad (4\text{-}2\text{-}3\text{-}2)$$

where,

$$I_1 = \int_0^\pi d\theta p_\ell(\theta)\sin^2\theta \quad ; \quad I_2 = \int_0^\pi d\theta p_\ell(\theta)\cos^2\theta \qquad (4\text{-}2\text{-}3\text{-}3)$$

and $p_\ell(\theta)$ is the probability density function of the leaf inclination angle.

In the frequency band 200 - 2000 Megahertz, leaves may be considered, nearly always, to be electrically thin [refer to Section 4.1.3].

The specific attenuation attributable to leaves as expressed by the imaginary part of Equations (4-2-3-1) and (4-2-3-2) is exemplified in Figure 4-9 for the case of a radiowave propagating parallel to the forest floor ($\theta_i = 90°$). These calculations are based upon a leaf radius of 5 centimeters, a leaf thickness of 1 millimeter, and a leaf number density of 200 leaves per cubic meter. The random orientation of the leaves is described by a probability density function assumed to be uniform in azimuth, and

uniform in elevation over the range of 0 - 30 degrees (the leaves tend to be horizontal). Three models are employed to describe the permittivity of the leaves [refer to Appendix A], but only model III can be considered realistic.

For electrically thin leaves, the frequency behavior of the specific attenuation is determined solely by the frequency behavior of a single scatterer. This is clearly evident from Equations (4-2-3-1) and (4-2-3-2) where the only frequency dependent parameter is the susceptibility of the leaf χ_ℓ. Further, since all three permittivity models satisfy the inequality [refer to Appendix A]

$$\chi''_\ell << \chi'_\ell \approx 39 \qquad (4\text{-}2\text{-}3\text{-}4)$$

it is apparent from Equations (4-2-33), (4-2-3-1) and (4-2-3-2) that for leaves

$$\alpha_h \approx (8.686)k_o(\rho/2)(\pi a^2 t)\chi''_\ell(1 - \tfrac{1}{2}I_1) \qquad (4\text{-}2\text{-}3\text{-}5)$$

$$\alpha_v \approx (8.686)k_o(\rho/2)(\pi a^2 t)\chi''_\ell(1 - I_2) \qquad (4\text{-}2\text{-}3\text{-}6)$$

Especially noteworthy is the strong similarity between the frequency behavior of the leaves [Figure 4-9] and that of the branches [Figure 4-10]. This similarity is a consequence of using quasi-static boundary conditions for both the leaf and the branch in developing expressions for their dyadic scattering amplitudes [refer to Section 3].

The empirically-derived behavior predicted by Saxton and Lane [refer to Figure 1-1] is also shown in Figure 4-9. Although the model predictions agree reasonably well with experiment so far as order of magnitude is concerned, only computations based upon leaf permittivity model I reflect a similar frequency dependence. However, because leaf permittivity model I does not properly account for ohmic losses within the leaves, it must be considered nonrealistic and the near agreement between the electrically thin leaf model employing it and experiment only coincidental. This is not to say, however, that the thin leaf model is invalid. It must be recognized that the empirically-derived behavior refers to atten-

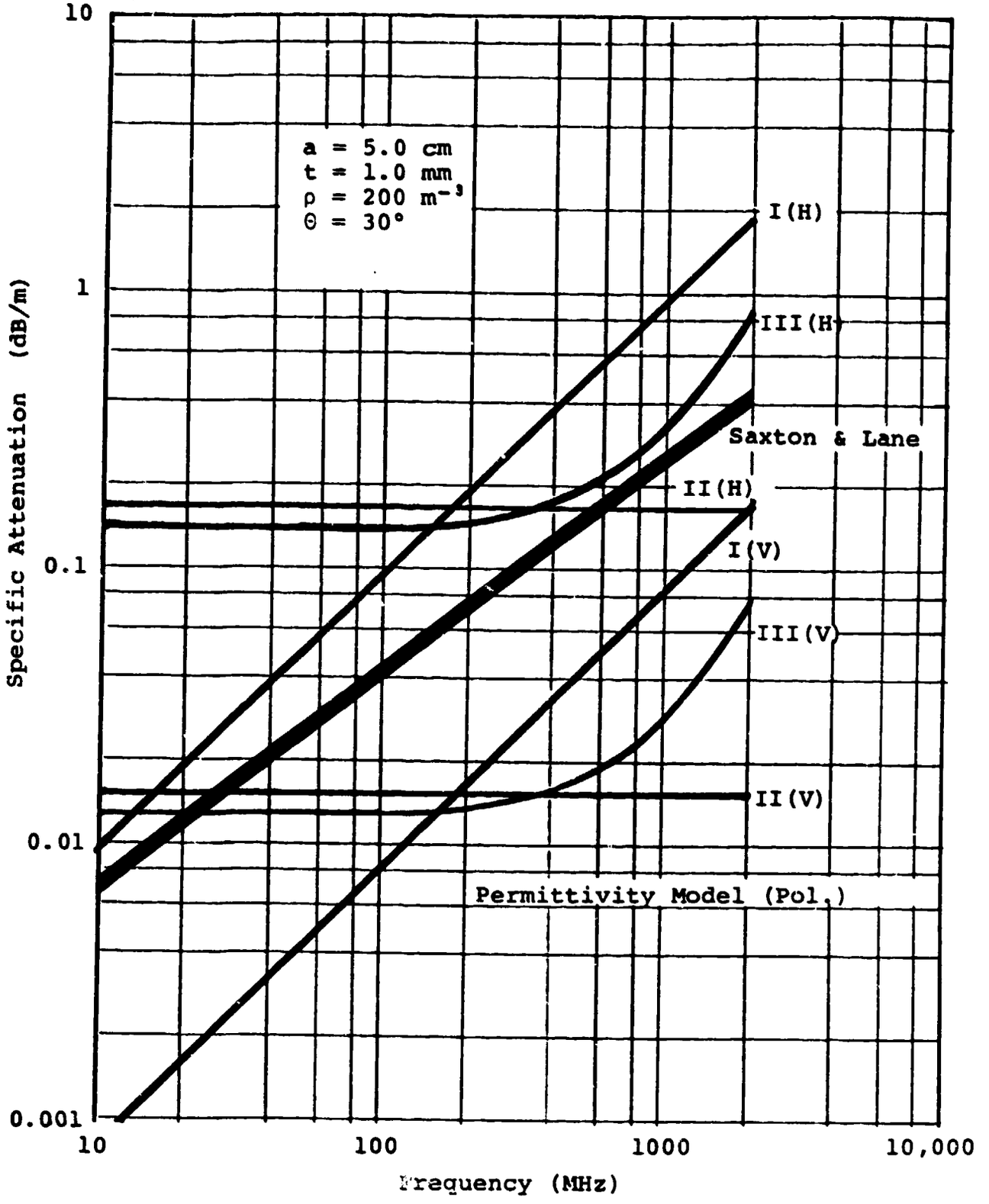

Figure 4-9: Specific Attenuation - Leaves

uation through a forest (tree trunks, branches and leaves) and not solely to attenuation through leaves. Thus, for example, if tree trunks were the dominant scatterers, the sub-resonant behavior contributed by the trunks [refer to Figure 4-6] could easily mask the essentially frequency-independent behavior predicted here for the leaves by using leaf permittivity models II and III. A similar caveat was discussed in the case of branches.

4.3 Salient Forest Descriptive Parameters

Experimental verification of the electromagnetic forest model requires the identification of measurable quantitative parameters to describe the forest. Some of these parameters are microscopic (e.g., the size and relative permittivity of individual tree trunks, branches and leaves); other parameters are macroscopic (e.g., the number of trees per acre and the number of leaves per unit volume of forest). Several of these parameters (microscopic and macroscopic) have been identified earlier in this report and are discussed below.

For tree trunks, the specific attenuation (α) experienced in the low-frequency (Rayleigh) regime by a horizontally or vertically polarized radiowave propagating through an unbounded forest can be determined from Equations (4-2-1-4) and (4-2-1-5). Using these equations, CyberCom has been able to derive the following explicit relations between the specific attenuation and select salient parameters of the trunks

$$\alpha_h = (1.13)a^2\rho f\chi_\ell''/|\chi_\ell| \qquad \text{(dB/m)} \qquad (4\text{-}3\text{-}1)$$

$$\alpha_v = (0.286)a^2\rho f\chi_\ell'' \qquad \text{(dB/m)} \qquad (4\text{-}3\text{-}2)$$

where a is the trunk radius (meters), ρ is the trunk number density (trees per square meter), f is the frequency (Megahertz, and χ_ℓ is the susceptibility of the wood. Note that the specific attenuation is directly proportional to the area occupied by the trunks and to the frequency. Analogous expressions for specific attenuation have not yet been determined (outside the Rayleigh regime, at higher frequencies).

For branches, CyberCom has been able to derive from Equations (4-2-2-4) and (4-2-2-5) the following explicit relations between the specific attenuation due to electrically-thin branches and select salient parameters:

$$\alpha_h = (0.143)a^2 \ell \rho f \chi_\ell'' \sin^2\theta_b \qquad \text{(dB/m)} \qquad \text{(4-3-3)}$$

$$\alpha_v = (0.286)a^2 \ell \rho f \chi_\ell'' \cos^2\theta_b \qquad \text{(dB/m)} \qquad \text{(4-3-4)}$$

where a is the branch radius (meters), ℓ is the branch length (meters), ρ is the branch number density (branches per cubic meter), f is the frequency (Megahertz), χ_ℓ is the susceptibility of the wood, and θ_b is the angle that the branch makes with the vertical. It is apparent from these equations that the specific attenuation depends upon the square of the branch radius, but only linearly upon branch length, number density, and χ_ℓ''.

For leaves, CyberCom has been able to derive from Equations (4-2-3-5) and (4-2-3-6) the following explicit relations between the specific attenuation due to electrically thin leaves and select salient foliage parameters:

$$\alpha_h = (0.286)a^2 t \rho f \chi_\ell''(1 - \tfrac{1}{2} I_1) \qquad \text{(dB/m)} \qquad \text{(4-3-5)}$$

$$\alpha_v = (0.286)a^2 t \rho f \chi_\ell''(1 - I_2) \qquad \text{(dB/m)} \qquad \text{(4-3-6)}$$

where a is the leaf radius (meters), t is the leaf thickness (meters), ρ is the leaf number density (leaves per cubic meter), f is the frequency (Megahertz), and χ_ℓ is the susceptibility of the leaves. The parameters I_1 and I_2 are related to the probability density function of the leaf inclination angles and are defined in Equation (4-2-3-3). It is apparent from these equations that the specific attenuation depends upon the square of the leaf radius, but only linearly upon the leaf thickness, number density, and χ_ℓ''.

It may be noted that each of the above expressions is of the form

$$\alpha = kV\rho fG \qquad (4\text{-}3\text{-}7)$$

where

k = constant

V = volume of element

ρ = density (no./m^3)

f = frequency in MHz

G = geometrical factor

$V\rho$ = fractional volume

As it is required in several developments in this report that fractional volume be small, a preliminary evaluation of this quantity has been made using Reference 15. This lists for forests in many parts of the world the following:

A = basal area in m^2/hectare ($10^4 m^2$)

M_w = dry mass of stem wood

M_b = dry mass of branches

M_f = dry mass of foliage

A cursory average of values for the United States gives the following fractional volumes:

Trunks	$A \times 10^{-4} = .0064$
Branches	$.0064 \times M_b/M_w = .0013$
Leaves	$.0064 \times M_f/M_w = .00016$

These values are clearly very small.

5.0 Anisotropic Forest Slab Model

Results were obtained above for an unbounded continuous medium equivalent to an infinitely high forest of model trunks, branches or leaves. In this section the medium is bounded at a forest-air upper interface to provide a more realistic overall model. This necessitates starting again from Maxwell's equations, inserting the dyadic permittivities from Section 3. The resulting inhomogeneous wave equation for an anisotropic medium is converted to a homogeneous equation for an isotropic medium by the substitution

$$z' = \sqrt{\varepsilon_t/\varepsilon_z}\, z \qquad (5\text{-}0\text{-}1)$$

The vector potentials are found by an asymptotic evaluation using integrations in the complex plane. The reflected component is found to include a lateral (tree-top) component. These, plus the direct wave are the potentials used to find the corresponding vertical components of the E field received by a vertical dipole.

5.1 Model Formulation

The basic slab model for the forest is shown in Figure 5-1. The trees and vegetation are assumed to be distributed uniformly between a smooth forest floor and the air interface at height h. Earlier efforts [93, 104, 107] have shown that the presence of the ground complicates the model significantly. The complications can be avoided, however, by allowing the ground plane to recede to $z \to -\infty$ so that the model reduces to the half-space representation shown in Figure 5-2. This simplification provides a very good approximation to the basic slab model if neither the transmitting or receiving antenna is located too close to the ground [107].

Consider a transmitting antenna which is representable as a vertical electric (Hertzian) dipole having a time-harmonic current moment $Idl \cdot \exp\{j\omega t\}$ and immersed a distance d below the interface of two semi-infinite media [refer to Figure 5-2]. The isotropic upper half-space ($z > 0$) represents the air and is characterized by the permittivity ε_o, and permeability μ_o of free-space. The electrically anisotropic lower half-space ($z < 0$)

represents the forest and is characterized (at least so far as the mean fields are concerned) by the effective dyadic permittivity $\underline{\varepsilon}\varepsilon_o$ and the free-space permeability μ_o. The relation between the relative effective dyadic permittivity $\underline{\varepsilon}$ and the biophysical parameters of the forest has been described in Section 4 of this report.

5.2 Mean Fields

In any charge-free medium where the electromagnetic fields vary harmonically as $\exp\{j\omega t\}$, Maxwell's equations may be written in the form

$$\nabla \times \underline{E} = -j\omega\underline{B} \qquad \nabla \cdot \underline{D} = 0$$
$$\nabla \times \underline{H} = j\omega\underline{D} + \underline{J} \qquad \nabla \cdot \underline{B} = 0 \tag{5-2-1}$$

If the medium is electrically anisotropic and characterized by the relative permittivity dyadic $\underline{\varepsilon}$, the constitutive relations

$$\underline{D} = \varepsilon_o\underline{\varepsilon} \cdot \underline{E} \qquad \underline{B} = \mu_o\underline{H} \tag{5-2-2}$$

may be introduced and Maxwell's equations re-written as

$$\nabla \times \underline{E} = -j\omega\mu_o\underline{H} \qquad \nabla \cdot \underline{\varepsilon} \cdot \underline{E} = 0$$
$$\nabla \times \underline{H} = j\omega\varepsilon_o\underline{\varepsilon}\cdot\underline{E}+\underline{J}_s \qquad \nabla \cdot \underline{H} = 0 \tag{5-2-3}$$

Because the forest may be considered uniaxially-anisotropic with respect to the mean fields [refer to Section 4],

$$\underline{\varepsilon} = \varepsilon_t\underline{x}^o\underline{x}^o + \varepsilon_t\underline{y}^o\underline{y}^o + \varepsilon_z\underline{z}^o\underline{z}^o \tag{5-2-4}$$

can be used to represent the effective relative complex permittivity of the forest, and $\underline{E}$, $\underline{H}$ the mean fields.

Because for any vector $\underline{A}$,

$$\nabla \cdot (\nabla \times \underline{A}) \equiv 0 \quad , \tag{5-2-5}$$

the relation

$$\nabla \cdot \underline{H} = 0 \tag{5-2-6}$$

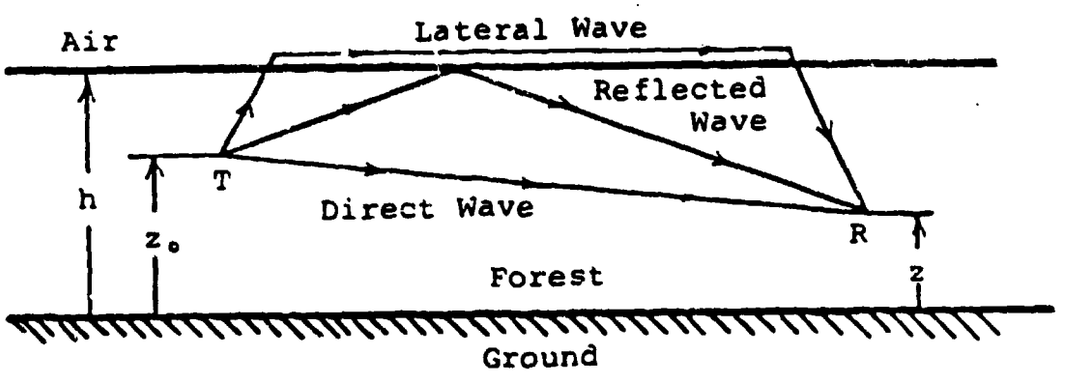

Figure 5-1: Slab Model for the Forest

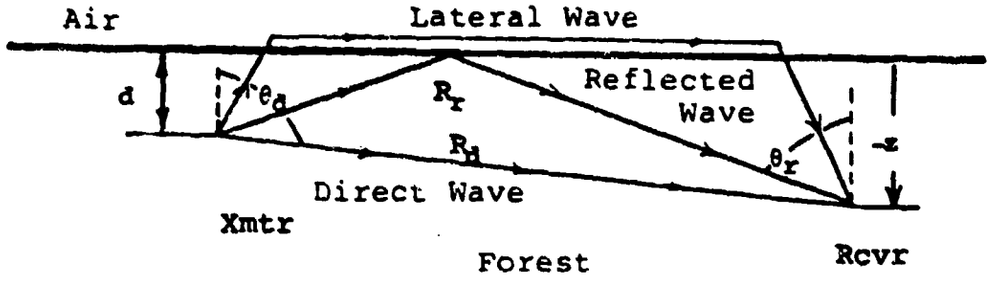

Figure 5-2: Half-Space Model for the Forest

suggests that there is a vector $\underline{A}$ satisfying the relation*

$$\underline{H} = j\omega\varepsilon_o\varepsilon_t(\nabla \times \underline{A}) \tag{5-2-7}$$

If this expression is introduced into Maxwell's equations, it may be shown that $\underline{A}$ satisfies the equation

$$\nabla^2\underline{A} + k_o^2\underline{\varepsilon} \cdot \underline{A} + \varepsilon_t^{-1}(\underline{\varepsilon}-\varepsilon_t\underline{I}) \cdot \nabla(\nabla \cdot A) = (-j\omega\varepsilon_o\varepsilon_t)^{-1}\underline{J}_s \tag{5-2-8}$$

and that the mean electric and magnetic fields may be derived from $\underline{A}$ using the relations

$$\underline{E} = k_o^2\varepsilon_t\underline{A} + \nabla(\nabla \cdot \underline{A}) \tag{5-2-9}$$

$$\underline{H} = j\omega\varepsilon_o\varepsilon_t(\nabla \times \underline{A}) \tag{5-2-10}$$

For an electrically isotropic medium where

$$\varepsilon_t = \varepsilon_z = \varepsilon \tag{5-2-11}$$

Equation (5-2-8) reduces to the inhomogeneous vector wave equation

$$\nabla^2\underline{A} + k_o^2\varepsilon\underline{A} = (-j\omega\varepsilon_o\varepsilon)^{-1}\underline{A} \tag{5-2-12}$$

and $\underline{A}$ is known as the electric Hertz potential [111].

In Region I (above the forest) where there are no electromagnetic sources

$$\underline{J}_s^I = 0 \tag{5-2-13}$$

the vector potential ($\underline{A}^I$) satisfies the homogeneous vector wave equation

$$\nabla^2\underline{A}^I + k_o^2\underline{A}^I = 0 \tag{5-2-14}$$

In Region II (within the forest) where a vertical electric (Hertzian) dipole of current moment+ Idl is immersed a distance d below the top of the forest canopy, the vector potential ($\underline{A}^{II}$) satisfies the inhomogeneous vector equation

---

* The scalar coefficient $j\omega\varepsilon_o\varepsilon_t$ has been included for mathematical convenience.

+ The harmonic factor $\exp\{j\omega t\}$ has been assumed and suppressed.

$$\nabla^2 \underline{A}^{II} + k_o^2 \underline{\underline{\varepsilon}} \cdot \underline{A}^{II} + \varepsilon_t^{-1} (\underline{\underline{\varepsilon}} - \varepsilon_t \underline{\underline{I}}) \cdot \nabla (\nabla \cdot \underline{A}^{II})$$

$$= (-j\omega\varepsilon_o\varepsilon_t)^{-1} Idl\delta(x)\delta(y)\delta(z+d)\underline{z}_o^o \qquad (5\text{-}2\text{-}15)$$

Because the current moment Idl is directed along the z-axis, a solution $\underline{A}^{II}$ will be sought having only a z-directed component, i.e.

$$\underline{A}^{II} = (0,0,A_z^{II}) \qquad (5\text{-}2\text{-}16)$$

Equation (5-2-16) permits Equation (5-2-15) to be reduced to the inhomogeneous scalar wave equation

$$\frac{\partial^2 A_z^{II}}{\partial x^2} + \frac{\partial^2 A_z^{II}}{\partial y^2} + \left(\frac{\varepsilon_z}{\varepsilon_t}\right) \frac{\partial^2 A_z^{II}}{\partial z^2} + k_o^2 \varepsilon_z A_z^{II}$$

$$= (-j\omega\varepsilon_o\varepsilon_t)^{-1} Idl\delta(x)\delta(y)\delta(z+d) \qquad (5\text{-}2\text{-}17)$$

By introducing the anisotropy factor

$$a = (\varepsilon_t/\varepsilon_z)^{\frac{1}{2}} \qquad (5\text{-}2\text{-}18)$$

and the change of variable

$$z' = az \qquad (5\text{-}2\text{-}19)$$

Equation (5-2-17) can be re-written as

$$\nabla'^2 A_z^{II} + k_o^2 \varepsilon_z A_z^{II} = (-j\omega\varepsilon_o\varepsilon_t)^{-1} Idl'\delta(x)\delta(y)\delta(z'+d') \qquad (5\text{-}2\text{-}20)$$

where ∇' represents the del operator transformed according to Equation (5-2-19). Note that as a consequence of the change of variable, the inhomogeneous scalar wave equation for the anisotropic medium [Equation (5-2-17)] has been transformed into the homogeneous scalar wave equation for an equivalent isotropic medium [111]. The possibility of such a transformation for unbounded anisotropic media apparently was first suggested by Clemmow [121].

The solution to Equation (5-2-20) consists of two parts: the complementary solution ($A_{z,c}^{II}$) to the homogeneous scalar wave

equation, and the particular solution ($A^{II}_{z,p}$) to the inhomogeneous scalar wave equation. The particular solution can be obtained by first introducing the three-dimensional Fourier transform pair

$$\tilde{A}_z(\underline{\beta}) = \int A_z(\underline{r})\exp\{j\underline{\beta}\cdot\underline{r}\}d\underline{r} \qquad (5\text{-}2\text{-}21)$$

$$A_z(\underline{r}) = (2\pi)^{-3}\tilde{A}_z(\underline{\beta})\exp\{-j\underline{\beta}\cdot\underline{r}\}d\underline{\beta} \qquad (5\text{-}2\text{-}22)$$

and subsequently using Jordan's Lemma to reduce the particular solution to the two-dimensional integral

$$A^{II}_{z,p}(\underline{r}) = A^{II}_{z,p}(\underline{\rho},z) = \frac{-Idl}{8\pi^2\omega\varepsilon_o\varepsilon_z}\int \frac{\exp\{-j(\underline{\beta}_t\cdot\underline{\beta} + \tau_2|z+d|)\}}{\tau_2}\, d\underline{\beta}_t \qquad (5\text{-}2\text{-}23)$$

where

$$\tau_2 = a(k_o^2\varepsilon_z - \beta_t^2)^{\frac{1}{2}} = \tau_2' - j|\tau_2''| \qquad (5\text{-}2\text{-}24)$$

The condition that $\tau_2'' < 0$ is necessary to ensure the convergence of the integral as $|z+d| \to \infty$.

Recognizing that the particular solution [Equation (5-2-23)] is a two-dimensional integral, complementary solutions to Equations (5-2-14) and (5-2-20) will be sought utilizing the two-dimensional Fourier transform pair

$$\tilde{A}_z(\underline{\beta}_t,z) = \int A_z(\underline{\rho},z)\exp\{j\underline{\beta}_t\cdot\underline{\rho}\}d\underline{\rho} \qquad (5\text{-}2\text{-}25)$$

$$A_z(\underline{\rho},z) = (2\pi)^{-2}\int \tilde{A}_z(\underline{\beta}_t,z)\exp\{-j\underline{\beta}_t\cdot\underline{\rho}\}d\underline{\beta}_t \qquad (5\text{-}2\text{-}26)$$

with appropriate consideration given to the transformation of Equation (5-2-19). Substitution of Equation (5-2-26) into Equations (5-2-14) and (5-2-20) yields the complementary solutions

$$\tilde{A}^{I,II}_{z,c}(\underline{\beta}_t,z) = C_+^{I,II}(\underline{\beta}_t)\exp\{j\tau_{1,2}z\} + C_-^{I,II}(\underline{\beta}_t)\exp\{-j\tau_{1,2}z\} \qquad (5\text{-}2\text{-}27)$$

where,

$$\tau_1 = (k_o^2 - \beta_t^2)^{\frac{1}{2}} = \tau_1' - j|\tau_1''| \qquad (5\text{-}2\text{-}28)$$

$$\tau_2 = a(k_o^2\varepsilon_z - \beta_t^2)^{\frac{1}{2}} = \tau_2 - j|\tau_2''| \qquad (5\text{-}2\text{-}29)$$

To ensure that the electromagnetic fields remain finite as $|z| \to \infty$, it is necessary that

$$C_+^I(\underline{\beta}_t) \equiv 0 \qquad (5\text{-}2\text{-}30)$$

$$C_-^{II}(\underline{\beta}_t) \equiv 0 \qquad (5\text{-}2\text{-}31)$$

Following a normalization of the coefficients $C_+^{II}(\underline{\beta}_t)$ and $C_-^I(\underline{\beta}_t)$ and the addition of the complementary and particular solutions associated with the wave equation for Region II, the potential functions for Region I and II may be written, respectively, in the following forms:

$$A_z^I(\underline{\rho},z) = \frac{-Idl}{8\pi^2\omega\varepsilon_o\varepsilon_z}\int M(\underline{\beta}_t)\exp\{-j\tau_1 z\}\exp\{-j\underline{\beta}_t\cdot\underline{\rho}\}d\underline{\beta}_t \qquad (5\text{-}2\text{-}32)$$

$$A_z^{II}(\underline{\rho},z) = \frac{-Idl}{8\pi^2\omega\varepsilon_o\varepsilon_z}\int[(1/\tau_2)\exp\{-j\tau_2|z+d|\} + N(\underline{\beta}_t)\exp\{j\tau_2 z\}]$$

$$\cdot\exp\{-j\underline{\beta}_t\cdot\underline{\rho}\}d\underline{\beta}_t \qquad (5\text{-}2\text{-}33)$$

Because the tangential components of the electromagnetic fields must be continuous across the air-forest interface, Equations (5-2-9), (5-2-10) and (5-2-16) require

$$A_z^I(\underline{\rho},0) = \varepsilon_t A_z^{II}(\underline{\rho},0) \qquad (5\text{-}2\text{-}34)$$

$$\partial[A_z^I(\underline{\rho},0)]/\partial z = \partial[A_z^{II}(\underline{\rho},0)]/\partial z \qquad (5\text{-}2\text{-}35)$$

Substitution of Equations (5-2-32) and (5-2-33) into Equations (5-2-34) and (5-2-35) reveals that

$$M(\underline{\beta}_t) = [2\varepsilon_t/(\tau_2 + \varepsilon_t\tau_1)]\exp\{-j\tau_2 d\} \qquad (5\text{-}2\text{-}36)$$

$$N(\underline{\beta}_t) = [(\tau_2 - \varepsilon_t\tau_1)/(\tau_2 + \varepsilon_t\tau_1)\tau_2]\exp\{-j\tau_2 d\} \qquad (5\text{-}2\text{-}37)$$

so that the potential functions for Region I and Region II are, respectively,

$$A_z^I(\underline{\rho},z) = \frac{-Idl}{8\pi^2\omega\varepsilon_o\varepsilon_z}\int\frac{2\varepsilon_t}{(\tau_2+\varepsilon_t\tau_1)}\exp\{-j\tau_2 d\}\exp\{-j\tau_1 z\}$$

$$\cdot\exp\{-j\underline{\beta}_t\cdot\underline{\rho}\}d\underline{\beta}_t \qquad (5\text{-}2\text{-}38)$$

$$A_z^{II}(\underline{\rho},z) = \frac{-Idl}{8\pi^2\omega\varepsilon_o\varepsilon_z}\int\left[\frac{e^{-j\tau_2|z+d|}}{\tau_2}+\left(\frac{\tau_2-\varepsilon_t\tau_1}{\tau_2+\varepsilon_t\tau_1}\right)\frac{e^{j\tau_2(z-d)}}{\tau_2}\right]$$

$$\cdot\exp\{-j\underline{\beta}_t\cdot\underline{\rho}\}d\underline{\beta}_t \qquad (5\text{-}2\text{-}39)$$

Equations (5-2-38) and (5-2-39), in conjunction with Equations (5-2-9) and (5-2-10), constitute the formal solution for the mean electromagnetic fields of a vertical electric (Hertzian) dipole immersed in an anisotropic forest half-space.

5.3 Asymptotic Evaluation

The integral representations for the potential functions afforded by Equations (5-2-38) and (5-2-39) are not amenable to exact analytic evaluation. Fortunately, analytic asymptotic approximations can be derived which will prove adequate for most engineering applications. However, before proceeding with the development of these asymptotic approximations, it will prove expedient to introduce the transformations

$$\beta_x = \lambda\cos\psi \qquad \rho_x = \rho\cos\phi$$
$$\beta_y = \lambda\sin\psi \qquad \rho_y = \rho\sin\phi \qquad (5\text{-}3\text{-}1)$$

so that with the help of the identity

$$J_o(\lambda\rho) = \frac{1}{2\pi}\int_{-\pi}^{\pi}\exp\{-j\lambda\rho\cos(\psi-\phi)\}d\psi \qquad (5\text{-}3\text{-}2)$$

the potential function within the forest can be written as

$$A_z^{II}(\underline{\rho},z) = \frac{-Idl}{4\pi\omega\varepsilon_o\varepsilon_z}\int_0^\infty\left[e^{-j\tau_2|z-d|} + \Gamma(\tau_1,\tau_2)e^{j\tau_2(z-d)}\right] \cdot \frac{J_o(\lambda\rho)}{\tau_2}\lambda d\lambda \qquad (5\text{-}3\text{-}3)$$

where

$$\Gamma(\tau_1,\tau_2) = \frac{\tau_2 - \varepsilon_t\tau_1}{\tau_2 + \varepsilon_t\tau_1} \qquad (5\text{-}3\text{-}4)$$

may be recognized as the Fresnel reflection coefficient associated with the air-forest interface and, as before,

$$\tau_1 = \tau_1' - j|\tau_1''| = (k_o^2 - \lambda^2)^{\frac{1}{2}} \qquad (5\text{-}3\text{-}5)$$

$$\tau_2 = \tau_2' - j|\tau_2''| = a(k_o^2\varepsilon_z - \lambda^2)^{\frac{1}{2}} \qquad (5\text{-}3\text{-}6)$$

If the identity [111, Equation (5.35a)]

$$\frac{\exp\{-jk_o\sqrt{\varepsilon}R\}}{R} = -j\int_0^\infty \frac{e^{-j\kappa|z+d|}}{\kappa} J_o(\lambda\rho)\lambda d\lambda \qquad (5\text{-}3\text{-}7)$$

where

$$\kappa = (k_o^2\varepsilon - \lambda^2)^{\frac{1}{2}} \qquad (5\text{-}3\text{-}8)$$

$$R = [\rho^2 + (z-d)^2]^{\frac{1}{2}} \qquad (5\text{-}3\text{-}9)$$

is analytically continued into the complex z-plane using the transformation of Equation (5-2-19), the potential function in the forest can be more conveniently written in the form

$$A_z^{II} = A_z^{(d)} + A_z^{(r)} \qquad (5\text{-}3\text{-}10)$$

where

$$A_z^{(d)} = \frac{-jIdl}{4\pi\omega\varepsilon_o\varepsilon_z} \cdot \frac{\exp\{-jk_o\sqrt{\varepsilon_z}R_d\}}{aR_d} \qquad (5\text{-}3\text{-}11)$$

$$R_d = [\rho^2 + a^2(z+d)^2]^{\frac{1}{2}} \qquad (5\text{-}3\text{-}12)$$

is the component of the potential function associated with the direct wave, and

$$A_z^{(r)} = \frac{-jIdl}{4\pi\omega\varepsilon_o\varepsilon_z} \int_0^\infty \Gamma(\tau_1,\tau_2) \frac{e^{j\tau_2(z-d)}}{\tau_2} \cdot J_o(\lambda\rho)\lambda d\lambda \qquad (5\text{-}3\text{-}13)$$

is the component of the potential function associated with the reflected wave.

The asymptotic evaluation of $A_z^{(r)}$ is most readily achieved by first analytically continuing the real integration variable λ into the complex plane. Unfortunately, the integral presented by Equation (5-3-13) presents a mathematical problem: the path of integration begins at the origin. This can be eliminated by expressing the Bessel function $J_o(\lambda\rho)$ in terms of the Hankel functions of the first and second kinds [$H_o^{(1)}(\lambda\rho)$ and $H_o^{(2)}(\lambda\rho)$], and then using analytic continuation to express the Hankel function of the first kind in terms of one of the second kind [111] so that the electromagnetic waves exhibit the proper asymptotic behavior at infinity as might be expected with the harmonic time dependence $\exp\{j\omega t\}$. As a consequence of these mathematical manipulations, the potential associated with the reflected wave can be recast into the form

$$A_z^{(r)} = \frac{-Idl}{4\pi\omega\varepsilon_o\varepsilon_z} \int_{-\infty}^\infty \Gamma(\tau_1,\tau_2) e^{j\tau_2(z-d)} \frac{H_o^{(2)}(\lambda\rho)}{2\tau_2} \lambda d\lambda \qquad (5\text{-}3\text{-}14)$$

It is especially important to note that without the constraints imposed by Equations (5-3-5) and (5-3-6) on the imaginary parts of τ_1 and τ_2, the integrand of Equation (5-3-14) would not be uniquely determined. Generally speaking, the integrand is four-valued (corresponding to the four possible combinations of signs

in the square roots defining τ_1 and τ_2), and its Riemann surface consists of four sheets. To insure the convergence of the integral at infinity and the uniqueness of the integral everywhere, the integration path in the complex λ-plane must be constrained to the permissible (upper) sheet defined by Equations (5-3-5) and (5-3-6). This can be achieved by joining the branch points (i.e., those points where τ_1 and τ_2 are zero) by two (essentially arbitrary) branch cuts and insuring that the branch cuts are not intersected by the path of integration.

An asymptotic approximation for the potential function in the forest suitable at relatively large distances from the transmitter ($k_o\rho >> 1$) can be obtained by evaluating Equation (5-3-14) using the method of steepest descent [111]. This approach involves the conformal re-mapping of the integrand from the λ-plane to the w-plane using the transformation

$$\lambda = k_o\sqrt{\epsilon_z}\sin w \qquad (5\text{-}3\text{-}15)$$

to eliminate the branch cut associated with τ_2; the subsequent deformation of the integration contour to coincide with the path of steepest descent passing through the saddle point associated with the exponential factor; and, finally, the approximate evaluation of the integral defining $A_z^{(r)}$.

The complex w-plane associated with the transformation of Equation (5-3-15) is shown in Figure 5-3. Under this transformation, the coordinate axes of the λ-plane are mapped into lines in the λ-plane defined by*

$$\tanh w'' \approx (\chi_z''/2)\tan w' \ , \qquad (\lambda'\text{-axis}) \qquad (5\text{-}3\text{-}16)$$

and

$$\tanh w'' \approx -(2/\chi_z'')\tan w' \ , \qquad (\lambda''\text{-axis}) \qquad (5\text{-}3\text{-}17)$$

The branch points associated with τ_1 are located at

$$w_B \approx \pm(2n+1)\pi/2 \pm \sqrt{\chi_z} \ , \qquad (n=1,2,\ldots) \qquad (5\text{-}3\text{-}18)$$

---

* Predicated upon the condition that $|\chi_z| = |\chi_z' - j\chi_z''| << 1$.

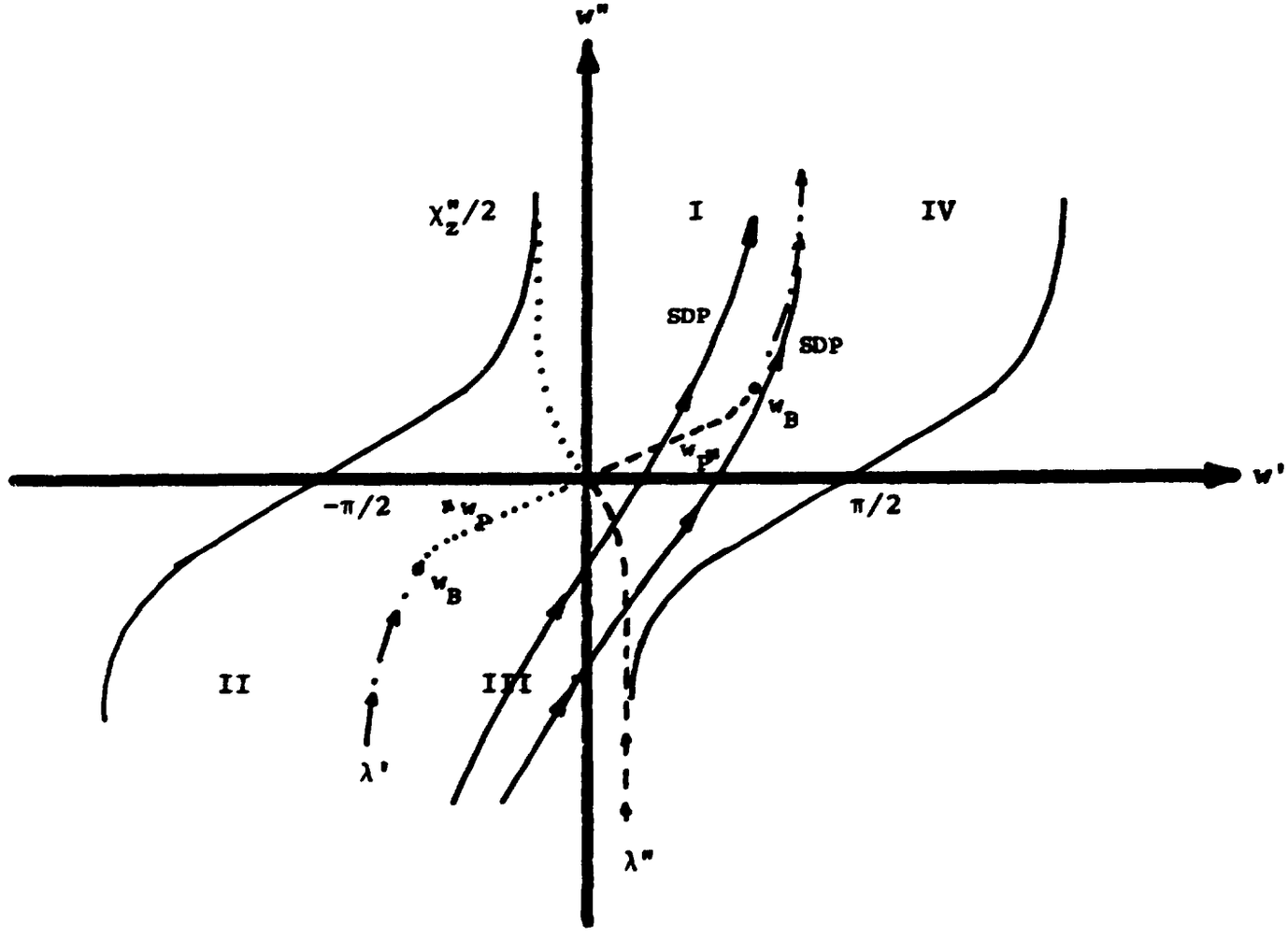

Figure 5-3: Complex w-plane

If the associated branch cuts are defined so that

$$\mathrm{Im}\{\tau_1\} = \mathrm{Im}\{k_o(1 - \varepsilon_z \sin^2 w)^{\frac{1}{2}}\} = 0 \qquad (5\text{-}3\text{-}19)$$

then from the branch point to the origin, the branch cut is defined by*

$$\tanh w'' \approx (\chi_z''/2)\tan w' \ , \qquad (w'w'' > 0) \qquad (5\text{-}3\text{-}20)$$

and from the origin to infinity by*

$$\tanh w'' \approx -(2/\chi_z'')\tan w' \ , \qquad (w'w'' < 0) \qquad (5\text{-}3\text{-}21)$$

Note that the branch cut proceeds from the branch point along the λ'-axis to the origin, experiences a clockwise angular rotation of $\pi/2$ radians, and then proceeds from the origin along the λ-axis to infinity.

Poles, associated with the denominator of the reflection coefficient $\Gamma(\tau_1, \tau_2)$, occur wherever

$$\cos w + \sqrt{\varepsilon_t}\, a(1 - \varepsilon_z \sin^2 w)^{\frac{1}{2}} = 0 \qquad (5\text{-}3\text{-}22)$$

These poles can be found on the top sheet where*

$$w_p \approx \pm(\pi/4 + j\chi_t''/4) \qquad (5\text{-}3\text{-}23)$$

and on the bottom sheet where*

$$w_p \approx \pm(3\pi/4 + j\chi_t''/4) \qquad (5\text{-}3\text{-}24)$$

Anticipating an asymptotic evaluation, the Hankel function in Equation (5-3-14) can be replaced by its approximation for large arguments

$$H_o^{(2)}(\lambda\rho) \approx \sqrt{\frac{2}{\pi\lambda\rho}}\, \exp\{-j(\lambda\rho - \pi/4)\} \qquad (5\text{-}3\text{-}25)$$

Introducing the transformation defined by the mapping of Equation (5-3-15) and the geometric transformation suggested by

---

* Predicated upon the condition that $|\chi_z| = |\chi_z' - j\chi_z''| \ll 1$.

Equation (5-2-19), viz.

$$\rho = R_r \sin\theta_r$$
$$-a(z-d) = R_r \cos\theta_r \qquad (5\text{-}3\text{-}26)$$

recasts the potential function into the form

$$A_z^{(r)} = \frac{-Idl}{4\pi\omega\varepsilon_o\varepsilon_z} e^{j\pi/4} \frac{(k_o\sqrt{\varepsilon_z})^{\frac{1}{2}}}{a(2\pi R_r \sin\theta_r)^{\frac{1}{2}}} \int \Gamma(w)\sqrt{\sin w}$$
$$\cdot \exp\{-jk_o\sqrt{\varepsilon_z}\, R_r \cos(w-\theta_r)\}dw \qquad (5\text{-}3\text{-}27)$$

When

$$k_o|\sqrt{\varepsilon_z}\, R_r| >> 1 \qquad (5\text{-}3\text{-}28)$$

Equation (5-3-27) can be evaluated asymptotically by defining the integration path P (which, in the λ-plane, coincides with the λ'-axis) into the steepest-descent path SDP (which, in the w-plane, passes through the saddle point $w = \theta_r$) defined by

$$R_e\{\sqrt{\varepsilon_z}\, R_r \cos(w-\theta_r)\} = R_e\{\sqrt{\varepsilon_z}\, R_r\} \qquad (5\text{-}3\text{-}29)$$

Integration of $A_z^{(r)}$ along the steepest-descent path yields

$$A_z^{(r)} \sim \frac{Idl}{4\pi\omega\varepsilon_o\varepsilon_z} \Gamma(\theta_r) \frac{\exp\{-jk_o\sqrt{\varepsilon_z}\, R_r\}}{aR_r} \qquad (5\text{-}3\text{-}30)$$

where

$$\Gamma(\theta_r) = \frac{\cos\theta_r - \sqrt{\varepsilon_t}(1-\varepsilon_z\sin^2\theta_r)^{\frac{1}{2}}}{\cos\theta_r + \sqrt{\varepsilon_t}(1-\varepsilon_z\sin^2\theta_r)^{\frac{1}{2}}} \qquad (5\text{-}3\text{-}31)$$

is the Fresnel reflection coefficient associated with the wave specularly reflected from the air-forest interface.

The validity of Equation (5-3-30) is predicated not only upon the condition that

$$k_o|\sqrt{\varepsilon_z}\, R_r| >> 1 \ , \qquad (5\text{-}3\text{-}32)$$

but also upon the condition that the value of the reflection coefficient $\Gamma(w)$ appearing in Equation (5-3-27) does not vary appreciably along the steepest descent path in the vicinity of the saddle point, i.e.

$$\Gamma'(w_s) \approx 0 \qquad (5\text{-}3\text{-}33)$$

This assumption will prove justified if [87]

$$k_o|R_r(\theta_r - \theta_c)^2| >> 1 \qquad (5\text{-}3\text{-}34)$$

where

$$\theta_c = \text{Arc sin}\,(1/\sqrt{\varepsilon_z}) \qquad (5\text{-}3\text{-}35)$$

For the forest, the effective permittivity ε is close to unity. Further, because the distance ρ between the transmitter and receiver will, nearly always, be much greater than their height differential $|z-d|$, the angle

$$\theta_r = \text{Arc tan}\,[\rho/a|z-d|] \qquad (5\text{-}3\text{-}36)$$

will, nearly always, be close to $\pi/2$. As a consequence, the requirement expressed by Inequality (5-3-34) is usually much more stringent than that expressed by Inequality (5-3-32).

Because θ_r will, nearly always, be close to $\pi/2$, the deformation of the contour P into the steepest-descent path SDP nearly always results in the capture of the branch point w_B. In order to avoid crossing the branch cut when the branch point is captured, an additional line integral about the branch cut must be introduced [refer to Figure 5-3]. Integration about the branch cut yields the asymptotic result that [87]

$$A_z^{(\ell)} = \frac{Idl}{2\pi\omega\varepsilon_o} \cdot \frac{1}{k_o(\varepsilon_z-1)^{\frac{1}{4}}\sqrt{\rho}} \cdot \frac{\exp\{-jk_o[\rho+a(\varepsilon_z-1)^{\frac{1}{2}}|z-d|]\}}{[(\varepsilon_z-1)^{\frac{1}{2}}\rho - a|z-d|]^{3/2}} \qquad (5\text{-}3\text{-}37)$$

subject to the constraint that

$$\frac{k_o[(\varepsilon_z-1)^{\frac{1}{2}}\rho - a|z-d|](\varepsilon_z-1)^{\frac{1}{2}}}{[k_o\varepsilon_z a|z-d|]^{\frac{1}{2}}} >> 1 \qquad (5\text{-}3\text{-}38)$$

If

$$\rho >> |a|\ |z-d|/(\varepsilon_z-1)^{\frac{1}{2}} \qquad (5\text{-}3\text{-}39)$$

then

$$A_z^{(\ell)} \sim \frac{Idl}{2\pi\omega\varepsilon_o} \cdot \frac{1}{k_o(\varepsilon_z-1)} \cdot \frac{\exp\{-jk_o[\rho + a(\varepsilon_z-1)^{\frac{1}{2}}|z-d|]\}}{\rho^2} \qquad (5\text{-}3\text{-}40)$$

Actually, the validity of Equation (5-3-37) is predicated, not only upon Inequality (5-3-38), but also upon the condition that the reflection coefficient $\Gamma(w)$ appearing in Equation (5-3-27) does not vary appreciably along the steepest-descent path in the vicinity of the branch point, i.e.

$$\Gamma'(w_B) \approx 0 \qquad (5\text{-}3\text{-}41)$$

This assumption is justified if

$$(k_o|R_r||\varepsilon_z-1|)^{\frac{1}{2}} >> 1 \qquad (5\text{-}3\text{-}42)$$

Observing that when $a = 1$, the phase factor appearing in the exponents of Equations (5-3-37) and (5-3-40) can be written in the form

$$\begin{aligned} k_o[\rho + (\varepsilon_z-1)^{\frac{1}{2}}|z-d|] &= k_o\sqrt{\varepsilon_z}(d/\cos\theta_c) \\ &\quad + k_o[\rho - d(\sin\theta_c/\cos\theta_c) - |z|(\sin\theta_c/\cos\theta_c)] \\ &\quad + k_o\sqrt{\varepsilon_z}(|z|/\cos\theta_c) \end{aligned} \qquad (5\text{-}3\text{-}43)$$

where

$$\theta_c = \text{Arc sin}\,(1/\sqrt{\varepsilon_z}) \qquad (5\text{-}3\text{-}44)$$

The three terms of Equation (5-3-43) suggest that the vector potential $A_z^{(\ell)}$ can be associated with a so-called "lateral" wave which propagates from the transmitter up through the forest at the critical angle θ_c to the air-forest interface, through the air along the air-forest interface, and down through the forest at the critical angle from the air-forest interface to the receiver.

As a consequence of this asymptotic evaluation, a radiowave propagating within the forest may be considered to consist of three components - the direct wave, the reflected wave, and the lateral wave - and the vector potential within the forest can be written in the form

$$A_z^{II} = A_z^{(d)} + A_z^{(r)} + A_z^{(\ell)} \qquad (5\text{-}3\text{-}45)$$

where $A_z^{(d)}$ is the vector potential associated with the direct wave [Equation (5-3-11)], $A_z^{(r)}$ is the vector potential associated with the reflected wave [Equation (5-3-30)], and $A_z^{(\ell)}$ is the vector potential associated with the lateral wave [Equation (5-3-37)].

5.4 Electromagnetic Fields

The electromagnetic fields ($\underline{E}$ and $\underline{H}$) within the forest can be derived from the vector potential A_z^{II} [Equation (5-3-45)] by using Equations (5-2-9) and (5-2-10). Because the electromagnetic fields are related linearly to the vector potential, just as the vector potential exhibits three asymptotic components (the direct, reflected, and lateral waves), so too will the electromagnetic fields. For example, the vertically-polarized components of the electric field vector $\underline{E}$, derived under the asymptotic approximation from Equation (5-2-9) upon substitution of Equations (5-3-11), (5-3-30) and (5-3-37), are

$$E_z^{(d)} = \sqrt{a}\left(\frac{\omega\mu_o}{4\pi}\right) Idl \sin^2\theta_d \frac{\exp\{-jk_o\sqrt{\epsilon_z}\, R_d\}}{R_d} \qquad (5\text{-}4\text{-}1)$$

$$E_z^{(r)} = \sqrt{a}\left(\frac{\omega\mu_o}{4\pi}\right) Idl \sin^2\theta_r \Gamma(\theta_r) \frac{\exp\{-jk_o\sqrt{\epsilon_z}\, R_r\}}{R_r} \qquad (5\text{-}4\text{-}2)$$

$$E_z^{(\ell)} = 60\, Idl \left(\frac{a}{\epsilon_z - 1}\right) \frac{\exp\{-jk_o[\rho + a(\epsilon_z-1)^{\frac{1}{2}}|z-d|]\}}{\rho^2} \qquad (5\text{-}4\text{-}3)$$

where,

$$R_d = [\rho^2 + a^2(z+d)^2]^{\frac{1}{2}} \qquad (5\text{-}4\text{-}4)$$

$$R_r = [\rho^2 + a^2(z-d)^2]^{\frac{1}{2}} \qquad (5\text{-}4\text{-}5)$$

$$\theta_d = \text{Arc tan}\left[\frac{\rho}{a\ (z+d)}\right] \qquad (5\text{-}4\text{-}5)$$

$$\theta_r = \text{Arc tan}\left[\frac{\rho}{a\ |z-d|}\right] \qquad (5\text{-}4\text{-}7)$$

$$\Gamma(\theta_r) = \frac{\cos\theta_r - \sqrt{\epsilon_t}(1-\epsilon_z \sin^2\theta_r)^{\frac{1}{2}}}{\cos\theta_r + \sqrt{\epsilon_t}(1-\epsilon_z \sin^2\theta_r)^{\frac{1}{2}}} \qquad (5\text{-}4\text{-}8$$

$$a = \sqrt{\epsilon_t/\epsilon_z} \qquad (5\text{-}4\text{-}9)$$

Note that in the limiting case of an isotropic forest, the anisotropy factor $a \to 1$, and the above results reduce to those obtained by Staiman and Tamir [114, Equation (28) with $\alpha = -\pi/2$]. In this limiting isotropic case, the parameters R_d, R_r, θ_d and θ_r acquire the geometric interpretation shown in Figure 5-2.

The remaining component of the electromagnetic field, the magnetic field intensity, can be obtained similarly. In this report, however, attention will be focused upon the vertical electric field E_z, the only component received by a vertical whip antenna.

6.0 Forest Pulse Response

The anisotropic half-space model of the forest developed in Section 5 of this report is a time-harmonic model. The transmitting antenna was assumed to be a vertical electric (Hertzian) dipole having a time-harmonic current moment $Id\ell \cdot \exp\{j\omega t\}$. However, because the effective dyadic permittivity characterizing the equivalent continuous medium of the mean wave is linear, the model can be extended using linear system theory to accommodate the transmission of arbitrarily-modulated waveforms. This extension is especially important if the model is to be employed in analysis and evaluation of wideband spread-spectrum radio communication systems.

Following a brief review of linear system theory in Section 6.1, the forest transfer function $F(f,t)$ is identified in Section 6.2 and employed in Section 6.3 to define the forest pulse response. In Section 6.4, the forest pulse response is evaluated for the important practical case of a broadband, rectangular, r-f pulse.

6.1 Linear System Theory

A system is a collection of interrelated components or objects for which there is specified a set of dynamic variables called excitations, or inputs, and another set called responses, or outputs [145]. The radio transmission channel through the forest represents such a system. The tree leaves, branches, and trunks constitute the collection of components or objects which are interrelated by mutually-induced currents excited within them by electromagnetic fields. The dynamic variable representing the input of this system can be the time-harmonic electric current momemt $Id\ell$ of an electrically small (Hertzian) dipole transmitting antenna. The dynamic variable representing the output of this system can be the electric field $\underline{E}$ at the location of the receiving antenna.

The objective of systems analysis is to determine how such a collection of components of objects behaves when subjected to an arbitrary, but specified, excitation. For the analysis of linear

systems (such as the forest transmission channel), which (by definition) satisfy the principle of superposition so that

$$F[\alpha_1 x_1 + \alpha_2 x_2] = \alpha_1 F[x_1] + \alpha_2 F[x_2] \qquad (6\text{-}1\text{-}1)$$

where F[x] represents the output response of the system to the input excitation x, there are two basic approaches. The first of these, which might be termed the "direct" approach, consists in directly solving the input-output relation

$$y = F[x] \qquad (6\text{-}1\text{-}2)$$

subject to a known set of initial conditions or boundary conditions. In the "indirect" approach, the input x is first resolved into a set of elementary functions all of which are similar in form. The response of the system to each elementary component (presumably determined more easily than the response of the system to an arbitrary input) is then obtained and the responses to all the elementary components of the input added to obtain (by virtue of system additivity) the output corresponding to the input.

Any one of a number of elementary components may be used for the decomposition of the input. Two often-employed choices for the elementary components are the Dirac delta function and the complex exponential. Resolution of the input x into a continuum of Dirac delta functions may be achieved with the help of the sifting integral

$$x(t) = \int_{-\infty}^{\infty} x(\tau)\delta(t-\tau)d\tau \qquad (6\text{-}1\text{-}3)$$

If the response to the linear system at time t to a Dirac δ-function applied at time $\tau[\delta(t-\tau)]$ is $f(t,\tau)$, the superposition principle [Equation (6-1-1)] and the sifting integral [Equation (6-1-3)] dictate that the response of the linear system to the arbitrary input x(t) is

$$y(t) = \int_{-\infty}^{\infty} x(\tau)f(t,\tau)d\tau \qquad (6\text{-}1\text{-}4)$$

The function $f(t,\tau)$ is termed the time-variant impulse response.

Alternatively, the input x may be resolved into a continuum of complex exponentials using the Fourier transform pair

$$x(t) = \int_{-\infty}^{\infty} X(f)\exp\{j2\pi ft\}df \qquad (6\text{-}1\text{-}5)$$

$$X(f) = \int_{-\infty}^{\infty} x(t)\exp\{-j2\pi ft\}dt \qquad (6\text{-}1\text{-}6)$$

The function X(f) is called the amplitude spectrum of the input x(t). If the response of the linear system at time t to the complex exponential of unit amplitude $\exp\{j2\pi ft\}$ is F(f,t), the superposition principle [Equation (6-1-1)] and the inverse Fourier transform [Equation (6-1-5)] dictate that the response of the linear system to the arbitrary input x(t) is

$$y(t) = \int_{-\infty}^{\infty} X(f)F(f,t)\exp\{j2\pi ft\}df \qquad (6\text{-}1\text{-}7)$$

The function F(f,t) is termed the time-variant transfer function.

6.2 Forest Transfer Function

The time-variant transfer function of a linear system represents the response of that linear system at time t to the complex exponential of unit amplitude $\exp\{j2\pi ft\}$. Inasmuch as the transmitting antenna of the anisotropic half-space model of the forest is taken to be a vertical electric (Hertzian) dipole having a time-harmonic current moment $Idl\cdot\exp\{j\omega t\}$ [refer to Section 5.1], the mean component of the vertically-polarized electric field found in response to that current-moment [refer to Section 5.4], may be considered to be the forest transfer function F(f,t) after normalizing the expressions for the mean field by Idl. Further, as a consequence of the relationship between the expressions for the mean field and the forest transfer function, the forest transfer function F(f,t) may be considered to consist of three components corresponding to the direct wave [$F_d(f,t)$], the reflected wave [$F_r(f,t)$], and the lateral wave [$F_\ell(f,t)$].

Inasmuch as a real input (excitation) to any linear system is always observed to produce a real output (response), it may

be shown as a consequence of Equations (6-1-6) and (6-1-7) that the real part of F(f,t) must be an even function of frequency, i.e.

$$F'(f,t) = F'(-f,t) \tag{6-2-1}$$

and the imaginary part of F(f,t) must be an odd function of frequency, i.e.

$$F''(f,t) = -F''(-f,t) \tag{6-2-2}$$

Further, inasmuch as d-c transmission through the forest is not possible,

$$F(0,t) = 0 \tag{6-2-3}$$

These relations have proved helpful in evaluating the field expressions of Section 5.4 at negative frequencies as required by Equation (6-1-7).

It is apparent from Equation (6-1-7) that the forest transfer function F(f,t) should be defined over the entire frequency range from minus infinity to plus infinity. In practice, however, the forest transfer function need only be defined over the spectral range occupied by the input signal X(f). This is fortunate because the forest transfer function (the normalized vertically-polarized electric field) is expressed on the basis of a high-frequency asymptotic evaluation [refer to Section 5.3] which may give incorrect results below one Megahertz.

Because each of the three forest transfer-function components may be considered to be a complex phasor, the received signal will be either enhanced or degraded depending upon their relative strength and phase. Their relative strengths and phases are clearly frequency-dependent [refer to Section 5.4] and, therefore, the forest transfer function is frequency-selective.

As a consequence of the frequency-dependent factor $(\omega\mu_o/4\pi)$ appearing in Equations (5-4-1) and (5-4-2), the effect of the direct- and reflected-wave components of the forest transfer function on the transmitted signal will be primarily one of differentiation. This is also true in free-space transmission as can be

clearly seen by setting $\varepsilon_t = \varepsilon_z = 1$ in Equation (5-4-1). Except for its exponential factor (which is primarily one of phase delay), the lateral-wave component of the forest transfer function is nearly frequency independent. This means that if an equalizer having a response inversely proportional to frequency (f^{-1}) is employed at the receiver to ensure distortionless free-space transmission, direct- and reflected-wave pulses are received nearly distortion free, whereas wide-band (400 MHz) lateral-wave pulses could be severely distorted.

6.3 Forest Pulse Response

Consider the current moment of the electrically small (Hertzian) dipole transmitting antenna to be the rectangular r-f pulse

$$x(t) = p(t) \cdot \sin(2\pi f_o t) \qquad (6\text{-}3\text{-}1)$$

where f_o is the r-f carrier frequency, and $p(t)$ is the pulse envelope defined here to be

$$p(t) = \begin{cases} 1, & |t| < L/2 \\ 0, & |t| > L/2 \end{cases} \qquad (6\text{-}3\text{-}2)$$

where L is the pulse length (duration).

The amplitude spectrum of the pulse envelope and of the rectangular r-f pulse can be determined from Equation (6-1-6) to be, respectively,

$$P(f) = L \operatorname{sinc}\{\pi L f\} \qquad (6\text{-}3\text{-}3)$$

and

$$X(f) = \tfrac{1}{2}jL\left|\operatorname{sinc}\{\pi L(f + f_o)\} - \operatorname{sinc}\{\pi L(f - f_o)\}\right| \qquad (6\text{-}3\text{-}4)$$

The spectral bandwidth occupied by the central lobe about the carrier frequency f_o is $2/L$.

The forest pulse response, if defined to be the vertically-polarized component of the mean electric field arising in response to a rectangular r-f input pulse of current moment, can be obtained from Equation (6-1-7) upon the substitution of Equation (6-3-4) for the amplitude spectrum of the input X(f) and the use of

Equations (5-4-1), (5-4-2) and (5-4-3) for the forest channel transfer functions.

6.4 Numerical Evaluation

The evaluation of Equation (6-1-7) is not easily effected analytically due to the complex frequency dependence exhibited by the effective dyadic permittivity of the forest $\underline{\varepsilon}$. As a consequence, numerical techniques based upon the fast Fourier transform (FFT) have been employed to expedite its evaluation. A review of the important properties of the FFT and special considerations bearing upon its application to the numerical evaluation of Equation (6-1-7) is presented in Appendix E.

To exemplify the numerical evaluation of the forest pulse response, CyberCom has elected to consider (1) a transmitting-antenna current moment representable by a rectangular r-f pulse; (2) a forest transfer function developed asymptotically on the basis of an anisotropic half-space consisting entirely of electrically-thin leaves; and a receiver with or without equalization for distortionless pulse transmission in free space. The channel model is illustrated in Figure 6-1.

The density of the leaves representing the forest has been taken as 200 leaves per cubic meter with each leaf represented as a dielectric disc 5 centimeters in radius and 1 millimeter in thickness; the leaves have been assumed to be randomly positioned in azimuth and location, and inclined from the horizontal with a probability density function uniform over the range 0 to 30 degrees. The transmitter has been positioned 4 meters (h_t) and the receiver 6 meters (h_r) below the air-forest interface; they have been separated by 1 kilometer (ρ) [refer to Figure 5-2].

The forest transfer functions corresponding to the direct-wave and lateral-wave components have been determined for the postulated forest parameters from Equations (5-4-1) and (5-4-3), respectively, and are shown (magnitudes only) in Figure 6-2 for both unequalized and free-space equalized receivers. The nearly linear frequency response of the unequalized direct-wave component

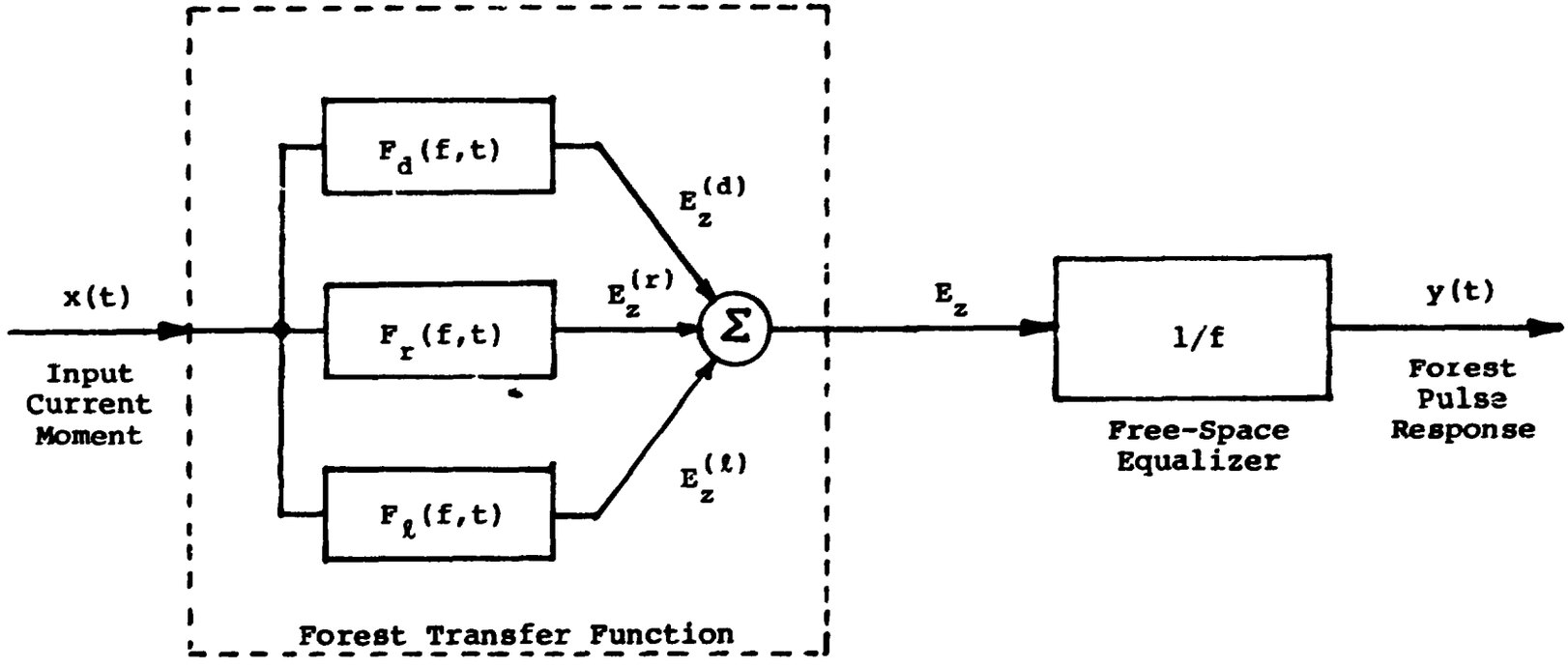

Figure 6-1: Forest Channel Model

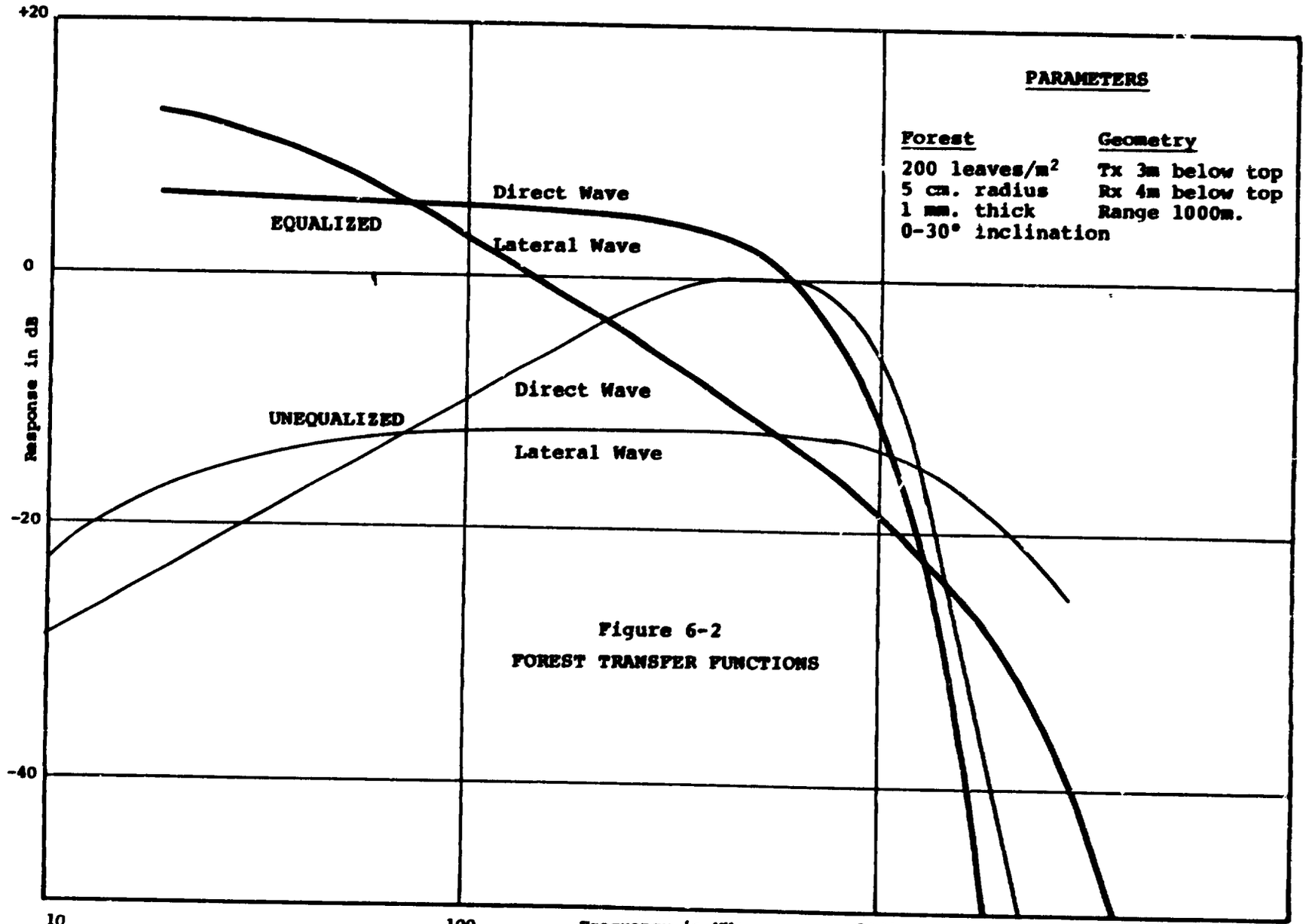

Figure 6-2
FOREST TRANSFER FUNCTIONS

apparent below 600 Megahertz will, as noted previously, lead to differentiation and distortion of a pulse propagated through the forest. The transfer function of the direct-wave component equalized for distortionless free-space transmission is nearly independent of frequency below 600 Megahertz. However, the transfer function of the equalized lateral-wave component appears now to behave as a low-pass filter. A comparison of the unequalized and equalized forest transfer functions suggests that, for distortionless transmission through arbitrary forests, adaptive equalization parametric upon path length, antenna heights, frequency, and forest susceptibility may be required.

The rectangular r-f input pulse of current moment x(t) is shown in Figure 6-3(a). This short pulse, only 5 nanoseconds long, consists of 3-cycles of a 600-Megahertz r-f carrier and occupies a spectral bandwidth (central lobe) of 400 Megahertz.

The unequalized r-f output pulse responses y(t) corresponding to the principal components of the forest transfer function are shown in Figure 6-3(b) to (e). These responses have been computed for the forest channel model of Figure 6-1 using a 256-point (2^8-point) FFT having a time resolution of 0.20833... nanoseconds and a frequency resolution of 53.33... Kilohertz. The direct- and reflected- wave pulses are distorted more than the lateral-wave pulse for reasons previously noted. For the equalized case shown in Figure 6-4, the direct- and reflected-wave pulses are distorted less than the lateral-wave pulse. Distortion of the lateral-wave pulse is primarily attributable to the poor low-frequency response of the asymptotic model, although some distortion is also attributable to the equalizer. Although the pulse distortion introduced by the forest appears to be relatively small (at least for the forest parameters employed here), multipath and intersymbol interference (ISI) could be substantial for multipath transmissions.

At the r-f carrier frequency of 600 Megahertz, the amplitude of the reflected-wave relative to that of the direct-wave is 0.986 (0.12dB down) and its phase almost directly opposite. Although the differential phase shift between

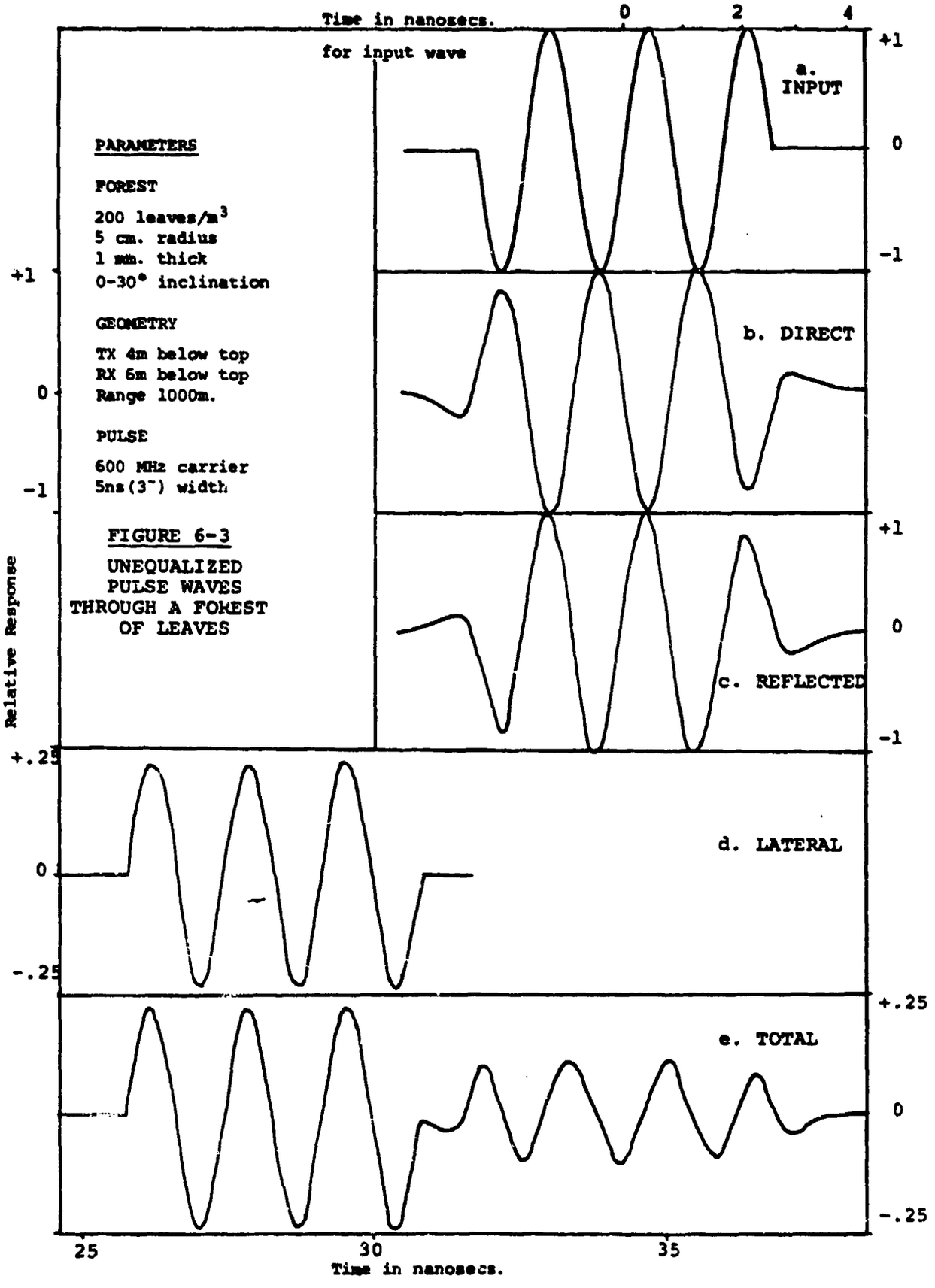

FIGURE 6-3
UNEQUALIZED PULSE WAVES THROUGH A FOREST OF LEAVES

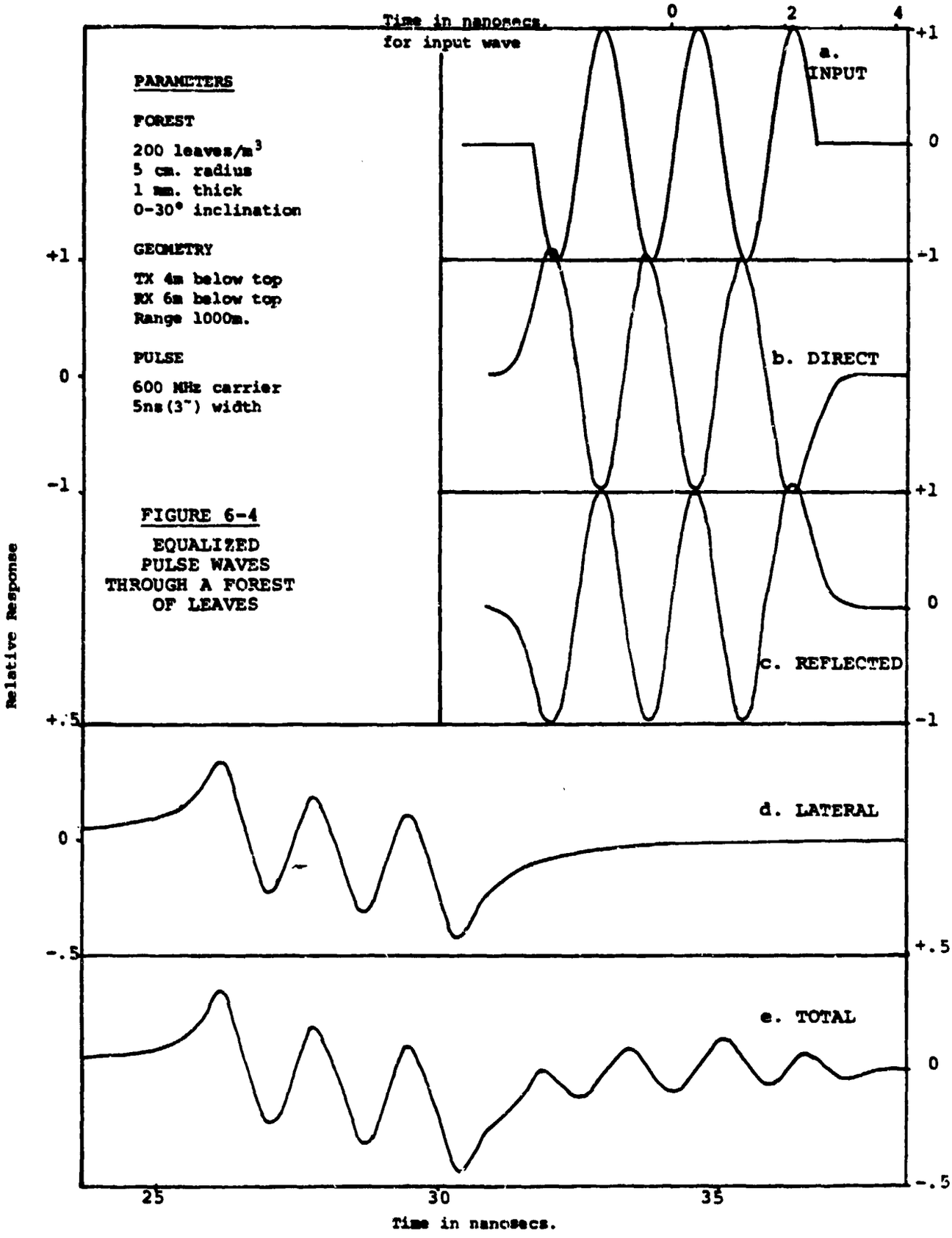

FIGURE 6-4

EQUALIZED PULSE WAVES THROUGH A FOREST OF LEAVES

direct- and reflected-waves attributable to path geometry

$$\Delta\phi = \frac{720\ h_t h_r}{\rho\lambda} \quad \text{(degrees)} \qquad (6\text{-}4\text{-}1)$$

is only about 35 degrees, the phase shift imparted upon reflection from the air-forest interface is about 172 degrees, Thus, the relative amplitude of the direct-plus-reflected wave is only 0.107 or about 19 dB below the direct. In the configuration considered, which may not be realistic because the effects of tree trunks and branches are not yet included, although the amplitude of the lateral-wave relative to that of the direct-wave is only 0.22 (13 dB down), it is approximately 6 dB above the direct-plus-reflected component propagating within the forest. The differential time of arrival (DTOA) between pulses arriving via the direct and lateral waves is approximately

$$[\rho\chi_z'/2 - (h_t+h_r)\sqrt{\chi_z'}]300 = 5.9 \text{ nanoseconds} \qquad (6\text{-}4\text{-}2)$$

7.0 Non-Coherent Forest Scattering

In the preceding three sections propagation through the forest has been described neglecting fluctuations about the mean field. This section will show that these become important as the frequency and propagation distance increase. In this section, the effect of the fluctuations will be taken into account for one specialized forest configuration. The results will give an indication of the importance of the fluctuating field in the forest environment.

In order to keep the analysis tractable, the scalar case of propagation through an infinite medium of vertical trunks will be considered. The trunks will be assumed to be identical vertical circular cylinders of radius a and relative dielectric constant ε_ℓ. In addition, their diameter will be chosen small enough so that the Rayleigh criterion is satisfied. Although the Rayleigh assumption is somewhat restrictive, physically meaningful results can still be attained over a portion if the frequency range of interest. The field is excited by an electric line source of unit magnitude which is parallel to the trunks. As has been pointed out in Section 2.2.1, the assumed source and scatterers give rise to an electric field vector wholly in the z direction. The problem can be exactly scalarized in terms of this component.

The strength of the random component will be examined by determining the intensity of the field

$$I(\underline{x}_t) = \langle \Psi(\underline{x}_t)\Psi^*(\underline{x}_t)\rangle \tag{7-1}$$

and relating it to the intensity of the mean component

$$I_o(\underline{x}_t) = \langle \Psi(\underline{x}_t)\rangle\langle \Psi^*(\underline{x}_t)\rangle \tag{7-2}$$

For two-dimensional Rayleigh scatterers, the intensity satisfies Equation (2-2-50) with $\underline{x}_t = \hat{\underline{x}}_t$. The equation is

$$I(\underline{x}_t) = |G(\underline{x}_t)|^2 - \beta\int d\underline{s}_t |G(\underline{x}_t - \underline{s}_t)|^2 I(\underline{s}_t) \tag{7-3}$$

where $\beta = k_o^4 |\alpha|^2 \rho$ with α being the polarizability constant appearing in Equation (2-2-21). For a circular cylinder, the polarizability is $\alpha = -\chi_\ell \pi a^2$ with $\chi_\ell = \varepsilon_\ell - 1$. In obtaining Equation (7-3) from

Equation (2-2-50) it has been assumed that the trunk medium is unbounded ($s = \infty$) and the density ρ is constant. These homogeneity assumptions lead to a translationally invariant Green's function:

$$G(\underline{x}_t, \underline{x}_t') = G(\underline{x}_t - \underline{x}_t') \tag{7-4}$$

The mean Green's function satisfies Equation (2-2-47). In the Rayleigh regime this equation reduces to

$$[\nabla_t^2 + k_o^2(1 + \rho\alpha)]G(\underline{x}_t) = \delta(\underline{x}_t) \tag{7-5}$$

The solution is given in terms of the zeroth order Hankel function of second kind. It is

$$G(\underline{x}_t) = \frac{j}{4} H_o^{(2)}(\kappa) \quad , \tag{7-6}$$

and

$$\kappa = k_o\sqrt{1 + \rho\alpha} \tag{7-7}$$

Before proceeding it should be pointed out that the intensity Equation (7-3) was derived under the assumption of small fractional area (two-dimensional analog of small fractional volume used for three-dimensional problems). Analytically, this condition states that $\pi a^2\rho << 1$. For a forest having a = 10cm and ρ = .1/m, the condition is met, since $\pi a^2\rho = 0.003 << 1$. Since $\rho\alpha = \chi_\ell(\pi a^2\rho)$ and $|\chi_\ell| \approx 40$, one can also conclude $\rho\alpha << 1$.

The exact solution to Equation (7-3) can be obtained by convolution techniques; however, the inverse transform involves a double integral. To simplify the form of the solution, the Green's function in Equation (7-3) is replaced by its far-field approximation. One obtains

$$G(\underline{x}_t) = \frac{j}{2\sqrt{2\pi\kappa x_t}} e^{-j(\kappa x_t - \pi/4)} \tag{7-8}$$

where $|\kappa x_t| >> 1$. Further simplification is obtained by using the fact that

$$\kappa \approx k_o(1 + \rho\,\alpha/2) \tag{7-9}$$

in the asymptotic expression for G. This result is:

$$G(\underline{x}_t) = \frac{j}{2\sqrt{2\pi k_o x_t}} e^{-j(k_o x_t - k_o \rho \alpha/2 - \pi/4)} \tag{7-10}$$

Now using Equation (7-10) in Equation (7-3), the approximate intensity equation is

$$I(\underline{x}_t) = K(x_t) - \beta \int d\underline{s}_t K(\underline{x}_t - \underline{s}_t) I(\underline{s}_t) \tag{7-11}$$

where

$$K(x_t) = \frac{e^{k_o \rho \alpha'' x_t}}{8\pi k_o x_t} \tag{7-12}$$

The solution to this equation can be obtained in terms of the single quadrature since now the Fourier transform of $K(\underline{x}_t)$ can be explicitly evaluated.

Before solving Equation (7-11), the physical restrictions imposed on the solution when the asymptotic form of the Green's function is used are addressed. First, the term $|G(\underline{x}_t)|^2$ appearing on the right hand side of Equation (7-3) has been replaced by its asymptotic approximation. This requires that $\kappa|\underline{x}_e| >> 1$ or that the receiving antenna be in the far field of the transmitter. Second, the Green's function in the integrand of Equation (7-3) has been replaced by its asymptotic expansion. This requires that $\kappa|\underline{x} - \underline{s}| >> 1$ or that the scatterers be in the far field of the observation point. Thus scatterers that are in the near field of the observation point are not treated correctly. This inaccuracy is small, however, if the far field distance is not too large. In this case, there are many more scatterers in the far field of the observation point than in the near field.

Integral Equation (7-11) can be solved exactly using Fourier transform theory. If the Fourier transform of I(x) is denoted by $\tilde{I}(\underline{k})$ where

$$I(\underline{x}_t) = \int d\underline{k}_t \tilde{I}(\underline{k}_t) e^{-j\underline{k}_t \cdot \underline{x}_t} \tag{7-13}$$

then the transform of Equation (7-11) becomes:

$$\tilde{I}(\underline{k}_t) = \tilde{K}(\underline{k}_t) + \tilde{\beta}\tilde{K}(\underline{k}_t)\tilde{I}(\underline{k}_t) \quad , \quad \tilde{\beta} = (2\pi)^2\beta \tag{7-14}$$

where

$$K(\underline{k}_t) = K(k_t) = \frac{1}{(4\pi)^2 k_o} \cdot \frac{1}{\sqrt{k_t^2 + (k_o\alpha^{-1}\rho)^2}} \tag{7-15}$$

with $k_t = |\underline{k}_t|$. Solving Equation (7-14) for $\tilde{I}(\underline{k}_t)$ gives

$$I(\underline{k}_t) = \frac{\tilde{K}(k_t)}{1 - \tilde{\beta}\tilde{K}(k_t)} \tag{7-16}$$

Now using this result in Equation (7-13), the intensity is

$$I(\underline{x}_t) = \int d\underline{k}_t \frac{\tilde{K}(k_t)}{1 - \tilde{\beta}\tilde{K}(k_t)} e^{-j\underline{k}_t \cdot \underline{x}_t} \tag{7-17}$$

Since $\tilde{I}(k_t)$ only depends on the absolute value of $\underline{k}_t$, the angular dependence in Equation (7-17) can be integrated explicitly. Let θ be the angle between $\underline{k}_t$ and $\underline{x}_t$; then

$$\underline{k}_t \cdot \underline{x}_t = k_t x_t \cos\theta \tag{7-18}$$

and $d\underline{k}_t = k_t dk_t d\theta$. Equation (7-17) becomes

$$I(\underline{x}_t) = I(x_t) = \int_0^\infty dk_t \int_0^{2\pi} d\theta \frac{k_t \tilde{K}(k_t)}{1 - \tilde{\beta}\tilde{K}(k_t)} e^{-jk_t x_t \cos\theta} \tag{7-19}$$

$$I(\underline{x}_t) = \frac{1}{2\pi} \int_0^\infty dk_t \frac{k_t J_o(k_t x_t)}{4k_o\sqrt{k_t^2 + (k_o\alpha^{-1}\rho)^2} - \beta} \tag{7-20}$$

The expression for the intensity given in Equation (7-20) is a function of x_t, k_o, α and β. This dependence on four parameters can be reduced to two parameters by appropriate scaling and normalization. For this purpose, the two-dimensional scattering cross section σ_s and total cross section σ_t are introduced. These quantities are related to the transform of the two-dimensional transition operator as follows (Appendix F)

$$\sigma_s = \frac{2\pi^3}{k_o} \int_0^{2\pi} d\theta |\tilde{t}(k_o\underline{o}, k_o\underline{i})|^2 \tag{7-21}$$

$$\sigma_t = -\frac{(2\pi)^2}{k_o} \text{Im } \tilde{t}(k_o\underline{o}, k_o\underline{i}) \tag{7-22}$$

For Rayleigh scatterers, $\tilde{t}(k_o\underline{o}, k_o\underline{i})$ becomes

$$\tilde{t}(k_o\underline{o}, k_o\underline{i}) = \frac{\alpha}{(2\pi)^2} k_o^2 \tag{7-23}$$

Using this in the expressions for σ_s and σ_t gives

$$\sigma_s = \frac{k_o |\alpha|^2}{4} \tag{7-24}$$

$$\sigma_t = -k_o \alpha'' \tag{7-25}$$

The albedo, W_o, and the optical distance, τ, can be introduced using the cross sections just defined. They are:

$$W_o = \frac{\sigma_s}{\sigma_t} \qquad \tau = \rho\sigma_t x_t \tag{7-26}$$

The albedo is a ratio of the scattered power to the total power, with the total power defined as the scattered power plus the power absorbed by the particle (Appendix F). The albedo lies between 0 and 1. For $W_o = 0$ there is no scattering (all absorption) and for $W_o = 1$ there is no absorption (all scattering).

The optical distance is a measure of the attenuation of the mean intensity, $I_o(\underline{x}_t)$. Thus, in the far field of the source

$$I_o(x_t) = |G(\underline{x}_t)|^2 \sim \frac{e^{-\rho\sigma_t x_t}}{8\pi k_o x_t} \tag{7-27}$$

where Equations (7-10) and (7-25) have been used. From Equation (7-27) it is seen that when $\tau = \rho\sigma_t x_t = 1$, the exponential has an argument of -1. Now Equation (7-20) can be normalized. Let $q = k_t/\rho\sigma_t$ and define a normalized intensity

$$\bar{I}(x_t) = I(x_t)/I_o(x_t) \tag{7-28}$$

The expression for the normalized intensity is then given by

$$\bar{I}(\tau) = \tau e^{\tau} \int_0^{\infty} \frac{dq\, q\, J_o(q\tau)}{\sqrt{q^2 + 1} - W_o} \tag{7-29}$$

Thus the normalized intensity $\bar{I}$ is only a function of τ and W_o.

The expression of $\bar{I}(\tau)$ given in Equation (7-29) is exact but slowly converging. As q becomes large, the integrand is proportional to $\cos(q\tau)/\sqrt{q}$. This convergence makes numerical evaluation difficult. Fortunately, by deforming the integral into the complex plane, a more rapidly converging representation can be obtained (see Appendix G). The result is

$$\bar{I}(\tau) = 2\tau W_o e^{\tau} K_o(\tau\sqrt{1 - W_o^2}) + \frac{2\tau}{\pi} e^{\tau} \int_0^{\infty} dp\, p^2 \frac{K_o(\tau\sqrt{1 + p^2})}{p^2 + W_o} \tag{7-30}$$

The integrand is now exponentially decaying for large p. As a check, it is interesting to note if $W_o = 0$, then $\bar{I}(\tau) = 1$. This means that if there is no scattering, the mean intensity is exactly equal to the total intensity.

The coherent and noncoherent intensities have been computed. Some representative results of the computations are shown in Figure 7-1. Because of the need to satisfy the Rayleigh criterion, $k_o\sqrt{\epsilon}\, a << 1$, the small trunk radius of 0.01 meters was chosen. Using this trunk radius and CyberCom permittivity modal III, the Rayleigh number was computed to be 0.4 at 300 MHz. It is also seen from Figure 7-1 that a density of $0.1/m^2$ has been used. This represents, on the average, one tree in every 10 square meter area.

It can be seen that the coherent intensities (related to the powers by a constant) decrease almost linearly with distance as expected in the assumed two-dimensional medium. The noncoherent intensities, however, fall off much more slowly with distance, thereby becoming an increasing fraction of the total intensity. At 300 MHz, the noncoherent intensity becomes greater than the

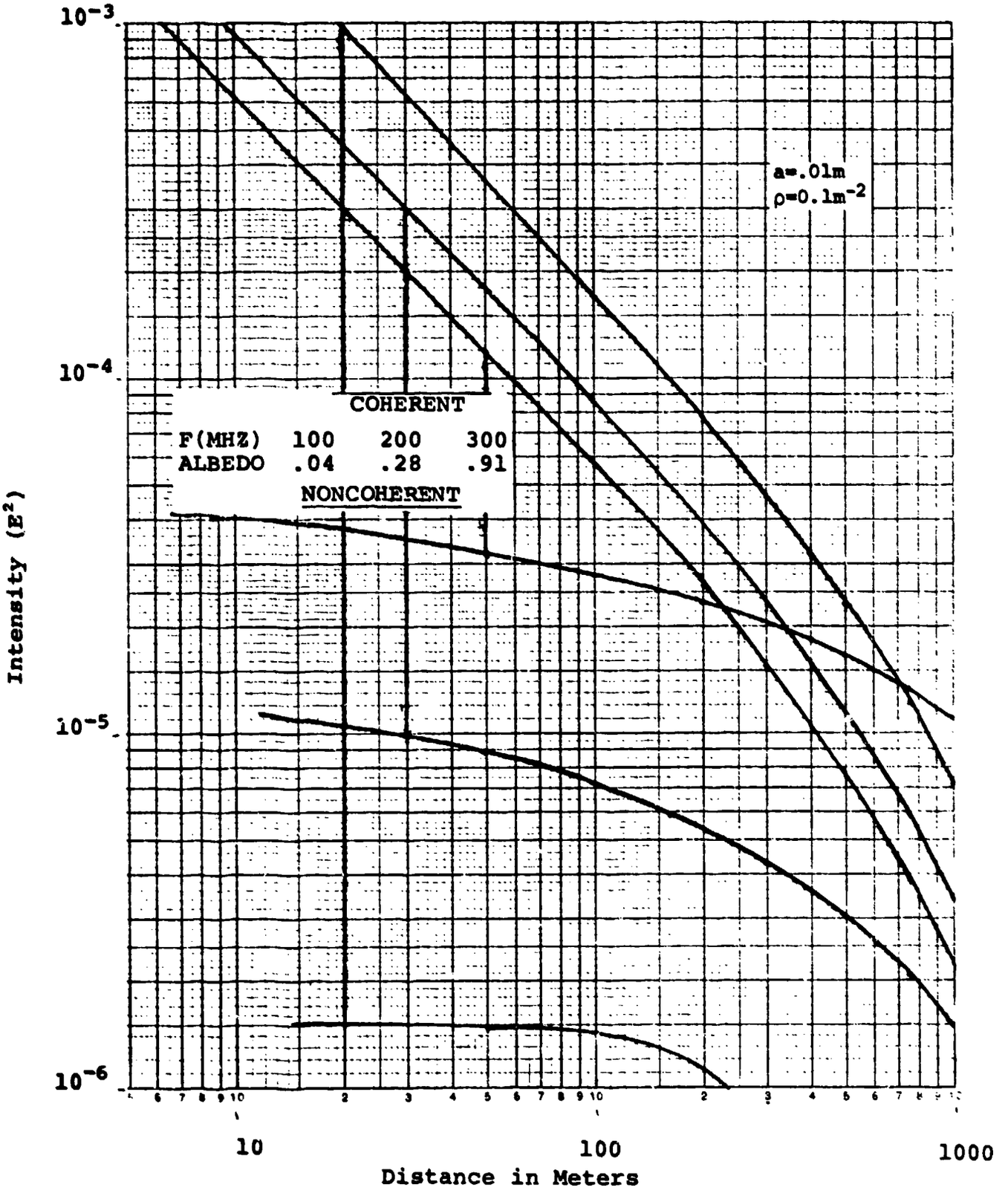

Fig. 7-1 Coherent and Noncoherent Intensities through Tree Trunks

coherent intensity beyond about 230 meters. This behavior is similar to that in Figure 8 of Schwering et al [28a], which also uses transport theory. If the total intensity is replotted on a linear distance scale as in Schwering et al, it is seen to fall off at a decreasing rate with distance.

In Figure 7-2 are plotted the normalized intensities (total/coherent). An examination of the curves shows that the normalized intensity increases with distance. At a frequency of 100 MHz or 200 MHz, the normalized intensity stays fairly close to unity for distances as great as one kilometer. This means that the random component of the intensity is relatively small for frequencies below 200 MHz and distances as large as 1 kilometer. The curve for 300 MHz increases rapidly with distance, however, and reveals that the random component will be important for distances in excess of 200 meters.

It appears that the random component of the intensity increases with frequency and propagation distance. Although the computed values presented in Figure 7-1 are interesting, to compute the intensity for a forest with larger trunks, the Rayleigh or low-frequency approximation can not be employed. The correlation equation must be used with the transition kernel for resonant trunks. This has yet to be done.

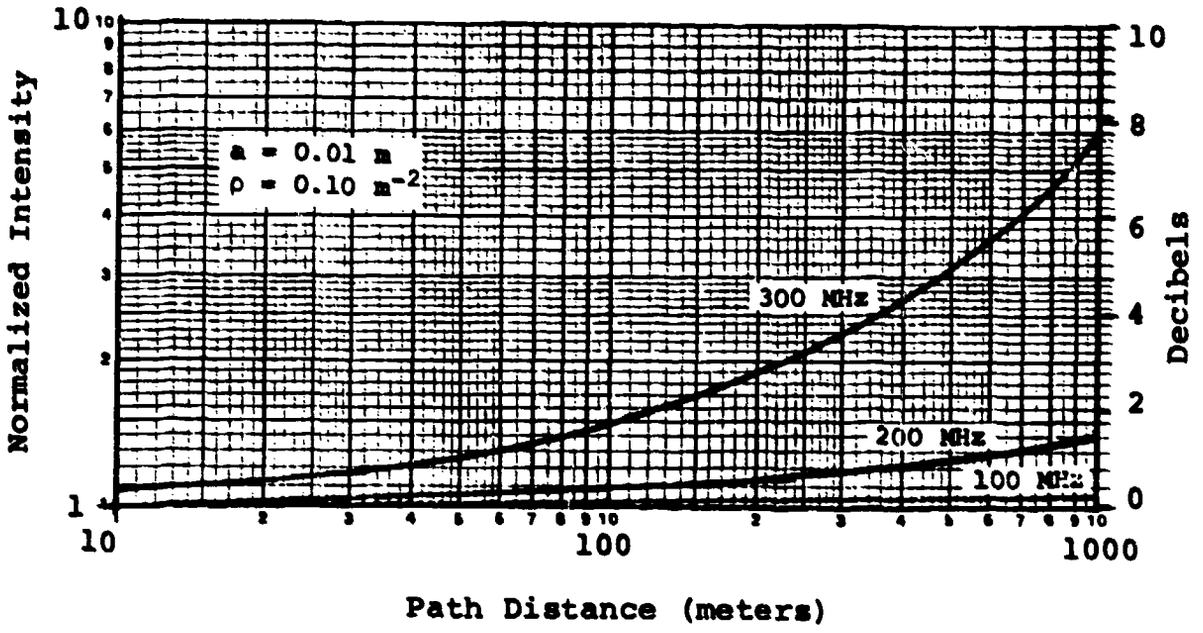

Figure 7-2: Normalized Intensity (Total/Coherent)

8.0 Conclusions

CyberCom has developed a stochastic radiowave propagation model useful for assessing the effects of forests and other vegetation upon radio communication systems operating in the 200 - 2000 Megahertz frequency band. The model considers the forest to be representable as a time-invariant ensemble of randomly positioned and oriented, discrete, canonical scatterers. Tree trunks are modeled as infinitely-long, circular, lossy-dielectric cylinders; branches as finitely-long, circular, lossy-dielectric cylinders; and leaves as flat, circular, lossy-dielectric discs. Mathematical expressions characterizing the scattering properties of these canonical scatterers in terms of their dyadic scattering amplitudes have been developed and integrated into the multiple-scattering theory of Foldy [53] to develop equations describing the behavior of a propagating radiowave. In the case of tree trunks and leaves, the model is suitable even in the difficult resonant scattering region where the physical dimensions of the scatterer are comparable to the radio wavelength within. However, in the case of branches, additional study would be required to extend the model into the resonant regime.

The propagating radiowave may be considered to consist of two components - a mean (or coherent) component and a random (or non-coherent) component. CyberCom has shown that, so far as the mean radiowave component is concerned, the ensemble of discrete canonical scatterers representing the forest can be replaced by an equivalent continuous medium characterized by an effective dyadic susceptibility $\underline{\chi}$. Simple mathematical expressions have been developed relating $\underline{\chi}$ to such biophysical parameters of the forest as tree trunk, branch and leaf dimensions, permittivity, number density, and orientation statistics. Expressions relating the specific attenuation of a radiowave propagating within an unbounded forest of tree trunks, branches or leaves to salient biophysical parameters of the forest have been developed and shown to agree favorably with experimental data. Utilization of these expressions in radio communication systems design still requires, however, a

global statistical classification and quantification of these biophysical forest parameters.

The effective dyadic susceptibility has been used by CyberCom in a half-space representation of the forest to extend an earlier isotropic model proposed by Sachs and Wyatt [101] and studied by Tamir [107]. This newer anisotropic model encompasses the lateral-wave contributions observed experimentally on long-distance paths above 200 Megahertz. For generality, it should be refined by consideration of the ground plane.

Using linear system theory, CyberCom has extended the harmonic anisotropic half-space model of the forest to the transmission of arbitrarily-modulated waveforms. This extension has been used to show the pulse distortion arising in the direct-, reflected- and lateral-wave components of the mean scattered field, and also in the total mean field. This extension of the model is especially important if the model is to be used in the analysis and evaluation of digital, spread-spectrum radio systems.

CyberCom has also investigated the random (or non-coherent) scattered field propagating within an unbounded forest of electrically-thin, infinitely-long, lossy-dielectric, parallel tree trunks. For this simple forest model, CyberCom has shown that the intensity of the non-coherent scattered field increases relative to that of the coherent (mean) field with increasing distance from the source and with increasing carrier frequency. This work should be extended so far as possible towards fully realistic models.

In summary, the homogenous isotropic, refracting slab model of a forest has been replaced by CyberCom with an inhomogenous, anisotropic, scattering ensemble of trunks, branches, and leaves. In consequence:

1. The lateral-wave contribution has been found even above 200 Megahertz.

2. Preliminary validation of the model has shown rough agreement with experiments.

3. Results have been obtained for narrow pulse transmission at 600 MHz.

4. A preliminary study (as well as field reports) has emphasized the importance of the incoherent component of the transmitted field.

As the CyberCom approach is ambitious in both scope and depth, the following remain to be done:

a. The techniques already developed must be exercised to determine the relative importance of forest components and the effects of varying critical parameters. For example, if the contribution of branches is major, the difficult characterization of the scattering properties should be advanced in the resonant region.

b. The effects of antenna directivity, the ground, and terminal movement should be incorporated into the model.

c. The difficult transport theory for the important noncoherent scattered wave should be developed as far as practical.

d. Forest studies must be pursued to quantify important biophysical parameters in areas of interest.

9.0 References

9.1 Forest Characteristics

1. M.G. Broadhurst, "Complex Dielectric Constant and Dissipation Factor of Foliage," National Bureau of Standards Report 9592 (October, 1970).

2. C.F. Brockman, Trees of North America, New York: Golden (1979).

3. N.L. Carlson, "Dielectric Constant of Vegetation at 8.5 GHz," Ohio State University, Electro-Science Laboratory, Tech. Report 1903-5 (1967).

4. P. Debye, Polar Molecules, New York: Dover (1929).

5. A. Feininger, Trees, New York: Viking (1968).

6. A. Fung, "Scattering from a Vegetation Layer," IEEE Trans. Geosci. Electron., Vol. 17, No. 1, pp 1-6 (1979).

7. R.F. Hearmon and J.N. Burcham, "The Dielectric Properties of Wood," Forest Products Research, Special Report No. 8, Her Majesty's Stationary Office (London) (1954).

8. W. James and D. Hamill, "Dielectric Properties of Douglas Fir Measured at Microwave Frequencies, " Forest Product J., Vol. 15, No. 2, p 57 (1965).

9. B.P. Kwok, "Time Domain Measurements for Determination of Dielectric Properties of Agricultural Materials," IEEE Trans. Instrum. & Meas., Vol, IM-28, No. 2, pp 109-122 (June, 1979).

10. G.P. de Loor, "Dielectric Properties of Heterogeneous Mixtures Containing Water," J. of Microwave Power, Vol. 3, No. 2, pp 67-73 (1968).

11. R. Lynn, "Review of Dielectric Properties of Wood and Cellulose," Forest Product J., Vol. 17, No. 7, pp 61- (1967).

12. A. Nanassy, "Electric Polarization Measurements on Yellow Birch," Can. J. Phys., Vol. 42, No. 6, pp 1270- (1964).

13. J.A. Saxton, "The Dielectric Properties of Water Vapour at Very High Radio Frequencies," in Meteorological Factors in Radio Propagation, London: The Physical Society (1946).

14. J.A. Saxton, and J.A. Lane, "The Anomalous Dispersion of Water at Very High Frequencies," in Meteorological Factors in Radio Propagation, London: The Physical Society (1946).

15. M.G. Cannell, World Forest Biomass and Primary Production Data, New York: Academic Press (1982).

16. C. Skaar, "Dielectric Properties of Wood at Several Radio Frequencies," New York State College of Forestry, Tech. Publication No. 69 (1948).

17. J.R. Smith, et al, "A comparison of Two Photographic Techniques for estimating Foliage Angle Distribution," Aust. J. Bot., Vol. 25, No. 6, pp545-553 (1977).

18. S.S. Stuchly, "A Method for Measurement of Permittivity of Thin Samples," J. Microwave Power, Vol. 14, No. 1, pp 7-13 (March, 1979).

19. V.W. Trapp and L. Pungs, "Einfluss von Temperature und Feuchte auf das Dielectrische Verhalten von Naturholz im Grossen Frequenzbereich," Holzforschung (Berlin), Vol. 10, No. 5, pp 144-150 (1956).

20. A.R. Von Hipple (ed.), Dielectric Materials and Applications, New York: Wiley (1954).

21. J.R. Wang and T.J. Schmugge, "An Empirical Model for the Complex Dielectric Permittivity of Soils as a Function of Water Content," IEEE Trans, Geosci. Electron., Vol. 18, No. 4, pp 288-295 (1980).

22. J.R. Wang, "The Dielectric Properties of Soil-Water Mixtures at Microwave Frequencies," Radio Science, Vol. 15, No. 5, pp 977-985 (September-October, 1980).

23. H.S. Zim and A.C. Martin, Trees - A Guide to Familiar American Trees, New York: Golden (1956).

24. U.S. Department of Agriculture, "Physical Properties of Wood," USDA Agricultural Handbook No. 72 - Wood Handbook: Wood as an Engineering Material, Chapter 8 (1974).

9.2 Propagation through Vegetation

25. G.S. Brown and W.J. Curry, "An Analytical Study of Wave Propagation through Foliage," Rome Air Development Center (RADC), Final Technical Report RADC-TR-79-359 (January, 1980).

26. L.J. Du and W.H. Peake, "Rayleigh Scattering from Leaves," Proc. IEEE, Vol. 57, No. 6, pp 1227-1229 (1969).

27. A. Fung and F.T. Ulaby, "A Scatter Model for Leafy Vegetation," IEEE Trans, Geosci. Electron., Vol. GE-16., No. 4, pp 281-285 (October, 1978).

28. G.H. Hagn, "VHF Radio System Performance Model for Predicting Communications Operational Ranges in Irregular Terrain," IEEE Trans. on Comm., Vol. COM-28, No. 9, pp 1637-1644 (September, 1980).

29. G.A. Hufford, et al, "Wideband Propagation Measurements in the Presence of Forest," Research and Development Technical Report CECOM-82-CS029-F (January, 1982).

30. J. Jones and L.G. Sturgill, "Tropical Propagation Research: Final Report," Vol. 1 (1966).

31. S. Krevsky, "HF and VHF Radio Wave Attenuation through Jungle and Woods," IEEE Trans. Antennas & Propagation, Vol. AP-11, No. 4, pp 506-507 (July, 1963).

32. A.G. Longley, and P.L. Rice, "Prediction of Tropospheric Radio Transmission Loss Over Irregular Terrain, A Computer Method - 1968," US Dept. of Commerce, Institute for Telecommunication Sciences, ESSA Technical Report ERL79-ITS67, (July, 1968).

33. R.A. Nelson, "UHF Propagation in Vegetative Media," SRI International, Final Report - Contract DAAG29-76-D-0100, Menlo Park, California (April, 1980).

34. R.I. Presnell, "PLRS Ground-to-Ground Propagation Measurements," SRI International, Final Report - Contract MDA903-78-C-0126, Menlo Park, California (June, 1980).

35. R.I. Presnell, "JTIDS Ground-to-Ground Propagation Measurements,' SRI International,..... as above

36. J.A. Saxton and J.A. Lane, "VHF and UHF Reception - Effects of Trees and Other Obstacles," Wireless World, Vol. 61, No. 5, pp 229-232 (May, 1955).

37. W.A. Stirrat, "UHF Propagation Through Foliage," US Army Electronic Warfare Laboratory, Fort Monmouth, New Jersey (May, 1981).

38. W.L. Stutzman, et al, "Microwave Transmission Measurements for Estimation of the Weight of Standing Pine Trees," IEEE Trans. Antennas & Propagation, Vol. AP-27, No. 1, pp22-26 (January, 1979).

39. S. Swarup and R.K. Tewari, "Radiowave Propagation Through Subtropical Pine Forest," Indian J. of Radio Space Phys., Vol. 3, pp 181-185 (June, 1974).

40. S. Swarup and R.K. Tewari, "Propagation Characteristics of VHF/UHF Signals in Tropical Moist Deciduous Forest," J. Inst. Electron. & Telecom. Engr. (India), Vol. 21, No. 3, pp 123-125 (March, 1975).

41. S. Swarup and R.K. Tewari, "Depolarization of Radio Waves in Jungle Environments," IEEE Trans. Antennas & Propagation, Vol. AP-27, No. 1, pp 113-116 (January, 1979).

42. J.R. Wait, et al, "Workshop on Radio Systems in Forested and/or Vegetated Environments," US Army Communications Command (USACC) Technical Report ACC-ACO-1-74 (February, 1974).

43. F.T. Ulaby, et al, Microwave Remote Sensing, New York: Wesley (1981).

44. E.J. Violette, et al, "SHF-EHF Propagation Through Vegetation on Colorado East Slope," US Dept. of Commerce, Institute for Telecommunication Sciences, Research and Development Technical Report CECOM-81-CS020-F (June, 1981).

45. M.A. Weissberger, et al, "Radio Wave Propagation: A Handbook of Practical Techniques for Computing Basic Transmission Loss and Field Strength," Electromagnetic Compatability Analysis Center (ECAC), Report No. ECAC-HDBK-82-049 (September, 1982).

46. "Radio Propagation through New Guinea Rain Forest," New Zealand Dept. of Scientific and Industrial Research, Operational Research Section, Report No. 8, Melbourne, Australia (1944).

47. "Tropical Propagation Research, Final Report, Vol. I,II,III," Atlantic Research Corp., Jansky and Bailey Engineering Dept., Alexandria, Virginia (1966-1969).

48. "The Influence of Trees on PLRS Communication Capability," Hughes Aircraft Company (July, 1978).

9.3 Propagation in Discrete Random Media

49. I.M. Besieris and W.E. Kohler, "Two-Frequency Radiative Transfer Equation for a Statistically Inhomogeneous and Anisotropic Absorptive Medium," in Multiple Scattering and Waves in Random Media, New York: North Holland (1981).

50. G.S. Brown, "Coherent Wave Propagation Through a Sparse Concentration of Particles," Radio Science, Vol. 15, No. 3, pp 705-510 (may-June, 1980).

51. S. Chandrasekhar, Radiative Transfer, London: Oxford (1960).

52. A. Cohen and C. Acquista, "Light Scattering by Tilted Cylinders: Properties of Partial Wave Coefficient," Optical Society of America, Vol. 72, No. 5, pp 531-534 (May, 1982).

53. L.O. Foldy, "The Multiple Scattering of Waves," Phys. Rev., Vol. 67, No. 3, pp 107-119 (March, 1945).

54. A. Ishimaru, "Theory and Application of Wave Propagation and Scattering in Random Media," Proc. IEEE, Vol. 65, No. 7, pp 1030-1061 (July, 1977).

55. A. Ishimaru, Wave Propagation and Scattering in Random Media (Vols. 1 & 2), New York: Academic Press (1978).

55a. M. Lax, "Multiple Scattering of Waves," Rev. Mod. Phys., Vol. 23, No. 4, pp 287-310 (1951).

56. J.B. Keller, "Wave Propagation in Random Media," Proc. Symp. Appl. Math., Vol. 13, pp 145-170 (1962).

57. R.H. Lang, "Electromagnetic Backscattering from a Sparse Distribution of Lossy Dielectric Scatterers," Radio Science, Vol. 16, No. 1, pp 15-30 (January-February, 1981).

58. R.H. Lang and J. Sidhu, "Electromagnetic Backscattering from a Layer of Vegetation: A Discrete Approach," to be published in IEEE Trans. Geosci. Electron. (January, 1983).

59. J.C. Lin and A. Ishimaru, "Multiple Scattering of Waves by a Uniform Random Distribution of Discrete Isotropic Scatterers," J. Acous. Soc. America, Vol. 59, pp 1695-1700 (1974).

60. S. Rosenbaum and L.W. Bowles, "Clutter Return from Vegetated Areas," IEEE Trans. Antennas and Propagation, Vol. AP-22, No. 2, pp 227-236 (March, 1974).

61. S.S. Seker, "Resonant Backscattering from Sparsely Distributed Lossy Dielectric Scatterers," George Washington University, D. Sc. Dissertation (1982).

62. L. Tsang, et al, "Radiative Transfer Theory for Active Remote Sensing of a Layer of Small Ellipsoidal Scatterers," Radio Science, Vol. 16, No. 3, pp 321-329 (May-June, 1981).

63. V. Twersky, "On Propagation in Random Media of Discrete Scatterers," Proc. Symp. Appl. Math., Vol. 16, pp 84-116 (1964).

64. V. Twersky, "Multiple Scattering of Electromagnetic Waves by Arbitrary Configurations," J. Math. Phys., Vol. 8, No. 3, pp 589-610 (1967).

65. V.K. Varadum and V.V. Varadum (eds.), Acoustic, Electromagnetic and Elastic Wave Scattering - Focus on the T-Matrix Approach, New York: Pergamon (1980).

66. M. Abramowitz and I.A. Stegun (eds.), Handbook of Mathematical Functions, New York: Dover (1965).

67. U. Frisch, "Wave propagation in a random medium," Probabilistic Methods in Applied Math., Vol. 1, pp 75-198, Academic, New York, (1968).

9.4 Scattering by Dielectric Objects

68. P.W. Barber, and C. Yeh, Scattering of Electromagnetic Waves by Arbitrarily Shaped Dielectric Bodies," Applied Optics, Vol. 14, No. 12, pp 2864-2872 (December, 1975).

69. M. Chiba and T. Ishiai, "On a Method of Eliminating the Resonant Solutions of Integral Equations for the Problem of Scattering from Dielectric Cylinders," Trans. Inst. Electron. and Commun. Eng. Japan, Vol. E62, No. 12, pp 916- , (December, 1979).

70. I.S. Gradshteyn and I.M. Ryzhik, Tables of Integrals, Series, and Products, New York: Academic (1965).

71. A.R. Holt, N.K. Uzunoglu, and B.C. Evans, "An Integral Equation Solution to the Scattering of Electromagnetic Radiation by Dielectric Spheroids and Ellipsoids," IEEE Trans. Antennas and Propagation, Vol. AP=26, pp 706-712 (1978).

72. A.R. Holt and J.W. Shepherd, "Electromagnetic Scattering by Dielectric Spheroids in the Forward and Backward Directions," J. Phys. A: Math. Gen., Vol. 12, pp 159-166 (1979).

73. D.M. LeVine, et al, "High Frequency Scattering from Arbitrarily Oriented Dielectric Disks," NASA Technical Memo. 83910 (1982).

74. K.N. Liau, "Electromagnetic Scattering by Arbitrarily Oriented Ice Cylinders," App. Optics, Vol. 11, No. 3, pp 667-67[illegible] (1972).

75. K.F. Mei, "Unimoment Method of Solving Antenna and Scattering Problems," IEEE Trans. Antennas Propagation, Vol. AP-22, pp 760-766 (1974).

76. C.R. Mullin, R. Sandburg, and C.O. Velline, "A Numerical Technique for the Determination of Scattering Cross Sections of Infinite Cylinders of Arbitrary Geometrical Cross Sections," IEEE Trans. on Antennas and Propagation, Vol. AP-13, No. 1, pp 141-149 (January, 1965).

77. J.F. Owen, et al, "Internal Electric Field Distribution of a Dielectric Cylinder at Resonance Wavelengths," Optics Letter, Vol. 6, No. 11, pp 540-542 (November, 1981).

78. G.T. Ruck, D.E. Barrick, W.D. Stuart, and C.K. Krichbaum, Radar Cross Section Handbook (Vols. 1 & 2), New York: Plenum (1970).

79. R. Schiffer and K.O. Thielheim, "Light Scattering by Dielectric Needles and Disks," J. Applied Phys., Vol. 50, pp 2476-2483 (1979).

80. M. Tomita and K. Yasuura, "Numerical Analyses of Plane Wave Scattering from Dielectric Cylinders," Trans. Inst. Electron. and Commun. Eng. Japan, Vol. E62, No. 2, pp 104-105 (Februrary, 1979).

81. J. Van Bladel, "Resonant Scattering by Dielectric Cylinders," Microwave, Optics and Acous., Vol. 1, No. 2, pp 41-50 (January, 1977).

82. J.R. Wait, "Scattering of a Plane Wave from a Right Circular Dielectric Cylinder at Oblique Incidence," Can. J. Phys., Vol. 33, pp 189-195 (1955).

83. J.R. Wait, Electromagnetic Radiation from Cylindrical Structures, New York: Pergamon (1959).

84. P.C. Waterman, "Matrix Formulation of Electromagnetic Scattering," Proc. IEEE, Vol. 53, pp 805-812 (1965).

85. H. Weil and C.M. Chu, "Integral Equation Method for Scattering and Absorption of Electromagnetic Radiation by Thin Lossy Dielectric Disks," J. Comp. Phys., Vol. 22, pp 111-124 (1976).

86. H. Weil and C.N. Chu, "Scattering and Absorption of Electromagnetic Radiation by Thin Dielectric Disks," Applied Optics, Vol. 15, pp 1832-1836 (1976).

9.5 Propagation in Stratified, Isotropic Media

87. L.M. Brekhovskikh, Waves in Layered Media, New York: Academic (1960).

88. D.C. Chang and R.J. Fisher, "A Unified Theory on Radiation of a Vertical Electric Dipole Above a Dissipative Earth," Radio Science, Vol. 9, No. 12, pp 1129-1138 (December, 1974).

89. D.C. Chang and J.R. Wait, "Appraisal of Near-Field Solutions for a Horizontal Dipole Over a Conducting Half-Space," Can. J. Phys., Vol. 48, pp 737-743 (1970).

90. P.C. Clemmow, "The Resolution of a Dipole Field into Transverse Electric and Transverse Magnetic Waves," Proc. IEEE, Vol. 110, No. 1, pp 107-111 (January, 1963).

91. R.E. Collin and F.J. Zucker, Antenna Theory (Parts 1 & 2), New York: McGraw-Hill (1969).

92. D. Dence and T. Tamir, "Transmission Losses in a Forest for Antennas Close to the Ground," US Army Electronics Command (ECOM), Research and Development Technical Report ECOM-2940 (February, 1968).

93. D. Dence and T. Tamir, "Radio Loss of Lateral Waves in Forest Environments," Radio Science, Vol. 4, No. 4, pp 307-318 (April, 1969).

94. L.B. Felsen, "Lateral Waves," in Electromagnetic Wave Theory Part 1, New York: Pergamon (1967).

95. L.B. Felsen and N. Marcuvitz, Radiation and Scattering of Waves, Englewood Cliffs, New Jersey: Prentice-Hall (1973).

96. D.S. Jones, The Theory of Electromagnetism, New York: Pergamon (1964).

97. R.W. King and B. Sandler, "Subsurface Communication Between Dipoles in General Media," IEEE Trans. Antennas & Propagation, Vol. AP-25, pp 770-775 (November, 1977).

98. R.W. King, B. Sandler, and L.C. Shen, "A Comprehensive Study of Subsurface Propagation from Horizontal Electric Dipoles," IEEE Trans. Geosci. and Remote Sensing, Vol. GE-18, No. 3, pp 225-233 (July, 1980).

99. R.W. King, G.S. Smith, M. Owens, and J.T. Wu, Antennas in Matter; Fundamentals, Theory, and Applications, Cambridge, Massachusetts: MIT Press (1981).

100. D.J. Pounds and A.H. LaGrone, "Considering Forest Vegetation as an Imperfect Dielectric Slab," University of Texas Electrical Engineering Research Laboratory Report 6-53 (May, 1963).

101. D.L. Sachs and P.J. Wyatt, "A Conducting-Slab Model for Electromagnetic Propagation Within a Jungle Medium," Radio Science, Vol. 3, No. 2, pp 125-134 (February, 1968).

102. M. Siegel and R.W. King, "Electromagnetic Fields in a Dissipative Half-Space: A Numerical Approach," J. Applied Phys., Vol. 41, No. 6 (May, 1970).

103. D. Staiman and T. Tamir, "On the Nature and Optimization of the Ground (Lateral) Wave Excited by Submerged Antennas," Polytechnic Institute of Brooklyn Microwave Research Institute Research Report No. PIBMRI-1292-65 (January, 1966).

104. D. Staiman and T. Tamir, "Nature and Optimization of the Ground (Lateral) Wave Excited by Submerged Antennas," Proc. IEE , Vol. 113, No. 8, pp 1299-1310 (August, 1966).

105. C.H. Stoyer, "Electromagnetic Fields of Dipoles in Stratified Media," IEEE Trans. Antennas and Propagation, Vol. AP-25, No. 4, pp 547-552 (July, 1977).

106. T. Tamir, "An Experimental Study of Radio Wave Propagation in Simulated Forests and Other Dissipative Environments," US Army Electronics Command (ECOM), Research and Development Technical Report ECOM-0222-1 (September, 1968).

107. T. Tamir, "On Radio Wave Propagation in Forest Environments," IEEE Trans. Antennas and Propagation, Vol. AP-15, No. 6, pp 806-817 (November, 1967).

108. T. Tamir, "Radio Wave Propagation Along Mixed Paths in Forest Environments," IEEE Trans. Antennas and Propagation, Vol. AP-25, No. 4, pp 471-477 (July, 1977).

109. T. Tamir and L.B. Felsen, "On Lateral Wave in Slab Configurations and Their Relation to Other Wave Types," IEEE Trans. Antennas and Propagation, Vol. AP-13, pp 410-422 (May, 1965).

110. L. Tsang, R. Brown J.A. Kong, and G. Simmons, "Numerical Evaluation of Electromagnetic Fields Due to Dipole Antennas in the Presence of Stratified Media," J. Geophys. Res., Vol. 79, No. 14, pp 2077-2080 (May, 1974).

111. G. Tyras, Radiation and Propagation of Electromagnetic Waves, New York: Academic (1969).

112. J.R. Wait, "The Electromagnetic Fields of a Horizontal Dipole in the Presence of a Conducting Half-Space," Can. J. Phys., Vol. 39, pp 1017-1028 (1961).

113. J.R. Wait, Electromagnetic Waves in Stratified Media, New York: Macmillan (1962).

114. J.R. Wait, "Asymptotic Theory for Dipole Radiation in the Presence of a Lossy Slab Lying on a Conducting Half-Space," IEEE Trans. Antennas and Propagation, Vol. AP-15, No. 5, pp 645-648 (September, 1967).

115. J.R. Wait, "Proceedings of a Conference on Environmental Effects on Antenna Performance," Boulder, Colorado (July, 1969).

116. A. Yokoyama, "Comments on the Solution of Dipoles in Semi-Infinite Media," IEEE Trans. Antennas and Propagation, Vol. AP-22, No. 1, pp 339-340 (March, 1974).

9.6 Propagation in Stratified, Anisotropic Media

117. S.M. Ali and S.F. Mahmoud, "Electromagnetic Fields of Buried Sources in Stratified Anisotropic Media," IEEE Trans. Antennas and Propagation, Vol. AP-27, No. 5, pp 671-678 (September, 1979).

118. E. Arbel and L.B. Felsen, "Theory of Radiation from Sources in Anisotropic Media," in Electromagnetic Theory and Antennas, New York: Pergamon (1963).

119. J.A. Arnaud and A.A. Salek, "Comments on 'Theorems of Bianisotropic Media'," Proc. IEEE, Vol. 61, No. 5, pp 667-668 (May, 1973).

120. P.C. Clemmow, "On the Theory of Radiation from a Source in a Magneto-Ionic Medium," in Electromagnetic Theory and Antennas, New York: Pergamon (1963).

121. P.C. Clemmow, "The Theory of Electromagnetic Waves in a Simple Anisotropic Medium," Proc. IEEE, Vol. 110, No. 1, pp 101-106 (January, 1963).

122. L.B. Felsen, "Lateral Waves on an Anisotropic Plasma Interface," IRE Trans. Antennas and Propagation, Vol. AP-10, No. 3, pp 347-348 (May, 1962).

123. J.A. Kong, "Electromagnetic Fields Due to Dipole Antennas Over Stratified Anisotropic Media," Geophys., Vol. 37, No. 6, pp 985-996 (December, 1972).

124. I.V. Lindell, "Elements of Dyadic Algebra and its Application in Electromagnetics," Helsinki University of Technology, Radio Laboratory Report S 126 (1981).

125. H.B. Phillips, Vector Analysis, New York: Wiley (1933).

126. C.T. Tai, Dyadic Green's Functions in Electromagnetic Theory, Scranton, Pennsylvania: Intext Educational (1971).

127. C.M. Tang, "Electromagnetic Fields Due to Dipole Antennas Embedded in Stratified Anisotropic Media," IEEE Trans. Antennas and Propagation, Vol. AP-27, No. 5, pp 665-670 (September, 1979).

128. J.R. Wait, "Fields of a Horizontal Dipole Over a Stratified Anisotropic Half-Space," IEEE Trans. Antennas and Propagation, Vol. AP-14, No. 6, pp 790-792 (November, 1966).

9.7 Pulses and Transients

129. R.T. Aiken, "Time-Variant Filters and Analytic Signals," IEEE Trans. on Info. Theory, Vol. IT-12, pp 331-333 (April, 1967).

130. W.R. Bennett and J.R. Davey, Data Transmisstion, New York: McGraw-Hill (1965).

131. J.C. Bolomey, et al, "Time Domain Integral Equation Approach for Inhomogeneous and Dispersive Slab Problems," IEEE Trans. Antennas and Propagation, Vol. AP-26, No. 5, pp 658-667 (September, 1978).

132. A.T. de Hoop, "Pulsed Electromagnetic Radiation from a Line Source in a Two-Media Configuration," Radio Science, Vol. 14, No. 2, pp 253-268 (March-April, 1979).

133. L.R. Duykers, "Deformation of an Exponential Pulse with a Finite Rise Time in the Region of Total Reflection," J. Acous. Soc. America, Vol. 37, No. 6, pp 1052-1055, (1965).

134. S.E. El-Khamy, "On Pulse Compression in Dispersive Media," IEEE Trans. Antennas and Propagation, Vol. AP-27, No. 3, pp 420-422 (May, 1979).

135. A. Ezzeddine, et al, "Transient Fields of a Vertical Electric Dipole Over a Two-Layer Non-Dispersive Dielectric," J. Applied Phys., Vol. 52, No. 3, pp 1202-1208 (March, 1981).

136. L.B. Felsen, "Transients in Dispersive Media, Part I: Theory," IEEE Trans. Antennas and Propagation, Vol. AP-17, No. 2, pp 191-200 (March, 1969).

137. L.B. Felsen (ed.), Transient Electromagnetic Fields, Vol. 10 in Topics in Applied Physics, New York: Springer-Verlag (1976).

138. H. Haddad and D.C. Chang, "Transient Electromagnetic Field Generated by a Vertical Electric Dipole on the Surface of a Dissipative Earth," Radio Science, Vol. 16, No. 2, pp 169-177 (March-April, 1981).

139. C.W. Helstrom "An Expansion of a Signal in Gaussian Elementary Signals," IEEE Trans. on Info. Theory, Vol. IT-12, No. 1, pp 81-82 (January, 1966).

140. R.F. Leach, "Propagation of Information-Bearing Signals Through Space," IEEE Trans. on Nuclear Science, Vol. NS-10, No. 1, pp 146-152 (January, 1963).

141. R.W. Lucky, J. Salz, and E.J. Weldon, Jr., Principles of Data Communication, New York: McGraw-Hill (1968).

142. S.F. Mahmoud, et al, "Transient Electromagnetic Fields of a Vertical Magnetic Dipole on a Two-Layer Earth," Proc. IEEE, Vol. 67, No. 7, pp 1022-1027 (July, 1979).

143. S.O. Rice, "Envelopes of Narrow-Band Signals," Proc. IEEE, Vol. 70, pp 692-299 (July, 1982).

144. M. Schwartz, W.R. Bennett, and S. Stein, Communication Systems and Techniques, New York: McGraw-Hill (1966).

145. R.J. Schwarz and B. Friedland, Linear Systems, New York: McGraw-Hill (1965).

146. K. Sivaprasad, et al,"Reflection of Pulses at Oblique Incidence from Stratified Dispersive Media," IEEE Trans. Antennas and Propagation, Vol. AP-24, No. 1, pp 95-99 (January, 1976).

147. S. Stein and J.J. Jones, Modern Communication Principles, New York: McGraw-Hill (1967).

148. A.M. Trakhtman, "Hilbert Transforms and Spectra," Telecom. and Radio Engineering, Part 2, Vol. 24, No. 7, pp 1-9 (1969).

149. J.R. Wait, "Ground Wave Pulses," Probing Geophys., Boulder, Colorado: Golem (19).

150. J.R. Wait, "Propagation of Pulses in Dispersive Media," Radio Science, Vol. 69D, No. 11, pp 1387-1401 (November, 1965).

151. L. Wetzel, "On the Theory of Signal Distortion Due to Ionospheric Dispersion," Institute for Defense Analyses Research Paper, p 317 (July 1967).

152. G.M Whitman and L.B. Felsen, "Transients in Dispersive Media, Part II: Excitation of Space Waves and Surface Waves in a Bounded Cold Magnetoplasma," IEEE Trans. Antennas and Propagation, Vol. AP-17, No. 2, pp 200-208 (March, 1969).

9.8 Discrete Fourier Transform

153. G.D. Bergland, "A Guided Tour of the Fast Fourier Transform," IEEE Spectrum, Vol. 6, No. 7, pp 41-52 (July, 1969).

154. E.O. Brigham, The Fast Fourier Transform, New York: Prentice-Hall (1974).

155. E.O. Brigham and R.E. Morrow, "The Fast Fourier Transform," IEEE Spectrum, Vol. 4, No. 12, pp 63-70 (December, 1967).

156. W.T. Cochran, et al, "What is the Fast Fourier Transform?", Proc. IEEE, Vol. 55, No. 10, pp 1664-1674 (October, 1967).

157. F.J. Harris, "On the Use of Windows for Harmonic Analysis with the Discrete Fourier Transform," Proc. IEEE, Vol. 66, No. 1, pp 51-59 (January, 1978).

158. F.J. Harris, "The Discrete Fourier Transform Applied to Time Domain Signal Processing," IEEE Comm. Mag., Vol. 20, No. 4, pp 13-22 (May, 1982).

159. T. Kaneko and B. Lui, "Accumulation of Round-off Error in Fast Fourier Transforms," J. Assn. Comput. Mach., Vol 17, No. 10, pp 637-654 (October, 1970).

160. B. Lui and T. Kaneko, "Round-off Error in Fast Fourier Transforms (Decimation in Time)," Proc. IEEE, Vol. 63, No. 6, pp 991-992 (June, 1975).

161. P.I. Richards, "Computing Reliable Power Spectra," IEEE Spectrum, Vol. 4, No. 1, pp 83-90 (January, 1967).

162. C.J. Weinstein, "Round-off Noise in Floating Point Fast Fourier Transform Computation,"IEEE Trans, Audio & Electroacoustics, Vol. AU-17, No. 3, pp 209-215 (September, 1969).

9.9 Spread-Spectrum Communications

163. P.F. Sass, "Army Spread Spectrum - Evolution or Revolution," Proc. 1982 IEEE Military Comm. Conf., Vol. 3, pp 4.1-1 to 8, (October, 1982).

164. P.F. Sass, "Propagation Measurements for UHF Spread Spectrum Communications," ibid. pp 4.4-1 to 7.

APPENDIX A

Susceptibilities of Wood and Leaves

The complex susceptibilities of green wood and leaves required for the modeling approach of CyberCom have been investigated. Measurements by Broadhurst [1] of the National Bureau of Standards appear to be the best available. They are summarized in Figure A-1. The spread of the results for the leaves represents the effects of different percentages of moisture (30-78%) and for the branches, different orientations relative to the branch axis. The curves show that the real parts of the susceptibilities χ_ℓ' are nearly constant with frequency; the imaginary parts of the susceptibilities χ_ℓ'' are inversely proportional to frequency at the lower frequencies of interest, and rise with frequency at the higher; the results for bamboo leaves and for tulip tree leaves and branches overlap.

CyberCom has developed and employed three simple models for the susceptibility of green wood and leaves, summarized in Table A-1. Model I describes a frequency-independent susceptibility which is convenient for ascertaining the effects of scatterer geometry on the scattered wave. Model II describes a susceptibility characterized by a real part which is frequency-independent and an imaginary part derived from a constant conductivity of 0.1 mho/meter. Model III best reflects the typical behavior of measured data and includes both a frequency-independent real part and an imaginary part related to both conduction and relaxation losses. It is shown in Figure A-1.

The imaginary parts of the susceptibilities (the loss factors) are shown in Figure A-2 for the three CyberCom models. The recovery of the Model III loss factor from its minimum near 1 GHz is clearly evident, and may be attributed to increased relaxation losses as the resonant frequency of the water molecule (approximately 22 GHz) is approached.

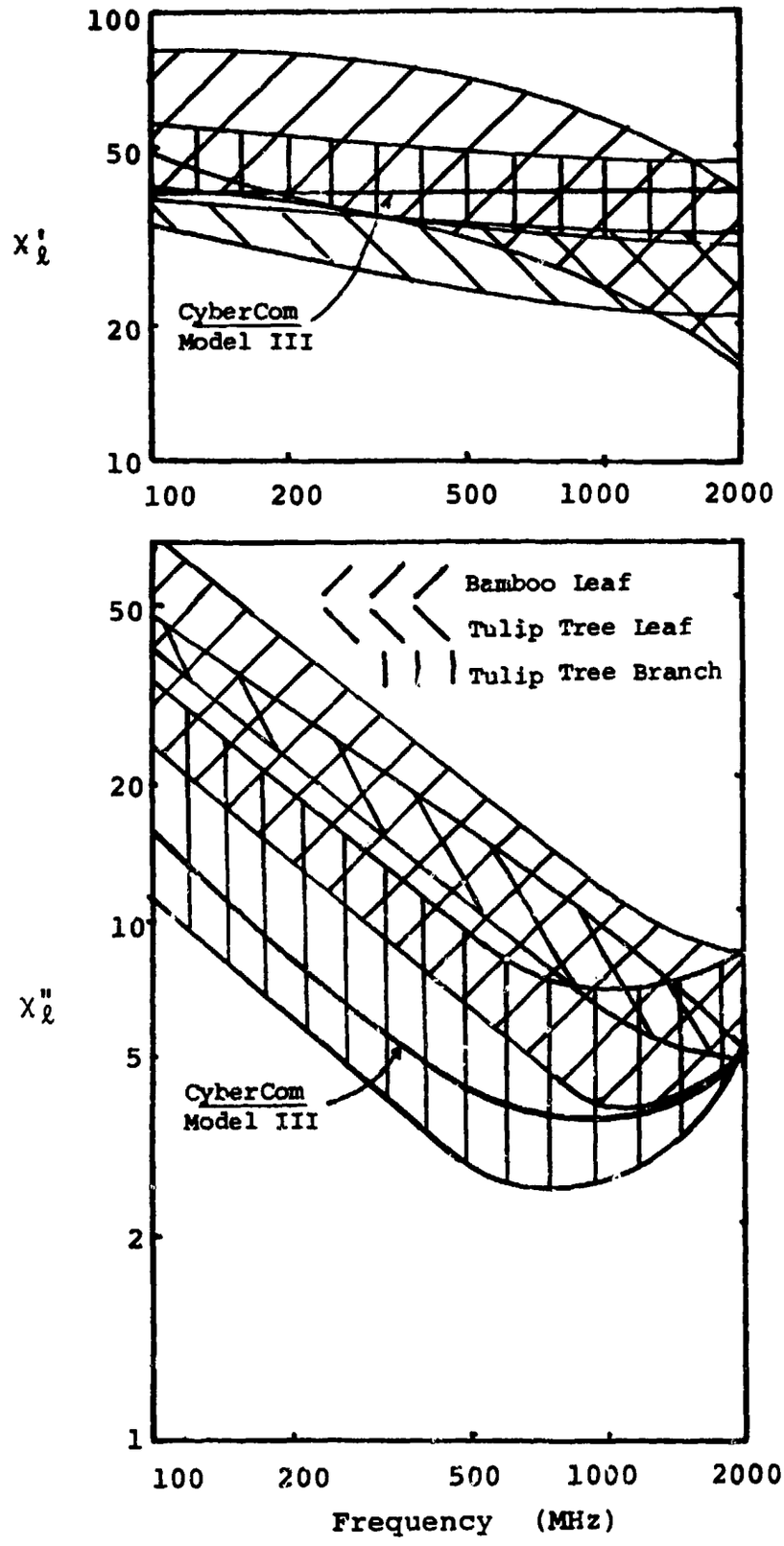

Figure A-1: Susceptibility of Wood and Leaves

TABLE A-1 Susceptibility of Wood and Leaves - CyberCom Models

CyberCom Model	$1+\chi_\ell'-j\chi_\ell'' = \varepsilon_\ell = \varepsilon_\ell'-j\varepsilon_\ell''$	
	$\chi_\ell'=\varepsilon_\ell'-1$	$\chi_\ell''=\varepsilon_\ell''$ (Loss Factor)
I	39	10
II	39	$1.8/f_{GHz}$ (σ = 0.1 mho/m)
III	39	$(1.5/f_{GHz}) + (2f_{GHz})/[1+(f_{GHz}/20)^2]$

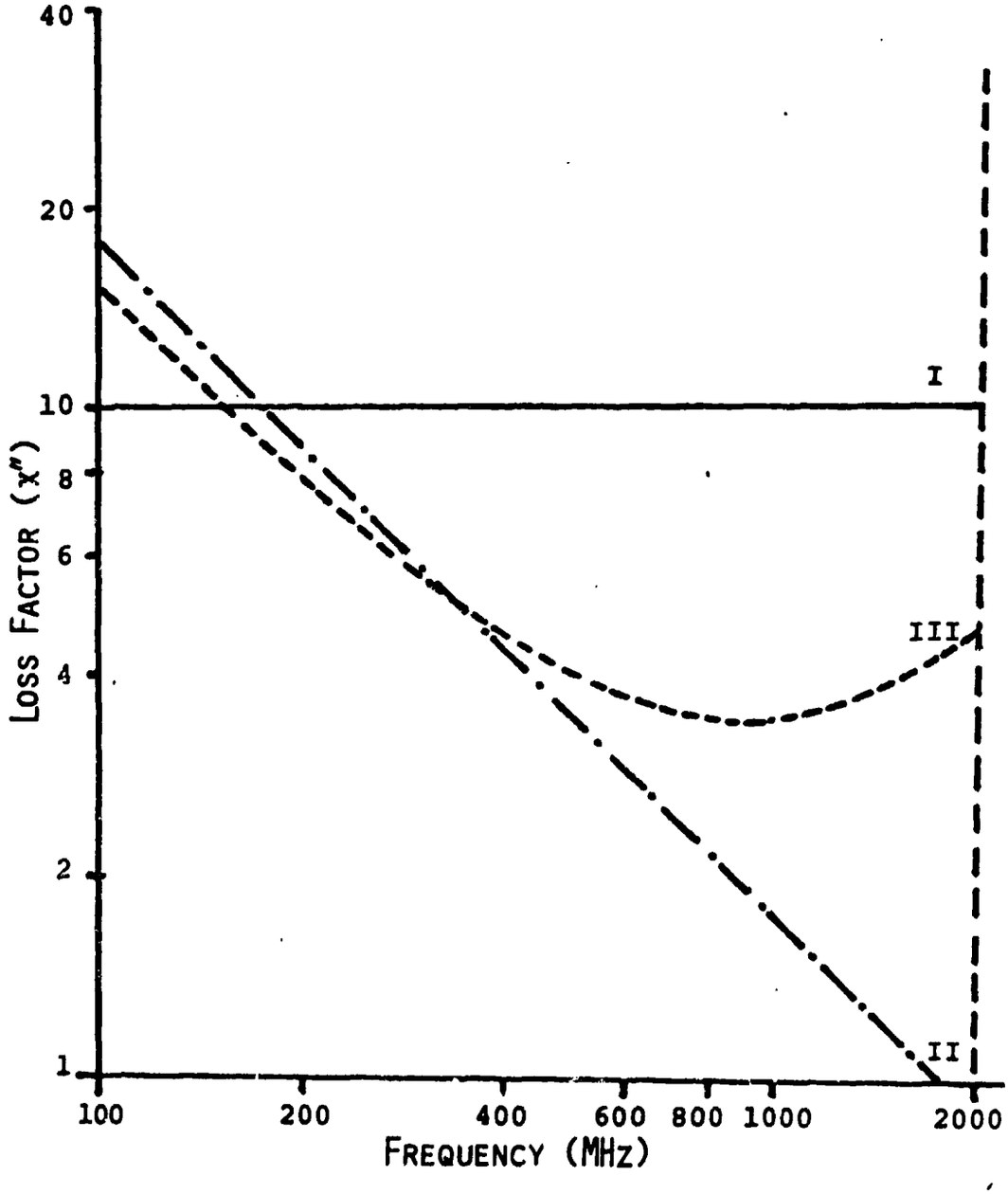

Figure A-2: Loss Factor of Wood & Leaves
[CyberCom Models]

Appendix B

Scattering Amplitude-Transition Operator Relationship for Two-Dimensional Scatterers

In this Appendix the relationship between the scattering amplitude and the transition operator will be obtained for two-dimensional scatterers. This will be done for both the vector case (oblique incidence) and the scalar case (normal incidence). The methodology used will parallel that of Lang [57] who derived the relationship for three-dimensional scatterers.

Assume a dyadic plane wave is incident on a two-dimensional scatterer as shown in Figure 2-4. The incident wave is of the form

$$\underline{\underline{e}}_o(\underline{x}) = (\underline{\underline{I}}-\underline{i}\underline{i})e^{-j(\underline{k}_t\cdot\underline{x}_t+k_z z)} \tag{B-1}$$

where $\underline{i}$ is in the direction of incidence, i.e.

$$\underline{i} = (\underline{k}_t + k_z\underline{z}^o)/k_o \tag{B-2}$$

with

$$k_o = \sqrt{k_t^2 + k_z^2} \quad , \quad k_t = |\underline{k}_t| \quad . \tag{B-3}$$

The dyadic scattered field is given by

$$\underline{\underline{e}}_s(x) = \int d\underline{x}'\ \underline{\underline{G}}(\underline{x}-\underline{x}') \cdot \int d\underline{x}''\ \underline{\underline{t}}(\underline{x}',\underline{x}'') \cdot \underline{\underline{e}}_o(\underline{x}'') \tag{B-4}$$

where the dyadic Green's function $\underline{\underline{G}}$ satisfies

$$\underline{\underline{L}} \cdot \underline{\underline{G}}(x) = \underline{\underline{I}}\delta(x) \tag{B-5}$$

with $\underline{\underline{L}}$ given by equation (2-3-5) and $\underline{\underline{t}}$ the kernel of the transition operator.

Since the scatterers are two-dimensional, they are invariant in the z direction, i.e.,

$$\underline{\underline{t}}(\underline{x}',x'') = \underline{\underline{t}}(\underline{x}_t',\underline{x}_t'',z'-z'') \tag{B-6}$$

Putting equation (B-6) into equation (B-4) and introducing the Fourier transform of the transition operator with respect to z yields

$$\underline{e}_s(x) = \int d\underline{x}_t'dz' \; \underline{\underline{G}}(\underline{x}_t-\underline{x}_t',\underline{z}-\underline{z}') \cdot \int d\underline{x}_t'' \; \hat{\underline{\underline{t}}}(\underline{x}_t',\underline{x}_t'', k_z) \cdot (\underline{\underline{I}}-\underline{i}\underline{i})e^{-j(\underline{k}_t\cdot\underline{x}_t''+k_z z')} \tag{B-7}$$

where

$$\hat{\underline{\underline{t}}}(\underline{x}_t,\underline{x}_t',k_z) = \int dz \; \underline{\underline{t}}(\underline{x}_t,\underline{x}_t',z)e^{+jk_z z} \tag{B-8}$$

Now introducing the Fourier transform of the dyadic Green's function with respect to z gives

$$\underline{e}_s(\underline{x}) = \int d\underline{x}_t'd\underline{x}_t'' \; \hat{\underline{\underline{G}}}(\underline{x}_t-\underline{x}_t',k_z) \cdot \hat{\underline{\underline{t}}}(\underline{x}_t',\underline{x}_t'',k_z) \cdot (\underline{\underline{I}}-\underline{i}\underline{i})e^{-j(\underline{k}_t\cdot\underline{x}_t''+k_z z)} \tag{B-9}$$

where

$$\hat{\underline{\underline{G}}}(\underline{x}_t,k_z) = \int dz \; \underline{\underline{G}}(\underline{x}_t,z)e^{jk_z z} \quad . \tag{B-10}$$

Before proceeding, the transformed Green's function must be found. This is accomplished by transforming the well-known expression for the three-dimensional dyadic Green's function [Van Bladel, 81]. The three-dimensional dyadic Green's function is

$$\underline{\underline{G}}(x) = (\underline{\underline{I}} - \frac{\nabla\nabla}{k_o^2})g(\underline{x}) \tag{B-11}$$

where $g(\underline{x})$ is the scalar Green's function;

$$g(\underline{x}) = \frac{e^{-jk_o r}}{4\pi r} \quad , \quad r = |\underline{x}| \tag{B-12}$$

This scalar Green's function satisfies the scalar wave equation

$$(\nabla^2+k_o^2)g(\underline{x}) = -\delta(\underline{x}) \; . \tag{B-13}$$

To find the transformed Green's function, first, the transformed scalar Green's function is found. This is done by Fourier-transforming equation (B-13) and then solving the resulting two-dimensional equation. The result is

$$g(\underline{x}) = -\frac{j}{4}\int H_o^{(2)}(k_t|\underline{x}_t|)e^{-jk_z z}\,dk_z \tag{B-14}$$

where

$$k_t = \begin{cases} \sqrt{k_o^2 - k_z^2}\,, & |k_z| < k_o \\ -j\sqrt{k_z^2 - k_o^2}\,, & |k_z| > k_o \end{cases}. \tag{B-15}$$

Now putting equation (B-14) in equation (B-11), bringing the dyadic portion of the operator through the integral and finally using equation (B-10) yields

$$\hat{\underline{\underline{G}}}(\underline{x}_t,k_z) = -\frac{j}{4}\left(\underline{\underline{I}} + \frac{\hat{\nabla}\hat{\nabla}}{k_o^2}\right) H_o^{(1)}(k_t|\underline{x}_t|) \tag{B-16}$$

where $\hat{\nabla} = \nabla_t - jk_z\underline{z}^o$.

To proceed with developing the relationship between the scattering amplitude and the transition operator, an asymptotic expression for $\underline{\underline{e}}_s(\underline{x})$ will be needed. An examination of equation (B-9) shows that this in turn requires a large $|\underline{x}_t|$ approximation for $\hat{\underline{\underline{G}}}(\underline{x}_t-\underline{x}_t',k_z)$. Assuming $|\underline{x}_t| >> |\underline{x}_t'|$ and using the asymptotic expression for the Hankel function results in

$$H_o^{(1)}(k_t|\underline{x}_t-\underline{x}_t'|) \sim \sqrt{\frac{2}{\pi k_t x_t}}\, e^{-j(k_t x_t - k_t \underline{o}_t\cdot\underline{x}_t' - \pi/4)} \tag{B-17}$$

where $\underline{o}_t = \underline{x}_t/|\underline{x}_t|$. Now substituting this result in equation (B-16) and keeping highest-order terms yields

$$\hat{\underline{\underline{G}}}(\underline{x}_t-\underline{x}_t',k_z) \sim -j\frac{(\underline{\underline{I}}-\underline{o}\,\underline{o})}{\sqrt{8\pi k_t x_t}}\, e^{-j(k_t x_t - k_t \underline{o}_t\cdot\underline{x}_t' - \pi/4)} \tag{B-18}$$

where $\underline{o} = \underline{o}_t + o_z\underline{z}^o$ with $o_z = k_z/k_o$.

The final form of the asymptotic expression for the scattered field $\underline{\underline{e}}_s(\underline{x})$ is obtained by substituting equation (B-18) into equation (B-9). The result is

$$\underline{\underline{e}}_s(\underline{x}) \sim \frac{(2\pi)^2}{\sqrt{8\pi k_t x_t}} (\underline{\underline{I}}-\underline{o}\underline{o})\cdot\underline{\underline{\tilde{t}}}(k_t\underline{o}_t, k_t\underline{i}_t; k_z)\cdot(\underline{\underline{I}}-\underline{i}\underline{i})e^{-j(k_t x_t + k_z z + \pi/4)} \quad \text{(B-19)}$$

where $\underline{i}_t$ is the transverse portion of $\underline{i}$ ($\underline{i}_t = \underline{k}_t/k_o$) and the two-dimensional transformed transition operator is given by

$$\underline{\underline{\tilde{t}}}(\underline{k}_t, \underline{k}_t'; k_z) = \frac{1}{(2\pi)^2}\int d\underline{x}_t d\underline{x}_t' \; \underline{\underline{\tilde{t}}}(\underline{x}_t, \underline{x}_t'; k_z) e^{j(\underline{k}_t\cdot\underline{x}_t - \underline{k}_t'\cdot\underline{x}_t')} \quad \text{(B-20)}$$

The desired relationship can be established by comparing the definition of scattering amplitude with equation (B-19). The two-dimensional dyadic scattering amplitude is defined as

$$\underline{\underline{e}}_s(x) \sim \underline{\underline{f}}(\underline{o}_t, \underline{i}_t; k_z) \frac{e^{-j(k_t x_t + k_z z)}}{\sqrt{x_t}} . \quad \text{(B-21)}$$

Comparing equations (B-19) and (B-21), one obtains

$$\underline{\underline{f}}(\underline{0}_t, \underline{i}_t; k_z) = \gamma(\underline{\underline{I}}-\underline{0}\underline{0})\cdot\underline{\underline{\tilde{t}}}(k_t\underline{o}_t, k_t\underline{i}_t; k_z)\cdot(\underline{\underline{I}}-\underline{i}\underline{i}) \quad \text{(B-22)}$$

where

$$\gamma = [2\pi^3/k_t]^{1/2} e^{-j\pi/4} \quad \text{(B-23)}$$

Before concluding this appendix a similar relationship will be derived for the scalar problem. Because the scalar problem is a special case of the two-dimensional vector work just presented, those results can be used.

The scalar problem restricts attention to propagation normal to the tree trunks and to sources that only excite vertical waves.

The vector problem reduces to the scalar problem as follows:

$$\begin{aligned} \langle \hat{\underline{E}}(\underline{x}_t, \underline{k}_z) \rangle \cdot \underline{z}^o &= 2\pi \langle \psi(\underline{x}_t) \rangle \delta(k_z) \\ \hat{g}(\underline{x}_t, k_z) \cdot \underline{z}^o &= 2\pi \, g(\underline{x}_t) \, \delta(k_z) \end{aligned} \tag{B-24}$$

If one dots equation (2-4-4) by $\underline{z}^o$ and introduces the scalar specializations as given by equation (B-24), one obtains the scalar mean-wave equation as given by equation (2-2-4) with

$$t(\underline{x}_t, \underline{x}_t') = \underline{z}^o \cdot \hat{\underline{\underline{t}}}(\underline{x}_t, \underline{x}_t'; o) \cdot \underline{z}^o \quad . \tag{B-25}$$

In addition, an examination of the definition of both the vector and scalar scattering amplitudes as given in equations (2-2-10) and (2-2-23) shows that

$$f(\underline{o}, \underline{i}) = \underline{z}^o \cdot \underline{\underline{f}}(\underline{o}, \underline{i}, o) \cdot \underline{z}^o \quad . \tag{B-26}$$

The desired relationship between the scalar scattering amplitude f and the transformed scalar transition operator $\tilde{t}$ is obtained by dotting equation (B-20) from the left and the right by $\underline{z}^o$, and then using equation (B-26) and the transform version of equation (B-25). The result is

$$f(\underline{o}, \underline{i}) = \delta \, t(k_o \underline{o}, k_o \underline{i})$$

where δ is given by equation (B-23).

Appendix C

Correlation Equation

In this Appendix the approximate equation for the correlation equation will be derived. The methodology employed in the derivation will parallel the Foldy development for the mean equation. The starting point is Equation (2-2-29) for the scalar field quantity Ψ. Multiplying this equation through from the left by L^{-1} gives an expression for Ψ in terms of the incident and scattered fields. It is

$$\Psi = \Psi_i + \sum_{j=1}^{N} L^{-1} T_j \Psi^{(j)} \tag{C-1}$$

Here the observation point for the field Ψ is $\underline{x}$, i.e., $\Psi = \Psi(\underline{x})$. An equation for the conjugate field $\Psi^* = \Psi^*(\hat{\underline{x}})$ at point $\hat{\underline{x}}$ can be obtained from Equation (C-1). The result is

$$\Psi^* = \Psi_i^* + \sum_{j=1}^{N} L^{-\dagger} T_j^* \Psi^{(j)*} \tag{C-2}$$

In the remainder of the appendix, the dependence of quantities on $\hat{\underline{x}}$ or $\underline{x}$ will be denoted by whether the symbols are starred (conjugate) or not.

Now forming the product $\Psi\Psi^*$ and averaging yields

$$\langle \Psi\Psi^* \rangle = \Psi_i \Psi_i^* + \Psi_i \sum_{j=1}^{N} L^{-\dagger} \langle T_j^* \Psi^{(j)} \rangle + \sum_{j=1}^{N} L^{-1} \langle T_j \Psi^{(j)} \rangle \Psi_i^*$$

$$+ \sum_{j=1}^{N} \sum_{k=1}^{N} L^{-1} L^{-\dagger} \langle T_j T_k^* \Psi^{(j)} \Psi^{(j)*} \rangle \tag{C-3}$$

The double sum appearing in the above equation can be broken into like terms (i=j) and unlike terms (i≠j). Doing this, the following expression results:

$$\langle\psi\psi^*\rangle = \psi_i\psi_i^* + \psi_i \sum_{j=1}^{N} L^{-1}\langle T_j^*\psi^{(j)*}\rangle + \sum_{j=1}^{N} L^{-1}\langle T_j\psi^{(j)}\rangle\psi_i^*$$

$$+ \sum_{j=1}^{N} L^{-1}L^{-1*}\langle T_jT_j^*\rangle\psi^{(j)}\psi^{(j)*}$$

$$+ \sum_{j=1}^{N}\sum_{\substack{k=1\\ j\neq k}}^{N} L^{-1}L^{-1*}\langle T_jT_k^*\rangle\psi^{(j)}\psi^{(k)*} \qquad \text{(C-4)}$$

To obtain an equation for the correlation function a closure approximation is employed. The approximation to be used is

$$\psi^{(j)} \approx \langle\psi\rangle$$

$$\psi^{(j)}\psi^{*(j)} \approx \langle\psi\psi^*\rangle \qquad \text{(C-5)}$$

$$\psi^{(j)}\psi^{*(k)} \approx \langle\psi\rangle\langle\psi^*\rangle \qquad j\neq k$$

This is a generalization of Foldy's closure approximation used to derive the mean equation. Using this approximation in Equation (C-4) gives:

$$\langle\psi\psi^*\rangle = \psi_i\psi_i^* + \psi_i \sum_{j=1}^{N} L^{-1^*}\langle T_j\rangle\langle\psi^*\rangle$$

$$+ \sum_{j=1}^{N} L^{-1}\langle T_j\rangle\langle\psi\rangle\psi_i^* + \sum_{j=1}^{N} L^{-1}L^{-1^*}\langle T_jT_j^*\rangle\langle\psi\psi^*\rangle$$

$$+ \sum_{j=1}^{N}\sum_{\substack{k=1\\ j\neq k}}^{N} L^{-1}\langle T_j\rangle\langle\psi\rangle L^{-1^*}\langle T_j^*\rangle\langle\psi^*\rangle \qquad \text{(C-6)}$$

Since the particles are identically distributed, the statistics for each particle are the same, i.e.,

$$\sum_{j=1}^{N}\langle T_j\rangle = N\langle T\rangle \qquad \text{(C-7)}$$

$$\sum_{j=1}^{N}\langle T_jT_j^*\rangle = N\langle TT^*\rangle \qquad \text{(C-8)}$$

Employing these simplifications in Equation (C-6) results in

$$\langle\Psi\Psi^*\rangle = \Psi_i\Psi_i^* + N\Psi_i L^{-\dagger} \langle T^*\rangle\langle\Psi^*\rangle$$

$$+ NL^{-1}\langle T\rangle\langle\Psi\rangle\Psi^* + NL^{-1}L^{-\dagger}\langle TT^*\rangle\langle\Psi\Psi^*\rangle$$

$$+ (N^2-N)L^{-1}\langle T\rangle\langle\Psi\rangle L^{-\dagger}\langle T^*\rangle\langle\Psi^*\rangle \qquad \text{(C-9)}$$

This is the desired equation for the correlation function $\langle\Psi\Psi^*\rangle$. It can be simplified substantially by making use of the mean-wave equation.

The mean-wave equation is given in the text by Equation (2-2-48). It is

$$\mathfrak{L}\langle\psi\rangle = g \qquad \text{(C-10)}$$

where

$$\mathfrak{L} = L - N\langle T\rangle \qquad \text{(C-11)}$$

In order to simplify Equation (C-9), the mean equation is put in a slightly different form. With this purpose in mind, multiply Equation (C-10) by L^{-1} from the left. This gives

$$\langle\psi\rangle = \Psi_i + NL^{-1}\langle T\rangle\langle\Psi\rangle \qquad \text{(C-12)}$$

Now using this result, Equation (C-9) becomes

$$\langle\Psi\Psi^*\rangle = \langle\Psi\rangle\langle\Psi^*\rangle + (N^2-N)L^{-1}\langle T\rangle\langle\Psi\rangle L^{-\dagger}\langle T\rangle\langle\Psi^*\rangle \qquad \text{(C-13)}$$

Multiplying from the left by $\mathfrak{L}\mathfrak{L}^*$, using the fact that $\mathfrak{L}L^{-1}$ and neglecting the N^2 terms in Equation (C-13) yields

$$\mathfrak{L}\mathfrak{L}^*\langle\psi\psi^*\rangle - N\langle TT^*\rangle\langle\psi\psi^*\rangle = gg^* \qquad \text{(C-14)}$$

The above steps can be justified by scaling the problems with respect to the characterstic size of the particle, then N is replaced by the fractional volume which is small.

The final form of the correlation equation as it appears in Equation (2-2-44) is obtained by writing the spatial average of TT^* out explicitly and by using Equation (2-2-38).

APPENDIX D

Dyadic Notation

According to Lindell [124], dyadic formalism is the most suitable notation for linear vector functions when applying the gibbsian vector notation to electromagnetic fields. Nevertheless, although conceived by J. Willard Gibbs nearly one-hundred years ago (1884), dyadic formalism has been introduced into electromagnetics only comparitively recently, and is not generally included in most engineering curricula. Thus, for the convenience of the uninformed reader, those basic definitions and properties of dyadics emplcyed in the body of the report are reviewed here.

D.1 Basic Definitions

A dyadic (more properly called a dyadic polynomial) is an operator representable as

$$\underline{D} = \underline{a}_1\underline{b}_1 + \underline{a}_2\underline{b}_2 + \ldots\ldots + \underline{a}_n\underline{b}_n \qquad \text{(D-1)}$$

where $\underline{a}_1, \underline{a}_2, \ldots \underline{a}_n$ and $\underline{b}_1, \underline{b}_2, \ldots \underline{b}_n$ are vectors and which, with an arbitrary vector $\underline{v}$, forms the scalar products

$$\underline{v}\cdot\underline{D} = (\underline{v}\cdot\underline{a}_1)\underline{b}_1 + (\underline{v}\cdot\underline{a}_2)\underline{b}_2 + \ldots\ldots + (\underline{v}\cdot\underline{a}_n)\underline{b}_n \qquad \text{(D-2)}$$

$$\underline{D}\cdot\underline{v} = \underline{a}_1(\underline{b}_1\cdot\underline{v}) + \underline{a}_2(\underline{b}_2\cdot\underline{v}) + \ldots\ldots + \underline{a}_n(\underline{b}_n\cdot\underline{v}) \qquad \text{(D-3)}$$

The vectors $\{\underline{a}_k\}$ are called antecedents; the vectors $\{\underline{b}_k\}$ are called consequents. Each term of the dyadic, $\underline{a}_k\underline{b}_k$ is called a dyad.

Dyadics arise naturally in electromagnetics when vector operators are to be separated mathematically from the field vectors being operated upon. For example, the projection of the electric field $\underline{e}$ along a linear antenna having the direction of a unit vector $\underline{u}$ can be written as $\underline{u}(\underline{u}\cdot\underline{e})$. Here, the vector $\underline{u}$ performs the projection operation upon the electric field vector $\underline{e}$. If these two vectors are to be separated mathematically, it is necessary to adopt the dyadic representation $\underline{uu}$ in the expression $(\underline{uu})\cdot\underline{e}$.

D.2 Basic Properties

Because in three-dimensional vector-space any vector $\underline{v}$ can be expressed in terms of any three vectors $\underline{a},\underline{b},\underline{c}$ forming a base (i.e., satisfying the condition $\underline{a} \times \underline{b} \cdot \underline{c} \neq 0$), any dyadic can be written as a polynomial of no more than three dyads. For example, the dyadic polynomial of Equation (D-1) can be recast in the form

$$\underline{D} = \underline{a}\,\underline{e} + \underline{b}\,\underline{f} + \underline{c}\,\underline{g} \tag{D-4}$$

where

$$\underline{e} = \frac{\underline{b}\times\underline{c}}{[\underline{a}\ \underline{b}\ \underline{c}]} \cdot \sum \underline{a}_i\underline{b}_i \tag{D-5}$$

$$\underline{f} = \frac{\underline{c}\times\underline{a}}{[\underline{a}\ \underline{b}\ \underline{c}]} \cdot \sum \underline{a}_i\underline{b}_i \tag{D-6}$$

$$\underline{g} = \frac{\underline{a}\times\underline{b}}{[\underline{a}\ \underline{b}\ \underline{c}]} \cdot \sum \underline{a}_i\underline{b}_i \tag{D-7}$$

Since the consequents $\underline{e},\underline{f},\underline{g}$ can also be expressed in terms of an arbitrary three-vector base, it is clear that the dyadic $\underline{D}$ is representable in terms of nine scalar coefficients.

For example, if the same three-vector orthonormal base is employed for both the antecedents and the consequents, $\underline{D}$ might be written in the form

$$\begin{aligned}\underline{D} = {} & d_{11}\underline{x}^\circ\underline{x}^\circ + d_{12}\underline{x}^\circ\underline{y}^\circ + d_{13}\underline{x}^\circ\underline{z}^\circ \\ & + d_{21}\underline{y}^\circ\underline{x}^\circ + d_{22}\underline{y}^\circ\underline{y}^\circ + d_{23}\underline{y}^\circ\underline{z}^\circ \\ & + d_{31}\underline{z}^\circ\underline{x}^\circ + d_{32}\underline{z}^\circ\underline{y}^\circ + d_{33}\underline{z}^\circ\underline{z}^\circ\end{aligned} \tag{D-8}$$

Although these nine scalar coefficients can be written as a matrix $[d_{ij}]$, a dyadic is not a matrix. The matrix $[d_{ij}]$ depends upon the base employed and so is coordinate-dependent; the dyadic is not.

A dyadic serves as a linear mapping from one vector to another. Conversely, any such linear mapping can be expressed in terms of a dyadic. This can be demonstrated by applying an orthonormal base $\{\underline{u}_i\}$ to an arbitrary linear function $\underline{f}(\underline{a})$ and noting that

$$\underline{f}(\underline{a}) = \sum\sum \underline{u}_i\underline{u}_i \cdot \underline{f}(\underline{u}_j\underline{u}_j \cdot \underline{a}) \tag{D-9}$$

$$= [\sum\sum \underline{u}_i \cdot \underline{f}(\underline{u}_j)\underline{u}_i\underline{u}_j] \cdot \underline{a} \tag{D-10}$$

The dyadic in the square brackets corresponds to the linear function $\underline{f}$.

The identity mapping has the property of mapping every vector into itself. The corresponding dyadic, $\underline{\underline{I}}$, is called the unit dyadic or idemfactor. Thus,

$$\underline{\underline{I}} \cdot \underline{a} = \underline{a} = \underline{a} \cdot \underline{\underline{I}} \tag{D-11}$$

Expressing $\underline{a}$ in an orthonormal base $\{\underline{u}_i\}$ shows that

$$\underline{\underline{I}} = \underline{u}_1\underline{u}_1 + \underline{u}_2\underline{u}_2 + \underline{u}_3\underline{u}_3 \tag{D-12}$$

More generally,

$$\underline{\underline{I}} = \underline{a}\,\underline{a}' + \underline{b}\,\underline{b}' + \underline{c}\,\underline{c}' \tag{D-13}$$

where $\{\underline{a}',\underline{b}',\underline{c}'\}$ is a base reciprocal to the arbitrary base $\{\underline{a},\underline{b},\underline{c}\}$. Thus, as for any dyadic, there exists an infinity of representations for the unit dyadic. As a consequence of Equation (D-11) the matrix of coefficients $[d_{ij}]$ associated with a given base $\{\underline{a}_i\}$ can be found in the relation

$$\underline{\underline{D}} = \underline{\underline{I}}\cdot\underline{\underline{D}}\cdot\underline{\underline{I}} = \sum\sum(\underline{a}_i'\cdot\underline{\underline{D}}\cdot\underline{a}_j)\underline{a}_i\underline{a}_j' = \sum\sum D_{ij}\underline{a}_i\underline{a}_j \tag{D-14}$$

APPENDIX E

The Fast Fourier Transform

The fast Fourier transform (FFT) is a highly efficient algorithm for computing the discrete Fourier transform (DFT). The FFT can be used in place of the continuous Fourier transform only to the extent that the DFT could before, but with a substantial reduction in computer time. This appendix reviews the basic properties of the DFT and its relation to the continuous Fourier transform, introduces the FFT and identifies the major pitfalls likely to arise in its use, and exemplifies the application of the DFT and the FFT by considering a band-limited, high-frequency, rectangular pulse.

C.1 Discrete Fourier Transform

The Fourier transform pair for continuous signals can be written in the form

$$X(f) = \int_{-\infty}^{\infty} x(t)\exp\{-j2\pi ft\}dt \qquad \text{(E-1)}$$

$$x(t) = \int_{-\infty}^{\infty} X(f)\exp\{+j2\pi ft\}df \qquad \text{(E-2)}$$

The integrals in Equations (E-1) and (E-2) are actually finite in any practical case since only a finite segment of an essentially band-limited signal will be available. This situation is commonly represented by setting $x(t) = 0$ for $0 > t > T$ when the signal $x(t)$ is available only over the time interval $(0,T)$, and $X(f) = 0$ for $-B/2 > f > B/2$ when the amplitude spectrum $X(f)$ is essentially band-limited to the frequency interval $(-B/2,+B/2)$.

The analogous discrete Fourier transform (DFT) pair that applies to sampled-data signals can be written in the form

$$X(f_m) = \Delta t \sum_{k=0}^{N-1} x(t_k)\exp\{-j2\pi f_m t_k\} \qquad \text{(E-3)}$$

$$x(t_k) = \Delta f \sum_{m=-N/2}^{N/2-1} X(f_m)\exp\{+j2\pi f_m t_k\} \qquad \text{(E-4)}$$

If the signal x(t) has been sampled uniformly at the Nyquist rate so that

$$\Delta t = T/N = 1/2B, \quad \Delta f = 2B/N = 1/T \tag{E-5}$$

then upon letting

$$t_k = k\Delta t, \quad f_m = m\Delta f \tag{E-6}$$

Equations (E-3) and (E-4) become

$$X(m) = \Delta t \sum_{k=0}^{N-1} x(k) \exp\{-j2\pi mk/N\} \tag{E-7}$$

$$x(k) = \Delta f \sum_{m=0}^{N-1} X(m) \exp\{+j2\pi mk/N\} \tag{E-8}$$

The periodicity of X(m) apparent in Equation (E-7) has been used in re-ordering (for ease of computation) the summation appearing in Equation (E-8). More generally, however, it is apparent from these equations that both X(m) and x(k) must be considered periodic, i.e.

$$X(m+N) = X(m) \tag{E-9}$$

$$x(k+N) = x(k) \tag{E-10}$$

This property has been anticipated in writing Equation (E-4) where the missing end point $X(f_{N/2})$ is considered to be the first point of the next period in a periodic extension of $X(f_m)$. Mathematically speaking, the interval from which samples of X(f) [and x(t)] are taken must be considered closed on the left and open on the right (or vice-versa). This property is illustrated in Figure E-1. Further discussion of this topic can be found in [157].

When the sampled-data signal x(k) is real, the real part of X(m) [denoted hereafter as X'(m)] is symmetric about the folding frequency B [m = N/2] and the imaginary part of X(m) [denoted hereafter as X"(m) is antisymmetric. Since X(m) has been

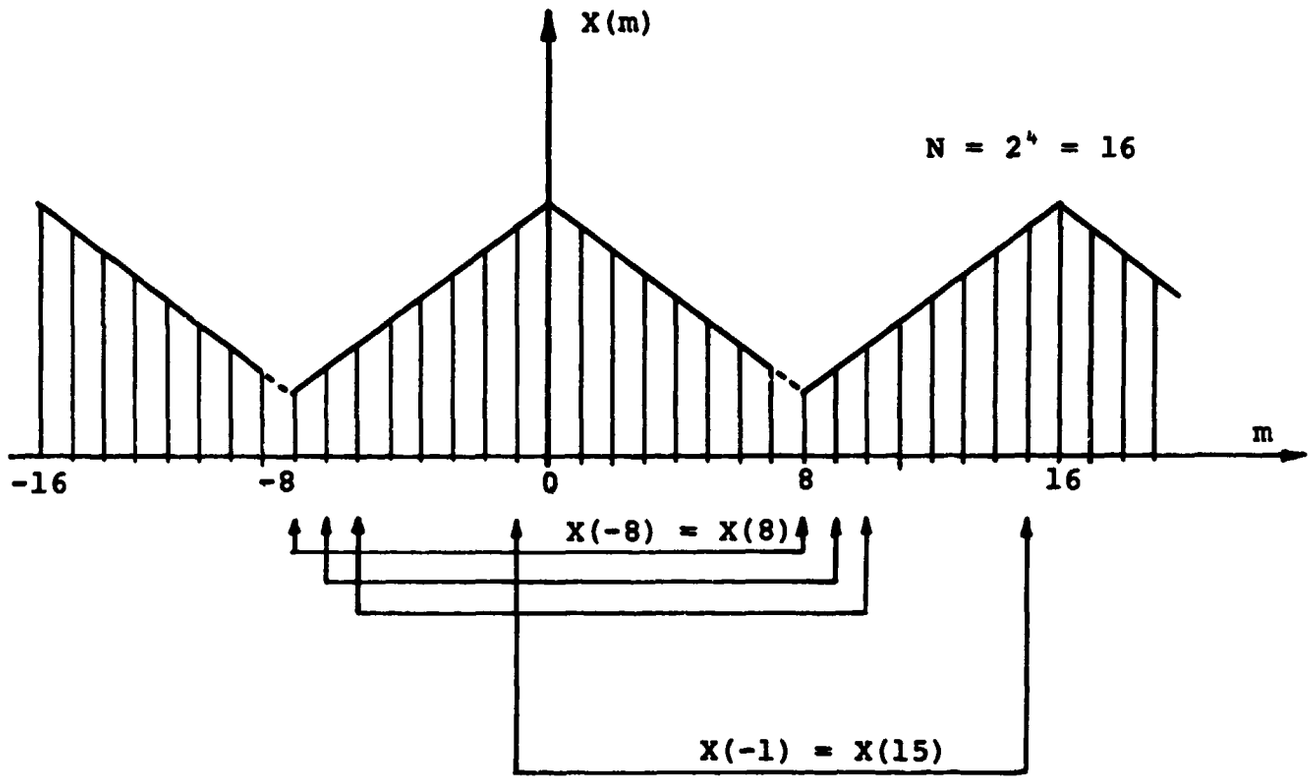

Figure E-1: Properties of Discrete Fourier Transform

interpreted as being periodic, these symmetries are equivalent to saying that X'(m) is an even function of m and X"(m) is an odd function. This also means that the Fourier coefficients between N/2 and N-1 can be viewed as the "negative frequency" harmonics between -N/2 and -1, respectively. Likewise, the last half of the sampled-data signal x(k) can be interpreted as negative time (that is, as occurring before t = 0).

Since the FFT algorithm provides an efficient transformation to the frequency domain, it is interesting to consider the product

$$Y(m) = F(m)X(m) \tag{E-11}$$

where Y(m) is the DFT of y(k), F(m) is the DFT of f(k), and X(m) is the DFT of x(k). According to Equation (E-7)

$$y(k) = \Delta f \sum_{m=0}^{N-1} \left[F(m)X(m) \right] \exp\{j2\pi mk/N\} \tag{E-12}$$

According to Equations (E-5) and (E-7) this can be written as

$$y(k) = \frac{\Delta t}{N} \sum_{m=0}^{N-1} \left[\sum_{\tau=0}^{N-1} x(\tau) e^{-j2\pi m\tau/N} \right] \left[\sum_{\hat{\tau}=0}^{N-1} f(\hat{\tau}) e^{-j2\pi m\hat{\tau}/N} \right] e^{j2\pi mk/N} \tag{E-13}$$

Since all of the sums are finite this can be written

$$y(k) = \frac{\Delta t}{N} \sum_{\tau=0}^{N-1} \sum_{\hat{\tau}=0}^{N-1} x(\tau) f(\hat{\tau}) \left[\sum_{m=0}^{N-1} e^{j2\pi(k-\tau-\hat{\tau})(m/N)} \right] \tag{E-14}$$

This can be simplified through the use of the orthogonality relation

$$\sum_{\ell=0}^{N-1} e^{j2\pi\ell m/N} e^{-j2\pi\ell n/N} = \begin{cases} N, & \text{if } n=m \text{ (modulo N)} \\ 0, & \text{otherwise} \end{cases} \tag{E-15}$$

Thus, Equation (E-14) is zero unless $\hat{\tau} = k-\tau$ and hence

$$y(k) = \Delta t \sum_{\tau=0}^{N-1} x(\tau) f(k-\tau) \tag{E-16}$$

Equation (E-16) may be recognized as the discrete form of the convolution integral

$$y(t) = \int_0^t x(\tau) f(t-\tau) d\tau \tag{E-17}$$

Equation (E-17) can be associated with the response y(t) of a fixed linear system to the input x(t), if that linear system can be characterized by the impulse response $f(t,\tau)$ where

$$f(t,\tau) = \begin{cases} f(f-\tau), & \text{if } t>\tau \\ o, & \text{if } t<\tau \end{cases} \qquad \text{(E-18)}$$

C.2 Fast Fourier Transform

The fast Fourier transform (FFT) is a highly efficient algorithm for computing the discrete Fourier transform (DFT). Taking advantage of the fact that the complex exponential weights appearing in the DFT can be calculated iteratively, the algorithm employs a clever computational technique for sequentially combining progressively larger partial sums of the exponentially weighted data samples to realize the DFT. Two mathematically equivalent versions of the FFT algorithm usually provide the basis for implementation: the Cooley-Tukey (decimation-in-time) algorithm and the Sande-Tukey (decimation-in-frequency) algorithm. The algorithm chosen for implementation is usually selected to exploit the characteristics of the sampled data and/or the hardware-software properties of the computer being used.

The value of the fast Fourier transformation lies in the reduction of computer execution time in evaluating the discrete Fourier transform. Whereas a direct N-point evaluation of the DFT typically requires a computer execution time proportional to N^2, the FFT requires a computer execution time proportional to only $N \cdot \log_2 N$. The approximate ratio of FFT to direct execution time is given by

$$\frac{N \cdot \log_2 N}{N^2} = \frac{\log_2 N}{N} \qquad \text{(E-19)}$$

For example, if $N = 256 = 2^8$, the FFT requires only about 3% of the time required by direct computation.

Four problems often encountered in using the FFT are: aliasing, leakage, picket-fence effect, and round-off error. The term "aliasing" refers to the fact that high-frequency spectral components of a band-limited signal can "impersonate" low-frequency spectral components if the sampling rate is too low [153]. This circumstance is reflected in its amplitude spectrum where the sidebands of frequency

translated baseband replicas are observed to overlap. This problem can be eliminated by sampling the signal at a rate at least twice as high as the highest frequency present in its amplitude spectrum. "Leakage" refers to distortion in the amplitude spectrum of a band-limited signal arising as a result of utilizing only a finite number of data samples from the signal's data record. This problem can be mitigated (but not eliminated) either by increasing the record length of the signal or by applying a data window to the data record [157]. The "picket-fence effect" refers to enhanced spectral responses at the discrete frequencies of the DFT due to interstitial, unresolved, spectral components of the signal. This problem can be mitigated (but not eliminated) by using an interpolation function between the discrete frequencies of the DFT or by extending the data record artificially with zero samples in order to increase the spectral resolution of the DFT. "Round-off error" arises in numerical computation as a result of the finite word length employed in digital computers for the representation of numbers. According to Kaneko and Lin [159,160] the total relative mean-square error (MSE) due to round-off error is bounded by

$$n\,\frac{2^{-2b}}{3} < \text{MSE} < 3n\,\frac{2^{-2b}}{3} \qquad \text{(E-20)}$$

where,

$$\text{MSE} = \frac{< \sum_{m=0}^{N-1} |e(m)|^2 >}{\sum_{m=0}^{N-1} |X(m)|^2} \qquad \text{(E-21)}$$

$$e(m) = \hat{X}(m) - X(m) \qquad \text{(E-22)}$$

$$n = \log_2 N \qquad \text{(E-23)}$$

and $\hat{X}(m)$ is the computer value of $X(m)$ based upon a b-bit representation for the mantissa (not including sign) of a real variable using binary floating-point arithmetic with double precision accumulation. For example, using double-precision real variables of 4 bytes each (3-byte mantissa, 1-byte exponent) so that $b = 23$ and a 512-point transform so that $n = 8$, the total relative MSE is bounded by

$$3.79\times10^{-14} < MSE < 1.14\times10^{-13} \qquad \text{(E-24)}$$

The total relative root-mean-square error (RMSE) in the amplitude spectrum is thus bounded by

$$1.95\times10^{-7} < RMSE < 3.37\times10^{-7} \qquad \text{(E-25)}$$

The relative accuracy in the calculation of the amplitude spectrum is thus, roughly speaking, about 1 part in 10^7.

In passing it may be noted that the FFT not only reduces the computation time of the DFT, it also substantially reduces the round-off errors associated with direct computation. In fact, both computation time and round-off error are reduced by the same factor of $(\log_2 N)/N$ [156]. Further, although the above discussion of the problems encountered in using the FFT was couched in terms relating to the forward transformation of variables from time to frequency [Equation (E-7)], the discussion remains valid in the inverse transformation of variables from frequency to time [Equation (E-8)].

C.3 Example: Bandpass Rectangular Pulse

The basic properties of the discrete Fourier transform (DFT) and its computation by the fast Fourier transform (FFT) may be exemplified by considering the bandpass rectangular pulse

$$x(t) = p(t)\cdot\cos(2\pi f_o t) \qquad \text{(E-26)}$$

where f_o is the r-f carrier frequency and $p(t)$ is the pulse envelope defined by

$$p(t) = \begin{cases} 1, & |t| < L/2 \\ 0, & |t| > L/2 \end{cases} \qquad \text{(E-27)}$$

where L is the pulse length (duration). In the numerical computations which follow, f_o will be taken to be 600 MHz and L to be 5 nanoseconds (3 r-f cycles).

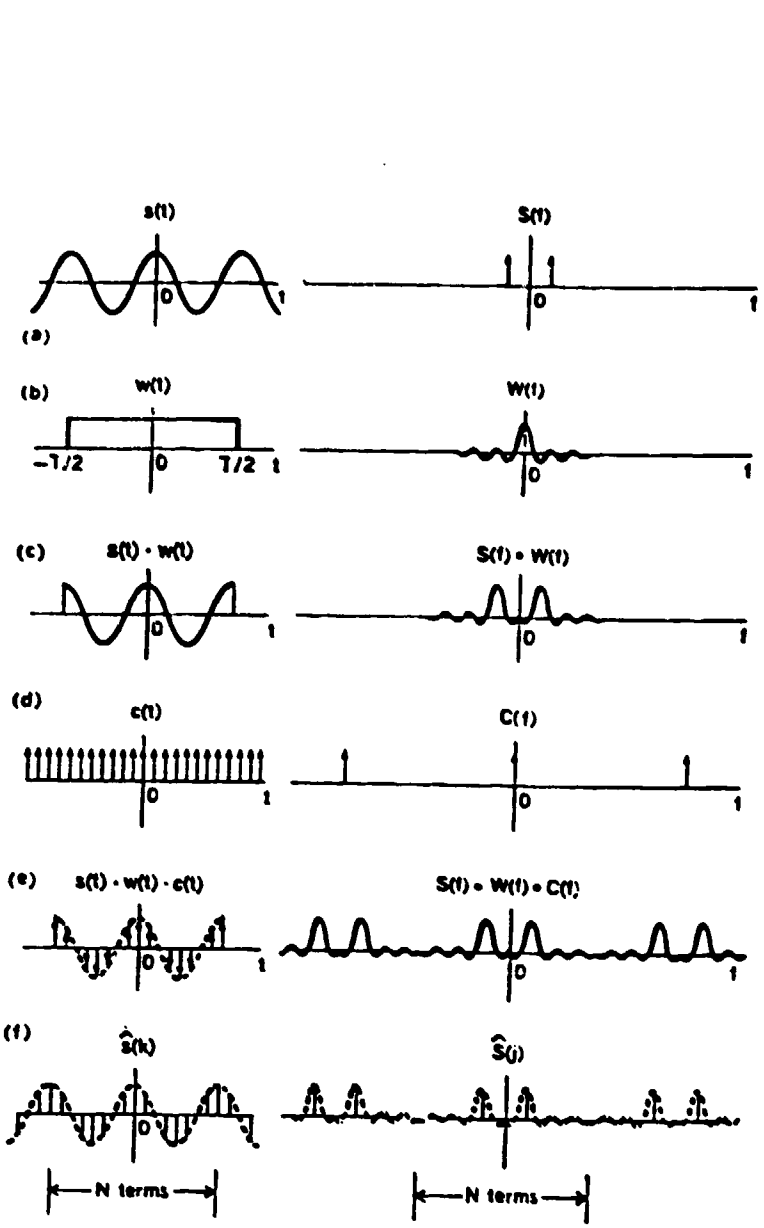

Figure E-2: Character of Discrete Fourier Transform [153]

The amplitude spectrum of the pulse envelope can be determined from Equation (E-1) to be

$$P(f) = L\,\mathrm{sinc}\{\pi fL\} \tag{E-28}$$

It should be noted that although the pulse p(t) is undefined for $|t| = L/2$, the inverse transformation of P(f) using Equation (E-2) converges to

$$P(|L/2|) = 0.5 \tag{E-29}$$

because of Gibb's phenomenon [ ]. As a consequence, the numerical representation of p(t) at the point of discontinuity ($|t| = L/2$) must be that afforded by Equation (E-29). Failure to accomodate Gibb's phenomenon at points of discontinuity in the signal (or even the spectrum) will lead to spurious oscillations in the transformed variable.

The r-f carrier $\cos(2\pi f_o t)$ and its amplitude spectrum [two δ functions at $\pm f_o$] and the pulse envelope p(t) and its amplitude spectrum P(f) are shown, respectively, in Figures E-2 (a) and (b). The bandpass rectangular pulse x(t) [refer to Equation (E-26)] and its amplitude spectrum.

$$X(f) = \tfrac{1}{2}L\,[\mathrm{sinc}\{\pi L(f+f_o)\} + \mathrm{sinc}\{\pi L(f-f_o)\}] \tag{E-30}$$

are shown, respectively, in Figure E-2 (c). In consonance with Equations (E-11) and (E-16) and the time-frequency duality of the Fourier transform [refer to Equations (E-1) and (E-2)], Equation (E-30) and Figure E-2 (c) reflect the fact that the amplitude spectrum of the product of two time functions is equal to the convolution of their respective amplitude spectra.

The sampled-data signal x(k) is obtained by multiplying the bandpass rectangular pulse x(t) by an infinite train of unit impulses (or Dirac comb) defined mathematically by

$$c(t) = \sum_{k=-\infty}^{\infty} \delta(t-k\Delta t) \tag{E-31}$$

The Dirac comb and its amplitude spectrum

$$C(f) = \frac{1}{\Delta t} \sum_{m=-\infty}^{\infty} \delta\left(f - \frac{m}{\Delta t}\right) \qquad \text{(E-32)}$$

are shown in Figure E-2 (d). The sampled-data signal x(t) and its amplitude spectrum C(f)*X(f) are shown, respectively, in Figure E-2 (e). It is apparent from this figure that, because the amplitude spectrum of the pulse [P(f)] is not strictly bandlimited, aliasing cannot be entirely avoided and some spectral overlapping is inescapable. However, CyberCom has found that the aliasing associated with non-bandlimited signals (which, strictly speaking, arise only in mathematical models and not in real systems) can be held within acceptable bounds, in most cases, by letting

$$\Delta t = [2(f_o + B_{99})]^{-1} \qquad \text{(E-33)}$$

where B_{99} is the low-pass equivalent bandwidth containing 99% of the signal power. Note that this rule is consistent with the low-pass Nyquist sampling rate when the signal is strictly bandlimited to B Hertz. For P(f) [refer to Equation (E-28)], the 99% containment bandwidth is [153]

$$B_{99} = \frac{10.5}{L} \qquad \text{(E-34)}$$

In the numerical computation which follow

$$L = \frac{3}{f_o} \qquad \text{(E-35)}$$

so that

$$\Delta t = \frac{1}{8f_o} \qquad \text{(E-36)}$$

which corresponds to a sampling rate of 8 samples per r-f cycle. It should be noted that the aliasing appearing in Figure E-2 (e) will not lead to distortion in recovering the sampled-data signal x(k) from C(f)*X(f) via the inverse Fourier tranformation. This is assured by the isomorphic (one-to-one) relation between a Fourier

transform and its inverse. However, subsequent signal processing operations which modify the amplitude spectrum C(f)*X(f) [e.g., convolution] will be affected.

The continuous frequency-domain function C(f)*X(f) shown in Figure E-2 (e) can also be made discrete (sampled) by treating the sample-data signal x(k) as one period of a periodic function with the data sample x(N/2) taken as the first sample of successive periods. This forces both the time-domain and frequency domain functions [x(k) and X(m), respectively] to be infinite in extent, periodic, and discrete as shown in Figure E-2 (f). The resolution in the frequency-domain is determined by the relation

$$\Delta f = \frac{1}{T} = \frac{1}{N\Delta t} \tag{E-37}$$

where T is the period in the time domain, Δt is the sampling rate, and N is the number of data samples. It is apparent from Equation (E-37) that the resolution can be increased by increasing the sampling rate and/or the number of data points. The number of data points can always be increased without changing the sampling rate by filling out the (truncated) data record x(k) with zeroes. In the numerical calculations which follow N was taken to be a power of 2, specifically

$$N = 2^8 = 256 \tag{E-38}$$

As a consequence of Equations (E-36) and (E-37)

$$f = \frac{f_o}{32} = \frac{75}{4}\ \text{MHz} \tag{E-39}$$

APPENDIX F

Optical Theorem for Scalar Fields in Two-Dimensional Media

The purpose of this appendix is to apply Poynting's vector theorem to two-dimensional scatterers that are normally illuminated. This will lead naturally to definitions of the total, scattering and absorption cross-sections for the scalar case.

Consider a two-dimensional scatterer of cross-section S_p as shown in Figure F-1. Assume that the scatterer is oriented in such a way that its generating elements are parallel to the z axis. The scatterer is illuminated by a unit amplitude plane wave.

$$\underline{E}_i(\underline{x}_t) = \psi_i(\underline{x}_t)\underline{z}^\circ \qquad \psi_i(\underline{x}_t) = e^{-jk_o\underline{i}\cdot\underline{x}_t} \tag{F-1}$$

where $\underline{i}\cdot\underline{z}^\circ = 0$.

Apply Poynting's vector theorem to a circular cylindrical volume of unit height and surface S_o. The cylinder has radius r which is assumed to be large. If $\underline{E}$ and $\underline{H}$ are the total electric and magnetic fields then

$$R_e \int_{S_o} \underline{S}_c \cdot d\underline{a} + \frac{1}{2}\int_{V_o} \sigma \underline{E}\cdot\underline{E}^* dV = 0 \tag{F-2}$$

where $\underline{S}_c$ is the complex Poynting vector,

$$\underline{S}_c = \tfrac{1}{2}\underline{E}\times\underline{H}^* \tag{F-3}$$

σ is the conductivity of the scatterer's material and V_o is the volume of the unit height cylinder. Because the scatterer and the incident field are both independent of z, it follows that

$$\underline{E} = \underline{E}(\underline{x}_t) = \psi(\underline{x}_t)\underline{z}^\circ \tag{F-4}$$

The scalar field $\psi(\underline{x}_t)$ is composed of an incident and scattered portion, thus

$$\psi(\underline{x}_t) = \psi_i(\underline{x}_t) + \psi_s(\underline{x}_t) \tag{F-5}$$

The scattering amplitude, $f(\underline{o},\underline{i})$, is introduced when the scattered wave is represented in the far field as follows:

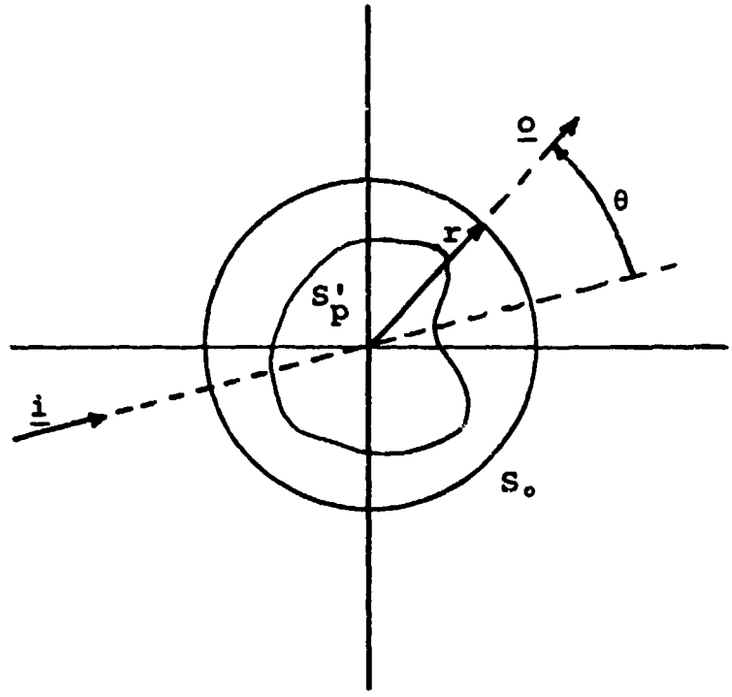

Figure F-1 Two-Dimensional Scattering Geometry

$$\psi_s(\underline{x}_t) \sim f(\underline{o},\underline{i})\frac{e^{-jk_t\underline{o}\cdot\underline{x}_t}}{\sqrt{r}}, \quad r = |\underline{x}_t| >> 1 \tag{F-6}$$

where $\underline{o} = \underline{x}_t/r$.

Finding the incident and scattered magnetic fields from Maxwell's equations for large r and then using them in equation (F-2) results in the following equation:

$$\int_0^{2\pi} |f(\underline{o},\underline{i})|^2 d\theta + \sqrt{r}\, R_e \int_0^{2\pi} [f(\underline{o},\underline{i}) e^{jk_o r(\cos\theta-1)} + f^*(\underline{o},\underline{i}) e^{-jk_o r(\cos\theta-1)} \cos\theta]\, d\theta = \sigma_a \tag{F-7}$$

where the angle θ is defined in Figure F-1 and the absorption cross-section σ_a is given by [55]

$$\sigma_a = \frac{\varepsilon_o}{\mu_o} \int_V \sigma \underline{E}\cdot\underline{E} dV \tag{F-8}$$

The derivation is completed by asymptotically evaluating the the integral in equation (F-7) for large $k_o r$. The integral can be divided into two integrals each of which can be treated by the method of stationary phase. A calculation shows that there are stationary points of $\theta = 0, r$ and 2π. Now using this asymptotic result in equation (F-7), one obtains

$$\int_0^{2\pi} |f(\underline{o},\underline{i})|^2 d\theta + \frac{2\sqrt{2\pi}}{\sqrt{k_o}} R_e f(\underline{i},\underline{i}) e^{-j\pi/4} + \sigma_a = 0 \tag{F-9}$$

Because the scattering cross-section σ_s is defined as

$$\sigma_s = \int_0^{2\pi} |f(\underline{o},\underline{i})|^2 d\theta \tag{F-10}$$

and the total cross-section is the sum of the scattering and absorption cross-section i.e.,

$$\sigma_t = \sigma_s + \sigma_a \tag{F-11}$$

one obtains

$$\sigma_t = -\frac{2\sqrt{2\pi}}{\sqrt{k_o}} R_e [f(\underline{i},\underline{i}) e^{-j\pi/4}] \tag{F-12}$$

The expressions for σ_s and σ_t in terms of the scattering amplitude f can be put in terms of the Fourier transform of the transition operator $\tilde{t}$. By using equation (2-2-24) in equations (F-10) and (F-12), the following expressions are obtained:

$$\sigma_s = \frac{2\pi^3}{k_o} \int_o^{2\pi} |\tilde{t}(k_o\underline{o}, k_o\underline{i})|^2 d\theta \qquad \text{(F-13)}$$

$$\sigma_t = - \frac{(2\pi)^2}{k_o} I_m \tilde{t}(k_o\underline{i}, k_o\underline{i}) \qquad \text{(F-14)}$$

APPENDIX G

Alternative Representation for the Intensity of Scalar Fields in Two-Dimensional Media

In Chapter 7 an integral representation for the normalized intensity [equation (7-28)] has been obtained. Unfortunately, the integral is very slowly convergent for large values of τq. To rectify the difficulty, the integral will be converted into an alternate form which is more rapidly convergent.

For convenience, the original expression for $\bar{I}(\tau)$ is repeated here. It is given by

$$\bar{I}(\tau)=\tau e^{\tau}\int_0^{\infty} \frac{dqqJ_o(\tau q)}{\sqrt{q^2+1}-W_o} \tag{G-1}$$

The alternative representation for $\bar{I}(\tau)$ can be obtained by deforming the integration path in the q plane. To do this an integral from $-\infty$ to $+\infty$ is needed. This is obtained by representing $J_o(\tau q)$ in terms of the Hankel function,

$$J_o(\tau q) = [H_o^{(1)}(\tau q) + H_o^{(2)}(\tau q)]/2 \tag{G-2}$$

and then substituting this expression into equation (G-1). This gives

$$\bar{I}(\tau) = \frac{\tau e^{\tau}}{2}\int_0^{\infty} dq \frac{qH_o^{(1)}(\tau q)}{\sqrt{q^2+1}-W} + \frac{\tau e^{\tau}}{2}\int_0^{\infty} dq \frac{qH_o^{(2)}(\tau q)}{\sqrt{q^2+1}-W_o} \tag{G-3}$$

The last integral in equation (G-3) is now transformed by letting $q' = qe^{i(\pi-\varepsilon)}$, $\varepsilon > 0$. The result when combined with the first integral of equation (G-3) is given by

$$\bar{I}(\tau) = \frac{\tau e^{\tau}}{2}\int_P \frac{dq\ qH_o^{(1)}(\tau q)}{\sqrt{q^2+1}-W_o} \tag{G-4}$$

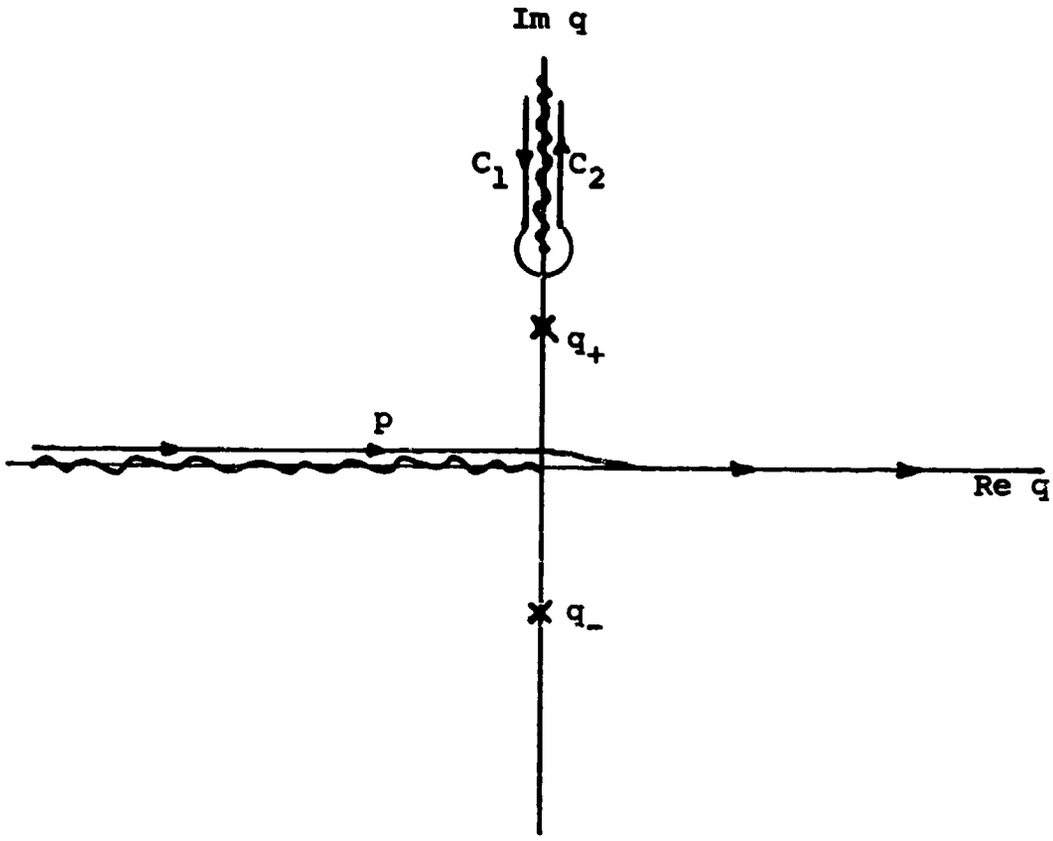

Figure G-1 Integration Paths for Normalized Intensity

where P is the resulting integration path shown in Figure G-1. The small parameter ε has been introduced in order to avoid the branch-cut of the Hankel function lying along the negative real q axis.

An examination of the singularities of equation (G-4) shows that in addition to the Hankel function branch-cut, there are simple poles at $q = q_{\pm} = \pm i\sqrt{1-W_o^2}$ and branch point singularities at $q = \pm i$. The branch cuts associated with these branch point singularities are chosen along the positive and negative imaginary axes. The alternative form of the integral is now obtained by deforming the integration path P into the upper half of the q plane. Because the integrand tends to zero as $|q| \to \infty$ in the upper half q plane, the inte ral is represented wholly by the contribution due to the pole $q = q_{\pm}$ and the upper branch-cut. The result is

$$\bar{I}(\tau) = 2\pi i \tau W_o e^{\tau} H_o^{(1)}\left(i\tau\sqrt{1-W_o^2}\right)/2 + \frac{\tau e^{\tau}}{2}\int_{C_1+C_2} dq\, q\, \frac{H_o^{(1)}(\tau q)}{\sqrt{q^2+1} - W_o} \qquad \text{(G-5)}$$

where the paths C_1 and C_2 are defined in Figure G-1.

The integrals over C_1 and C_2 can each be transformed to the real positive axis and combined. The result is

$$\bar{I}(\tau) = 2W_o \tau e^{\tau} K_o\left(\tau\sqrt{1-W_o^2}\right) + \frac{2\tau}{\pi} e^{\tau}\int_o^{\infty} dp\; p^2 \frac{K_o\left(\tau\sqrt{1+p^2}\right)}{p^2 + W_o^2} \qquad \text{(G-6)}$$

Here $K_o(z)$ is the modified Hankel function. Because $K_o(z)$ is decaying exponentially for large z, the integral converges rapidly for large values of p.

Distribution List

	Number of Copies
Defense Technical Information Center Cameron Station Alexandria, VA 22314	12 copies
US Dept of Commerce Institute for Telecommunications Sciences/NTIA Boulder, CO. 80303	
ATTN: Dr. G. Hufford	2 copies
Mr. E. Violette	1 copy
SRI International 333 Ravenswood Avenue Menlo Park, CA 94025	
ATTN: Dr. M. Frankel	1 copy
Dr. R. Nelson	1 copy
Dr. A. Spiridon	1 copy
Prof. T. Tamir Dept of EE/Electrophysics Polytechnic Institute of New York 333 Jay Street Brooklyn, NY 11201	1 copy
Mr. George Hagn SRI International 1611 N. Kent Street Arlington, VA 22209	1 copy
Prof. A. H. LaGrone Dept of EE University of Texas Austin, Texas 78712	1 copy
Dr. K. Chamberlin Dept of EE Ohio University Athens, OH 45701	1 copy
Dr. R. Luebbers Lockheed Palo Alto Research Labs 3251 Hanover Street Palo Alto, California 94304	1 copy

Dr. G. S. Brown
Applied Science Assoc., Inc.
105 East Chatham
Apex, N.C. 27502
1 copy

Commander
USA ERADCOM
EW Laboratory
ATTN: DELEW-V (W. Barr)
Fort Monmouth, NJ 07703
1 copy

Commander
USACECOM
CENSEI
ATTN: DRSEL-SEI-A (P. Major)
Fort Monmouth, NJ 07703
2 copies

Commander
USACECOM
CENCOMS
ATTN: DRSEL-COM-RM-4 (F. Schwering)
Fort Monmouth, NJ 07703
2 copies

Commander
USACECOM
CENCOMS
ATTN: DRSEL-COM-RM-4 (G. Whitman)
Fort Monmouth, NJ 07703
1 copy

IIT Research Institute
ATTN: Mark Weissberger
c/o DOD ECAC
Annapolis, Md. 21402
1 copy

Commander
USACECOM
CENCOMS
ATTN: DRSEL-COM-RM-4 (R. Johnson)
Fort Monmouth, NJ 07703
1 copy

Commander
USACECOM
CENCOMS
ATTN: DRSEL-COM-RF-2 (P.Sass)
Fort Monmouth, NJ 07703
64 copies

Dr. J. Olsen
Hughes Aircraft Company
Ground Systems Group
Fullerton, CA 92634
1 copy

Dr. F. Amoroso
Hughes Aircraft Company
Ground Systems Group
Fullerton, CA 92634

1 copy

Mr. Richard Robertson
Atlantic Research Corp.
5390 Cherokee Avenue
Alexandria, VA 22314

1 copy